

The role of RNA binding proteins in motoneuron diseases

**Die Rolle von RNA-bindenden Proteinen in
Motoneuronerkrankungen.**



**Doctoral thesis for a doctoral degree
at the Institute for Clinical Neurobiology,
University hospital Würzburg
and Graduate School of Life Sciences,
Julius-Maximilians-Universität Würzburg**

Submitted by

Rajeeve Sivadasan

from

Kadakkal, India

Würzburg 2016

Submitted on:

Office stamp

Members of the Promotionskomitee:

Chairperson: Prof. Dr. Thomas Dandekar

Primary Supervisor: Prof. Dr. Michael Sendtner

Supervisor (Second): Prof. Dr. Hermann Schindelin

Supervisor (Third): Prof. Dr. Erich Buchner

Date of Public Defence:

Date of Receipt of Certificates:

For Mummy, Papa, Karthika, Adithya and Aarav

TABLE OF CONTENTS

1. ABSTRACT	1
2. ZUSAMMENFASSUNG	3
3. INTRODUCTION	5
3.1 Clinical phenotype and genetic basis of spinal muscular atrophy.	5
3.2 Cellular functions of the SMN protein and model system.....	8
3.3 Clinical phenotype and genetic basis of amyotrophic lateral sclerosis.....	12
3.4 Discovery of C9ORF72 mutations.....	19
3.5 Pathogenic mechanism of the C9ORF72 repeat expansion.....	20
3.6 Current model systems to study C9ORF72 functions.....	22
3.7 The current state of knowledge on the function of C9ORF72.....	25
4. MATERIALS	28
4.1. Cell lines.....	28
4.2 Bacterial strains.....	28
4.3 Primary mouse motoneuron culture.....	29
4.4 Buffers for Immunofluorescence.....	31
4.5 Buffers for Western blotting.....	32
4.6 Commercial kits and molecular ladders.....	33
4.7 Stock buffers for protein purification.....	33
4.7.1 Buffers for purification of hnRNP R.....	34
4.7.2 Buffers for purification of SMN.....	34
4.7.3 Buffers for purification of TDP-43.....	35
4.7.4 Buffers for His-Trap HP column stripping and cleaning.....	35
4.7.5 Columns used for protein purification.....	36
4.8 Antibodies.....	36
4.9 EMSA buffers.....	39
4.10 Instruments used.....	39
4.11 Software used.....	40
5. METHODS	41
5.1 Animals and ethics statement.....	41
5.2 Cell Culture.....	41
5.3 Cryo stocking of cell lines.....	41
5.4 Transfection of HEK-293, HeLa and NSC-34 cell.....	42

5.5	Primary motoneuron culturing.....	42
5.6	Overexpression and knockdown of C9ORF72 by shRNA in cultured mouse motoneurons.....	43
5.7	Standardization of lentiviral concentration on NSC-34 cells.....	44
5.8	Sample preparation for LC-MS analysis using NSC-34 cells.....	44
5.9	LC-MS data acquisition and analysis.....	45
5.10	Data analysis.....	45
5.11	Immunofluorescence analysis of primary mouse motoneurons and cell lines.....	46
5.12	Lentivirus Production.....	46
5.13	Protein Purification.....	48
5.13.1	<i>Preparation of bacterial lysates for recombinant protein purification.....</i>	48
5.13.2	<i>Setup of FPLC for purification and maintenance.....</i>	48
5.13.3	<i>Chromatography.....</i>	48
5.13.4	<i>Immobilized metal affinity chromatography (IMAC).....</i>	49
5.13.5	<i>Chitin-Intein system.....</i>	49
5.13.6	<i>Ion exchange chromatography.....</i>	49
5.13.7	<i>Size-exclusion chromatography.....</i>	50
5.14	Co-immunoprecipitations of recombinant proteins.....	50
5.15	Electrophoretic Mobility Shift Assay (EMSA).....	51
5.15.1	<i>Linearisation of beta-actin 3'UTR cDNA (vector).....</i>	52
5.15.2	<i>Radiolabeling beta-actin 3'UTR mRNA using MEGAscript Transcription kit (Ambion).....</i>	52
5.16	Cytosolic and nuclear fractionation.....	53
5.17	Immunoprecipitations from cultured mouse motoneurons and cells.....	54
5.18	Live cell imaging of actin dynamics.....	54
5.19	G/F-actin ratio measurement.....	55
5.20	SDS-PAGE and Western blotting.....	56
5.21	Coomassie staining for protein gels.....	58
5.22	Cloning.....	59
5.22.1	<i>Polymerase chain reaction (PCR).....</i>	59
5.22.2	<i>Restriction enzyme digestion and analysis of DNA fragments.....</i>	59
5.22.3	<i>Ligation of restricted fragment into vector.....</i>	60
5.22.4	<i>Sequencing.....</i>	61
5.22.5	<i>Transformation of chemical competent E.coli.....</i>	62

5.22.6	<i>Easy prep plasmid purification</i>	62
5.23	Cross linking antibody to beads for LC-MS analysis.	63
5.24	Quantitative PCR.	64
5.25	Immunoprecipitation of protein-RNA complexes.	65
5.26	Statistical analysis.....	66
6.	Results	68
6.1	Protein purification of murine recombinant hnRNP R and SMN.....	68
6.2	Protein purification of murine recombinant TDP-43.....	71
6.3	HnRNP R interaction with SMN in motoneurons.	73
6.4	Direct SMN interaction with hnRNP R modulates affinity of hnRNP R.	75
6.5	Depletion of SMN alters the subcellular distribution of hnRNP R in motoneurons... 77	
6.6	TDP-43 interaction with SMN and hnRNP R influenced by the mutation.....	81
6.7	Direct interaction of SMN with TDP-43.....	83
6.8	HnRNP R SMN interaction enhance the binding of the 3'UTR of β -actin mRNA to the hnRNP R complex.....	85
6.9	TDP-43 binds to the 3'UTR of β -actin.	87
6.10	TDP-43 SMN interaction enhanced the binding of the 3'UTR of β -actin mRNA to TDP-43.....	88
6.11	TDP-43 mutations in the C-terminal region influence the binding of mRNA.	89
6.12	Cloning of plasmids for overexpression of C9ORF72 and shRNA for mouse C9ORF72.	91
6.13	C9ORF72 expression regulates axonal growth in cultured motoneurons.	94
6.14	Identification of the C9ORF72 interactome.	95
6.15	C9ORF72 regulates cofilin phosphorylation.	99
6.16	Cloning of a vector for combining actin visualisation with C9ORF72 knockdown.....	101
6.17	Actin dynamics is disturbed after knockdown of mouse C9ORF72.....	102
6.18	Altered G/F actin ratio in motoneurons after overexpression and knockdown of C9ORF72.	104
7.	DISCUSSION	106
7.1	SMN interacts directly with hnRNP R and TDP-43 and regulates the binding to the 3'UTR of β -actin mRNA.....	106
7.2	Depletion of SMN alters the subcellular distribution of hnRNP R in motoneurons. 107	

7.3	Mutations in the C-terminal region of TDP-43 regulate the binding of protein and RNA.	109
7.4	C9ORF72 interaction with cofilin modulates actin dynamics in motoneurons.	110
8.	REFERENCES FOR THIS THESIS	114
9.	APPENDIX	126
9.1	List of Figures:	126
9.2	List of Tables:	129
9.3	Abbreviations.	131
10.	AFFIDAVIT	134
11.	ACKNOWLEDGMENTS	135
12.	CURRICULUM VITAE	138

1. ABSTRACT

Motoneuron diseases form a heterogeneous group of pathologies characterized by the progressive degeneration of motoneurons. More and more genetic factors associated with motoneuron diseases encode proteins that have a function in RNA metabolism, suggesting that disturbed RNA metabolism could be a common underlying problem in several, perhaps all, forms of motoneuron diseases. Recent results suggest that SMN interacts with hnRNP R and TDP-43 in neuronal processes, which are not part of the classical SMN complex. This points to an additional function of SMN, which could contribute to the high vulnerability of spinal motoneurons in spinal muscular atrophy (SMA) and amyotrophic lateral sclerosis (ALS). The current study elucidates functional links between SMN, the causative factor of SMA (spinal muscular atrophy), hnRNP R, and TDP-43, a genetic factor in ALS (amyotrophic lateral sclerosis). In order to characterize the functional interaction of SMN with hnRNP R and TDP-43, we produced recombinant proteins and investigated their interaction by co-immunoprecipitation. These proteins bind directly to each other, indicating that no other co-factors are needed for this interaction. SMN potentiates the ability of hnRNP R and TDP-43 to bind to β -actin mRNA. Depletion of SMN alters the subcellular distribution of hnRNP R in motoneurons both in SMN-knockdown motoneurons and SMA mutant mouse ($\Delta 7$ SMA). These data point to functions of SMN beyond snRNP assembly which could be crucial for recruitment and transport of RNA particles into axons and axon terminals, a mechanism which may contribute to SMA pathogenesis and ALS.

ALS and FTLD (frontotemporal lobar degeneration) are linked by several lines of evidence with respect to clinical and pathological characteristics. Both sporadic and familial forms are a feature of the ALS-FTLD spectrum, with numerous genes having been associated with these pathological conditions. Both diseases are characterized by the pathological cellular aggregation of proteins. Interestingly, some of these proteins such as TDP-43 and FUS have also common relations not only with ALS-FTLD but also with SMA. Intronic hexanucleotide expansions in C9ORF72 are common in ALS and FTLD but it is unknown whether loss of function, toxicity by the expanded RNA or dipeptides from non ATG-initiated translation is responsible for the pathophysiology. This study tries to characterize the cellular function of C9ORF72 protein. To address this, lentiviral based knockdown and overexpression of C9ORF72 was used in isolated mouse motoneurons. The results clearly show that survival of these motoneurons was not affected by altered C9ORF72 levels,

whereas adverse effects on axon growth and growth cone size became apparent after C9ORF72 suppression. Determining the protein interactome revealed several proteins in complexes with C9ORF72. Interestingly, C9ORF72 is present in a complex with cofilin and other actin binding proteins that modulate actin dynamics. These interactions were confirmed both by co-precipitation analyses and in particular by functional studies showing altered actin dynamics in motoneurons with reduced levels of C9ORF72. Importantly, the phosphorylation of cofilin is enhanced in C9ORF72 depleted motoneurons and patient derived lymphoblastoid cells with reduced C9ORF72 levels. These findings indicate that C9ORF72 regulates axonal actin dynamics and the loss of this function could contribute to disease pathomechanisms in ALS and FTL D.

2. ZUSAMMENFASSUNG

Motoneuronerkrankungen bilden eine heterogene Gruppe von Pathologien, die durch die progressive Degeneration von Motoneuronen charakterisiert sind. Zunehmend werden genetische Faktoren in Assoziation mit Motoneuronerkrankungen identifiziert, die eine Funktion im RNA Metabolismus besitzen, was dafür spricht, dass ein gestörter RNA Metabolismus ein gemeinsames zugrunde liegendes Problem in mehreren, vielleicht allen, Formen von Motoneuronerkrankungen sein könnte. Neuere Ergebnisse legen nahe, dass SMN mit hnRNP R und TDP-43 in neuronalen Prozessen interagiert, die nicht Teil der klassischen Rolle des SMN Komplexes sind. Dies deutet auf eine zusätzliche Funktion von SMN hin, die zur hohen Störanfälligkeit von spinalen Motoneuronen in spinaler Muskelatrophie (SMA) und amyotropher Lateralsklerose (ALS) beitragen könnte. Die vorliegende Arbeit beleuchtet funktionelle Beziehungen zwischen SMN, dem auslösenden Faktor der SMA, und hnRNP R, sowie TDP-43, einem weiteren genetischen Faktor bei ALS. Um die funktionelle Interaktion von SMN mit hnRNP R und TDP-43 zu charakterisieren, wurden rekombinante Proteine hergestellt und ihre Interaktion durch co-Immunpräzipitation untersucht. Diese Proteine binden direkt an einander, was darauf hindeutet, dass für diese Interaktion keine weiteren co-Faktoren erforderlich sind. SMN potenziert die Fähigkeit von hnRNP R und TDP-43, β -Aktin mRNA zu binden. Depletion von SMN verändert die subzelluläre Verteilung von hnRNP R in Motoneuronen sowohl in SMN-knock-down Motoneuronen, als auch in der SMA Mausmutante (delta7 SMA). Diese Daten deuten auf Funktionen von SMN jenseits der snRNP Assemblierung hin, die entscheidend für die Rekrutierung und den Transport von RNA Partikel in Axonen und Axon Terminalen sein könnten, einem Mechanismus, der zur Pathogenese von SMA und ALS beitragen könnte.

ALS und FTLD (fronto-temporale Lobus Degeneration) sind aufgrund mehrerer Nachweislinien bezüglich klinischer und pathologischer Charakteristika vernetzt. Sowohl sporadische als auch familiäre Formen sind Merkmal des ALS-FTLD Spektrums, wobei zahlreiche Gene mit diesen pathologischen Erscheinungen assoziiert wurden. Beide Krankheiten sind durch pathologische zelluläre Proteinaggregation charakterisiert. Interessanterweise haben einige dieser Proteine, wie TDP-43 und FUS, einen gemeinsamen Bezug nicht nur mit ALS-FTLD, sondern auch mit SMA. Intronische Hexanukleotid-Expansionen in C9ORF72 sind häufig in ALS und FTLD, es ist jedoch unbekannt, ob Funktionsverlust, Toxizität aufgrund der verlängerten RNA, oder Dipeptide von non-ATG

initiiertes Translation für die Pathophysiologie verantwortlich sind. Die vorliegende Arbeit versucht die zelluläre Funktion von C9ORF72 Protein zu charakterisieren. Hierfür wurde lentiviraler knock-down und Überexpression von C9ORF72 in isolierten Motoneuronen eingesetzt. Die Ergebnisse zeigen deutlich, dass das Überleben dieser Motoneurone durch veränderte C9ORF72 Konzentrationen nicht beeinflusst wurde, wohingegen negative Auswirkungen auf Axonwachstum und Wachstumskegelgröße nach C9ORF72 Suppression deutlich wurden. Die Bestimmung des Protein Interaktoms identifizierte mehrere Proteinkomplexe mit C9ORF72. Interessanterweise liegt C9ORF72 in einem Komplex mit Cofilin und anderen Aktin-bindenden Protein vor, welche die Aktin Dynamik modulieren. Diese Interaktionen wurden sowohl durch Analyse von co-Präzipitationen als auch besonders durch funktionelle Studien bestätigt, die eine veränderte Aktin Dynamik in Motoneuronen mit reduzierter C9ORF72 Konzentration zeigten. Wichtig ist die Beobachtung, dass die Phosphorylierung von Cofilin in C9ORF72 depletierten Motoneuronen und in Lymphoblastoid-Zellen mit reduzierter C9ORF72 Konzentration verstärkt ist. Diese Ergebnisse zeigen, dass C9ORF72 die axonale Aktin Dynamik reguliert und dass der Verlust dieser Funktion zu Krankheits-Pathomechanismen in ALS und FTLD beitragen könnte.

3. INTRODUCTION.

Neurodegenerative diseases represent a heterogeneous group of neurological conditions primarily involving dementia and movement disorders. A wide variety of different pathophysiological and genetic mechanisms are involved in this group. Knowledge regarding the genetic basis of sporadic and familial cases of neurodegenerative disorders is growing. New evidence about the involvement of previously uncharacterized genes opens new dimensions for basic research. This is particularly true in cases with complex motor and cognitive phenotypes. Neurodegenerative diseases can be classified into two type main subtypes, one associated with motoneuron dysfunction and the other with a degeneration involving the cerebral cortex (dementia). Motoneuron disorders are diseases leading to degeneration of motoneurons. These diseases comprise four main different clinical forms of upper and lower motor neuron involvement: primary lateral sclerosis; progressive muscular atrophy; progressive bulbar palsy; and amyotrophic lateral sclerosis (ALS).

3.1 Clinical phenotype and genetic basis of spinal muscular atrophy.

Spinal muscular atrophy (SMA) is a comprehensive term that summarizes a range of diseases affecting motoneurons in the spinal cord and brainstem. Werdnig and Hoffmann were the first to independently describe clinical cases of children affected by muscular atrophy and progressive paralysis [1]. Studies have shown clear atrophy of the ventral roots of the spinal nerves, along with severe loss of motoneurons in the anterior horn of the spinal cord as the main pathological hallmarks.

SMA, an autosomal recessive disease, is the most frequent monogenic cause of death in infancy and a major cause of childhood morbidity due to weakness [2-4]. Among inherited diseases with an autosomal recessive pattern, the incidence of SMA is second only to cystic fibrosis. Reported SMA incidence is 1:10,000 live births; 1:40-1:60 of the general population are *SMN1* mutation carriers [2-4]. SMA comprises a wide spectrum of clinical conditions characterized by a rather selective degeneration of spinal motoneurons within the central nervous system (CNS), along with a complex profile of accompanying symptoms that point to the crucial systemic role of the SMN protein.

SMA has been divided into five subgroups based on the decreasing spectrum of severity that consider the age of onset, the most advanced motor milestone reached and the typical age of death. The clinical phenotype for an individual seems to be influenced by the

amount of copies of the paralogous gene *SMN2* [5]. SMA can be classified according to the severity into type 0, type 1, type 2, type 3 and type 4 [6]. SMA type 0 is the most severe form of SMA. The disease onset occurs *in utero*, with reduced fetal movements. At birth, affected children present symptoms such as failure to swallow, breath, facial diplegia, and joint contractures. Life expectancy is usually not beyond the first weeks after birth [7].

SMA type 1, also called Werdnig–Hoffman disease, is the most frequent subtype of SMA, accounting for 50% of all cases. The most common genotype in SMA type 1 is a homozygous *SMN1* deletion in the presence of two functional copies of the *SMN2* gene. The disease becomes overt during the first months (usually within 4-5) of life, and infants do not reach basic developmental motor milestones, such as the ability to sit without assistance. In the absence of external intervention, death usually occurs within the second year of life. Patients with SMA type 1 can be further classified into three internal subgroups, with the mildest phenotype represented by type 1c, which is characterized by a certain degree of impairment of head and postural control [8, 9].

Patients with SMA type 1 display generalized muscular weakness with severe hypotonia, often displaying the floppy infant syndrome (ragdoll-like limpness). Infants can present a typical frog-leg position owing to hypotonia of proximal muscles. Impaired ribcage expansion can cause a bell-shape-like conformation of the thorax, with a relative sparing of the diaphragm. Deep-tendon reflexes can be decreased or absent. Difficulties in breathing and feeding are invariably present. Tongue fasciculation and weak cry are consequences of the involvement of bulbar motoneurons. High-level cognitive functions seem to be spared. Congenital heart defects with potential impairment of the cardiac autonomic innervation have been reported in severe SMA type 1 [10-12] suggesting a potential role of SMN protein in human cardiogenesis.

Onset of SMA type 2, also named Dubowitz disease, is usually 7–18 months after birth. Children with SMA type 2 are able to sit once properly positioned, and sometimes acquire the ability to stand even though they are unable to walk [13]. The most frequent clinical feature at onset is a delay in reaching developmental milestones for gross motor skills. Individuals with SMA type 2 have shortened life expectancy, which varies from 2 years to over 40 years.

Clinical presentation of SMA type 3, also known as Kugelberg–Welander disease, is highly variable. Onset of SMA type 3a is between 18 months and 3 years after birth, whereas

SMA type 3b typically becomes overt after 3 years of age. Children often maintain the ability to sit, stand, and ambulate at least until puberty, when many patients become unable to walk [14]. Patients present varying degrees of muscular hypotonia and weakness, with a preferential wasting of proximal muscle groups. Bulbar motoneuron involvement is less frequent than in more severe forms of SMA.

Type 4 SMA is characterized by a late onset. It is usually diagnosed after the second or third decade of life. Type 4 SMA is considered as adult-onset SMA and represents the mildest form of the disease. Although individuals with SMA type 4 can manifest signs of spinal motoneuron degeneration, such as flaccid hypotonia, fasciculations, muscular atrophy and decreased deep-tendon reflexes, the disease course is stable and mild. Patients remain able to ambulate throughout adulthood and their life expectancy is generally not shortened [15].

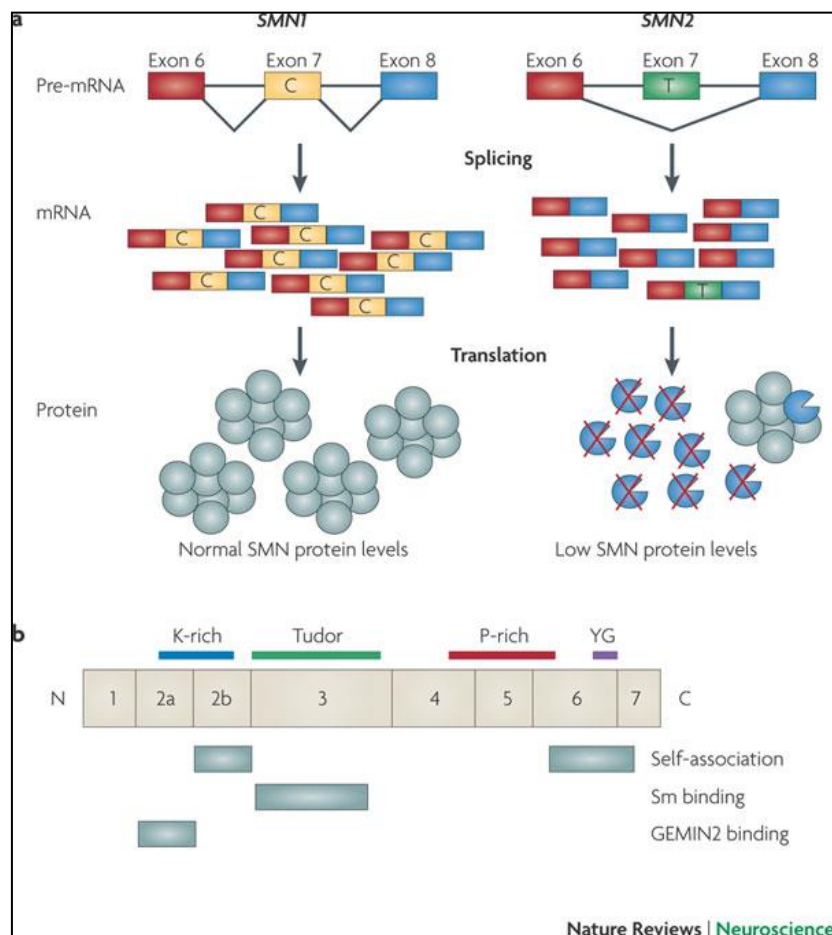


Figure 1: Genetics of SMA in humans.

- (a) Graphical representation of SMN genotype from control and SMN mutated individuals.
 (b) Graphical representation of corresponding SMN protein. The image was taken from [16]

Survival motor neuron (SMN) is a 38 kDa protein found both in the cytoplasm and nucleus of all cells [17-19]. An isoform of SMN comprising only the amino terminus (exons 1–3 and a part of intron 3) and found only in axons has also been reported [20]. However, this isoform is unlikely to have a role in SMA, as some patients with SMA carry missense mutation in exon 6 that would not alter this isoform's coding sequence [21]. Figure 1 describes the genetics of proximal SMA in humans. Protein derived from the *SMN2* gene is unstable and is not able to compensate for the loss of the *SMN1* gene, but multiple copies of the *SMN2* gene may modulate the disease severity [22].

Survival motor neuron genes *SMN1* and *SMN2* have an identical structure and are 99.9% identical at the sequence level. The essential difference between the two genes is a single-nucleotide change in exon 7 (C or T, as indicated in Figure 1). This single-nucleotide change affects the splicing of the gene, so most *SMN* transcripts from *SMN2* lack exon 7, whereas those from *SMN1* contain exon 7 [23-28]. *SMN2* produces full-length protein and therefore can be viewed as a gene with reduced function but not loss of function. However, the loss of the amino acids that are encoded by exon 7 results in the production of SMN protein with severely decreased oligomerization efficiency and stability [29, 30], and the SMN monomers are rapidly degraded [29]. In this way, loss of *SMN1* results in reduced SMN levels in most tissues. The SMN forms oligomer spanning dimer to octamer range based on gel filtration of SMN complexes formed *in vitro* [31]. Exon 2B encodes a domain that is important in binding Gemin2, as well as for self-association [32]. Both exon 2A and exon 2B are conserved. The K domain is rich in lysine (K-rich), and there is a Tudor domain in exon 3 that binds Sm proteins and has homology to other Tudor domains. Exon 5 and part of exon 6 contain a proline-rich (P-rich) domain that may influence profilin binding [33]. The C-terminal domain of exon 6 contains the conserved YG box and is important for self-association [32, 34].

3.2 Cellular functions of the SMN protein and model system.

SMN can be functional classified by its presence in two main cellular complexes based on four criteria, reciprocal immunoprecipitation of the endogenous forms, isolation of complexes containing SMN, colocalization of SMN and the protein in question and finally the complexes containing SMN-interacting proteins, which all should show a functional deficit upon SMN reduction. The best-characterized SMN complex is involved in small nuclear

ribonucleoprotein (snRNP) assembly [35-38]. Certain snRNPs are crucial for the recognition of splice sites and the catalytic removal of introns from pre-mRNA. snRNPs known to be assembled by SMN are composed of an U small nuclear RNA (snRNA) (U1, U2, U4, U5, U11 or U12) and, for those snRNPs involved in splicing, a heptameric ring of Sm proteins [39]. Although Sm proteins can self-associate onto snRNA *in vitro* [39], the SMN complex is required for this process *in vivo* [38, 40]. The SMN complex that performs this function in vertebrates consists of SMN, GEMIN2–8 and UNR-interacting protein (UNRIP, also known as STRAP). Their assembly reaction is ATP dependent [41-44].

SMN proteins secondly also play a major role in assembly of snRNPs. SMN has been called the master ribonucleoprotein (RNP) assembler. Many RNA-binding protein targets of SMN have RG and RGG domains. Of particular relevance are the Sm-like proteins (LSm proteins), hnRNP R [45-47], TDP-43 [48-50] and FUS/TLS [51]. A large number of these are mRNA-binding proteins implicated in multiple aspects of post-transcriptional gene regulation [52-57], including mRNA transport, stability and local translation in neurons. These RBPs bind SMN directly through their RG-rich domains in a methylation-dependent manner that is often disrupted by SMA-linked mutations of SMN [52-54, 58, 59]. In cultured neurons, SMN localizes with mRNA-binding proteins like hnRNP R, HuD, KSRP and IMP1 in axonal and dendritic granules that exhibit rapid, bidirectional movements [52-54, 58, 59]. These granules also contain other integral components of the SMN complex but not Sm proteins [57], suggesting a function for SMN unrelated to snRNP assembly. Importantly, SMN deficiency decreases localization of these RBPs and several associated transcripts in axons and growth cones of developing neurons [52, 60, 61]. Consistent with the requirement for local translation of mRNAs in neuronal pathfinding, these SMN-deficient neurons display reduced neurite length and smaller growth cones [52, 60, 61]. Altogether, these findings suggest that SMN may contribute to neuronal mRNA trafficking perhaps by facilitating the interaction of RBPs with their mRNA targets (Figure 2). Several SMN-associated RBPs are also involved in other aspects of mRNA regulation and associate with hundreds of transcripts, many of which contain AU-rich elements (AREs) in their 3'-UTRs that are key for the regulation of their turnover. One well investigated example is *Cdkn1a* mRNA, which is subject to antagonistic regulation by both KSRP [55] and HuD [59]. It accumulates upon SMN deficiency due to increased stability. This constitutes a particularly prominent event in SMA motoneurons [62]. Thus, SMN may play a role in the cytoplasmic turnover of transcripts such as ARE-containing mRNAs by modulating their association with RBPs (Figure 2). However, the molecular function(s) of SMN in the biology of mRNPs and other RNPs not described here is

unknown and awaits the development of specific assays to provide solid mechanistic insights into the full spectrum of SMN-mediated RNA regulation.

SMN has also been suggested to be important for the assembly of small nucleolar ribonucleoproteins (snoRNPs) [25, 63], and knockdown of SMN alters the level of U3 small nucleolar RNA (snoRNA) [64]. In snoRNPs, the snoRNA acts as a guide for the modification (methylation or pseudouridylation) of ribosomal RNA, tRNA and snRNA [65]. It remains to be explained how the loss of the ubiquitously expressed SMN protein which is a spliceosome assembling component in all cell types, can be responsible for a specific degeneration of motoneurons. To address this questions, various model systems have been generated and studied in detail [66]. The homozygous deletion of SMN in mice is embryonic lethal [67], but heterozygous knockdown mice (*Smn*^{+/-}) are useful as a model for less severe forms of the disease. Two mouse lines, *Smn*^{-/-};*SMN2Tg* [68, 69] and *Smn* Δ 7(*SMN2*^{+/+};*Δ7*^{+/+};*Smn*^{-/-}) [70], have been widely used as model for the most severe form of type I SMA. Studies done on cultured embryonic motoneurons have indicated that SMN has additional motoneuron specific roles [71]. RNA binding protein hnRNP R was found as interaction partner of SMN by yeast two-hybrid screen [47]. *Smn*^{-/-};*SMN2Tg* isolated motoneurons show shorter axon length when cultured on laminin111. In addition, overexpression of hnRNP R in a SMN deficient condition rescues the axon length [46] and also SMN hnRNP R association with β -actin mRNA. Reduced level of hnRNP R shows reduced level of β -actin mRNA in isolated motoneurons.

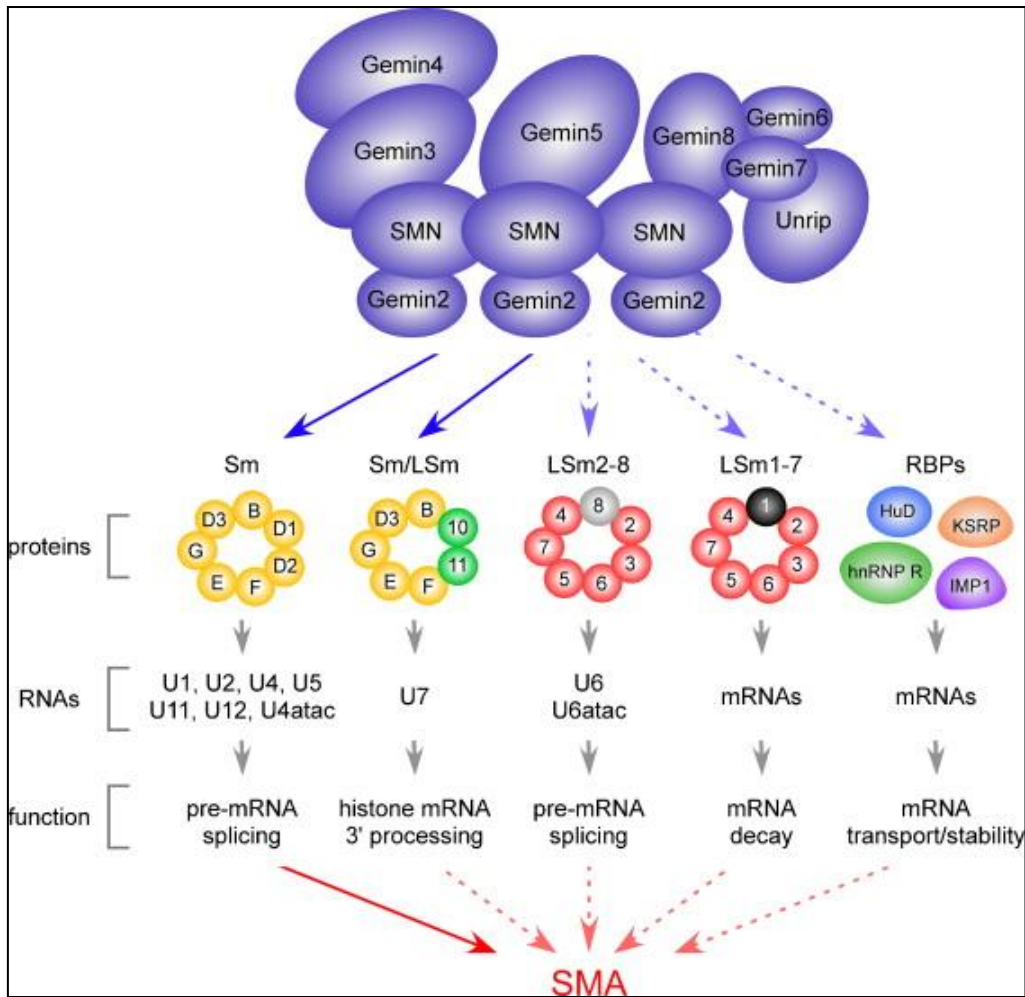


Figure 2: SMN-dependent RNP assembly pathways and their link to SMA.

The SMN complex—depicted with known integral subunits according to [72] and the protein and RNA components of each of its proposed RNP targets are shown above the RNA pathway in which they function. Solid arrows indicate connections that are established both molecularly and functionally. The image was taken from [73].

Morpholino based knockdown of hnRNP R in zebrafish embryos showed increased branching and shorter motor axons [45]. β -actin mRNA was found to be enriched in the growth cones of cultured embryonic motoneurons isolated from the spinal cords of *Smn*^{+/+};*SMN2* mice, whereas there was significant decrease in the β -actin mRNA in the growth cones of motoneurons isolated from *Smn*^{-/-};*SMN2Tg* mice as seen by in situ hybridization against β -actin mRNA, indicating that the SMN protein may be involved in the transport of the β -actin mRNA. There is reduction in the size of the growth cones of *Smn*^{-/-};*SMN2Tg* motoneurons and also defective calcium channel clustering in growth cones [45, 46, 71, 74].

3.3 Clinical phenotype and genetic basis of amyotrophic lateral sclerosis.

Amyotrophic Lateral Sclerosis (ALS) is the most prevalent late-onset motoneuron disorder worldwide. It is a progressive disease generally affecting patients aged 45–75 years, and primarily targets, fast-fatigable cortical and spinal motoneurons [75]. The disease is found worldwide, with a prevalence of roughly 3-5 per 100,000 individuals. Onset of symptoms is usually in the fourth or fifth decade of life with about 10% of the cases beginning before the age of 40 and less than 5% before the age of 30 [76]. Common clinical features of ALS include muscle weakness and wasting, followed by paralysis [77]. The disease progresses rapidly with a mean survival of three years after diagnosis. Respiratory failure, due to respiratory muscle paralysis, is the primary cause of patient death [77, 78].

ALS causes neural degeneration, neurite shortening and cell death, eventually resulting in fatal paralysis [79-82]. The majority of patients represent seemingly sporadic ALS [83]. Only 5–10% of patients have a familial history of the disease and usually of autosomal dominant inheritance [84, 85]. However, these groups remain symptomatically indistinguishable. The clinical presentation of ALS may differ depending on the extent of involvement of each type of motoneuron. The classical form of ALS involves primarily the upper motoneurons and the lower motoneurons that innervate the limbs. ALS is characterized depending on the stage of disease. At early stages, hyperactive reflexes and spasticity more predominant as at late stages. Muscle weakness, muscle wasting, and fasciculation which often predominate in the lower limbs, as well as by hyperactive tendon reflexes, spasticity, which often predominate in the upper limbs (also referred as Hoffman and Babinski signs) [75, 76, 86-88].

Likewise, all genes associated with familial ALS have also been found mutated in sporadic ALS (Table 1). The central pathological hallmark of ALS is the presence of cytoplasmic inclusions or aggregates in degenerating motoneurons and surrounding astrocytes [89]. Inclusions are not restricted to the spinal cord but are also present in other brain regions such as the frontal and temporal cortices, hippocampus and cerebellum [90-92]. The predominant aggregates found in ALS patients are ubiquitinated aggregates that are classified as either Lewy body-like hyaline inclusions or skein-like inclusions. At the ultrastructural level, Lewy body-like or skein-like inclusions appear as randomly oriented filaments covered by fine granules [93, 94]. Additional subclasses of aggregates found in ALS are bunina bodies, which are small eosinophilic ubiquitin-negative inclusions [95, 96] and round hyaline inclusions without a halo. Bunina bodies consist of amorphous electron-dense material

surrounded by tubular and vesicular structures [95, 96]. Furthermore, neurofilamentous inclusions are found in the axonal hillock in close proximity to ubiquitinated inclusions. Other cellular abnormalities include the presence of mitochondrial vacuolization [97], fragmentation of the Golgi apparatus [98, 99] and abnormalities at the neuromuscular junction [100]. In 1993, SOD1 (Superoxide dismutase 1) was the first protein to be identified to be mutated in familial ALS (FALS) cases carrying a mutation in the *SOD1* gene [101]. Later, mutations in *VAPB* (Vesicle-associated membrane protein-associated protein B) were also shown to cause ALS in a group of FALS patients [102]. Due to exponential development of genetic techniques, several new proteins have been identified to be involved in ALS pathophysiology during the past few years, including TDP-43 [103], FUS [104, 105], OPTN [106], UBQLN2 [107], Senataxin [108] and Alsin [109]. Recently, a gene defect in the C9ORF72 region leading to hexanucleotidic G2C4 repeats expansion was identified as the most common mutation in both familial (38%) and sporadic ALS (7%) [110, 111].

Table 1: Genes associated with familial ALS.

Genetic subtype	Chromosomal locus	Gene	Onset/inheritance	Reference
<i>Oxidative stress</i>				
ALS1	21q22	Superoxide dismutase 1 (<i>SOD1</i>)	Adult/AD	Rosen (1993)
<i>RNA processing</i>				
ALS4	9q34	Senataxin (<i>SETX</i>)	Juvenile/AD	Chen et al. (2004)
ALS6	16p11.2	Fused in sarcoma (<i>FUS</i>)	Adult/AD	Kwiatkowski et al. (2009)
				Vance et al. (2009)
ALS9	14q11.2	Angiogenin (<i>ANG</i>)	Adult/AD	Greenway et al. (2006)
ALS10	1p36.2	TAR DNA-binding protein (<i>TARDBP</i>)	Adult/AD	Sreedharan et al. (2008)

<i>Endosomal trafficking and cell signaling</i>				
ALS2	2q33	Alsin (<i>ALS2</i>)	Juvenile/AR	Yang et al. (2001)
ALS11	6q21	Polyphosphoinositide phosphatase (<i>FIG4</i>)	Adult/AD	Chow et al. (2009)
ALS8	20q13.3	Vesicle-associated membrane protein-associated protein B (<i>VAPB</i>)	Adult/AD	Nishimura et al. (2004)
ALS12	10p13	Optineurin (<i>OPTN</i>)	Adult/AD and AR	Maruyama et al. (2010)
<i>Glutamate excitotoxicity</i>				
ND	12q24	d-amino acid oxidase (<i>DAO</i>)	Adult/AD	Mitchell et al. (2010)
<i>Ubiquitin/protein degradation</i>				
ND	9p13–p12	Valosin-containing protein (<i>VCP</i>)	Adult/AD	Johnson et al. (2010)
ALSX	Xp11	Ubiquilin 2 (<i>UBQLN2</i>)	Adult/X-linked	Deng et al. (2011)
<i>Cytoskeleton</i>				
ALS– dementia –PD	17q21	Microtubule-associated protein tau (<i>MAPT</i>)	Adult/AD	Hutton et al. (1998)
<i>Other genes</i>				
ALS5	15q15–q21	Spatascin (<i>SPG11</i>)	Juvenile/AR	Orlacchio et al. (2010)
ALS–	9p13.3	σ Non-opioid	Adult/AD	Luty et al. (2010)

FTLD		receptor (<i>SIGMAR1</i>)	1	Juvenile/AR	Al-Saif et al. (2011)
ALS– FTLD	9q21–q22	Chromosome 9 open reading frame 72 (<i>C9ORF72</i>)		Adult/AD	Hosler et al. (2000)
					Renton et al. (2011)
					De Jesus-Hernandez et al. (2011)
<i>Unknown genes</i>					
ALS3	18q21	Unknown		Adult/AD	Hand et al. (2002)
ALS7	20ptel–p13	Unknown		Adult/AD	Sapp et al. (2003)
Abbreviations: AD, autosomal dominant; ALS, amyotrophic lateral sclerosis; AR, autosomal recessive; FLTD, fronto-temporal dementia; PD, Parkinson disease.					

TAR DNA-binding protein 43-kDa (TDP-43), encoded by the TARDBP gene on chromosome 1, is a major component of tau-negative and ubiquitin-positive inclusions that characterize amyotrophic lateral sclerosis (ALS) and fronto-temporal lobar degeneration (FTLD) linked to TDP-43 pathology (FTLD-TDP) [103]. TDP-43 aggregation and neuropathology have been observed in a spectrum of distinct neurodegenerative disorders collectively known as the TDP-43 proteinopathies, suggesting a central role for TDP-43 in neurodegenerative disease pathogenesis [112]. Indeed, the identification of more than 35 missense mutations in the TARDBP gene has further implicated abnormal TDP-43 function as a cause, rather than a consequence of neurodegeneration in ALS and FTLD-TDP [113, 114]. TDP-43 is predominantly nuclear in normal tissues, in disease TDP-43 is mislocalized to the cytoplasm, ubiquitinated, and hyperphosphorylated. TDP-43 is the prototype of this type of pathological process, but there are other RNA binding proteins fused in sarcoma/translocated in liposarcomas (FUS/TLS) and other heterogeneous nuclear ribonucleoproteins (hnRNPs) that are also mutated or aggregated in diseased brains. Like TDP-43, they are involved in the general control of mRNA processing steps. TDP-43 was initially described as a transcription factor [114]. However, the roles played by TDP-43 have rapidly expanded to include regulation of splicing [115], mRNA stability (including its own) [116], microRNA processing [117], mRNA transport and translation [118]. Dysregulation of

many of these processes might precede or follow the aberrant aggregation and modification of TDP-43 in affected cells. The discovery that mutated TDP-43 is involved in neurodegeneration, followed closely by similar findings for FUS/TLS and C9ORF72, have opened up the entire field of RNA binding proteins (RBPs) and RNA metabolism as a new and promising area of research in neuroscience.

Dominant mutations in the *TARDBP* gene encoding TDP-43 account for up to 4% of familial ALS cases and *de novo* mutation of TDP-43 causes approximately 1% of sporadic ALS [119]. TDP-43 contains a nuclear localization signal (NLS), a nuclear export signal (NES) and two RNA-recognition motifs (RRM1 and RRM2) (Figure 3A). Of these, RRM1 is essential for RNA binding, whereas RRM2 may mediate interactions with ssDNA and TDP-43 self-association [120, 121]. TDP-43 shows a clear preference for binding to (UG)_n repeat sequences in target RNA sequences [122, 123]. TDP-43 binds to a minimum of six single-stranded dinucleotide stretches, and binding affinity increases with the number of repeats through the highly conserved phenylalanine residues in RRM1 [120]. In addition to the RRM1, TDP-43 contains an unstructured carboxyl-terminal Gly-rich domain, in which all but one of the 32 identified ALS mutations has been identified. The Gly-rich domain mediates an ever-growing number of interactions between TDP-43 and proteins implicated in various aspects of RNA splicing and RNA metabolism [112]. This domain also contains a Q/N-rich prion-like element that mediates its aggregation with polyQ aggregates [124] [125]. Finally, cellular TDP-43 migrates as multiple complexes on size exclusion media, suggesting that distinct roles of TDP-43 may be carried out by different protein-protein interactions [126].

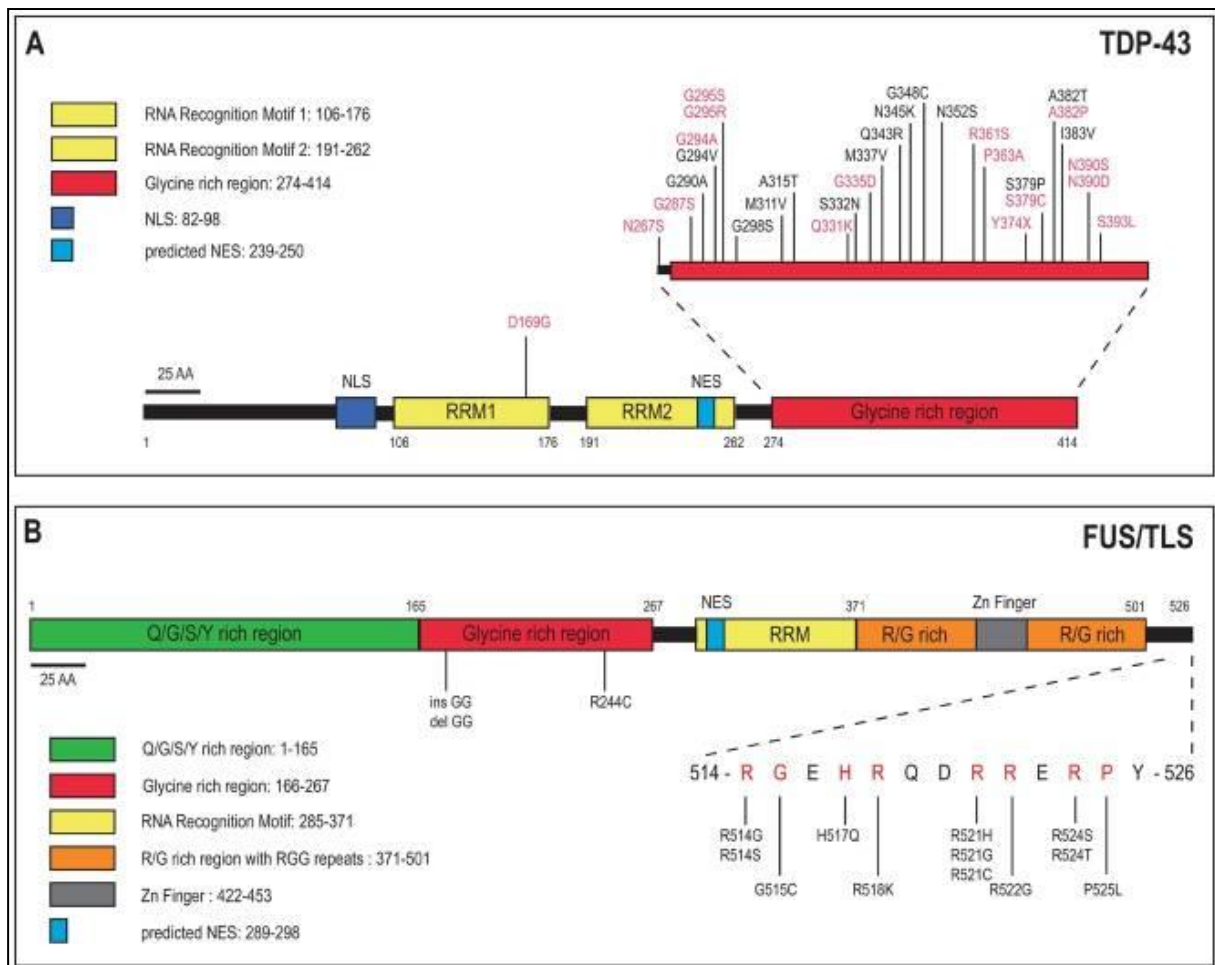


Figure 3: TDP-43 and FUS/TLS mutations in ALS.

(A.) Twenty dominant mutations in TDP-43 have been identified in sporadic (red) and familial (black) ALS patients, with most lying in the C-terminal glycine-rich region. All are missense mutations, except for the truncating mutation TDP-43Y374X. RRM1 and RRM2: RNA recognition motifs; NLS, nuclear localization signal; (NES), predicted nuclear export signal. (B.) Fifteen mutations have been identified in FUS/TLS in familial ALS cases, with most lying in the last 13 amino acids of the 526 amino acid protein. (Q/G/S/Y rich), an amino terminal region rich in serine, tyrosine, glutamine and glycine residues; (RRM) a RNA recognition motif (RRG), an arginine and glycine rich region with several RGG repeats; (NES), a predicted nuclear export signal. The image was taken from [127].

Mutations in the *FUS* gene have been described in ~4% of familial ALS cases and, more rarely, in cases with apparently sporadic etiology [104, 105]. *FUS* is predominantly localized to the nucleus, with established functions in transcription, mRNA splicing and transport, and gene silencing. *FUS* harbors a single centrally located RRM and a Gly-rich domain, which lies just amino-terminal to the RRM (Figure 3B). *FUS* also contains an amino-terminal ~160-amino acid S/Y/Q/G domain rich in Ser, Tyr, Gln, and Gly amino acids, three RGG domains rich in Arg and Gly residues that are also implicated in RNA binding, and a zinc finger domain that binds to GGUG RNA sequences [128, 129]. The vast majority of ALS

associated mutations in FUS are missense substitutions occurring in the Gly-rich, RGG, or NLS motifs.

TDP-43 binding is enriched in long intronic regions, the 3'UTR of pre-mRNA, and nuclear non-coding (nc) RNAs. The strong preference of TDP-43 for (UG)_n repeat motifs was confirmed in different studies [123]. However, UG repeats were neither necessary nor sufficient for binding [130]. The binding of TDP-43 to intronic sequences correlated positively with expression and suggested that this could reflect a role for TDP-43 in suppressing cryptic splice site expression and aberrant splicing. In addition, binding of TDP-43 to deep intronic regions upstream of an alternatively spliced exon promotes its exclusion, whereas binding of TDP-43 to proximal intronic sequences downstream of the alternatively spliced exon promotes its inclusion [123, 130]. Finally, binding of TDP-43 to 3'UTR sequences was enriched in the cytoplasm, which is consistent with the notion that TDP-43 regulates RNA post-splicing events such as stabilization and translation [123].

These interaction studies identified 7,000 protein-coding RNA substrates for TDP-43 [131, 132]. Within this list are many RNAs involved in neuronal development, neuronal survival, and synaptic transmission. TDP-43 splicing targets include myocyte enhancer factor 2D (MEF2D), myocardial infarction associated transcript (MIAT), and Bcl-2 interacting mediator of cell death (BIM) [123]. Interestingly, a number of TDP-43 RNA targets are directly implicated in neurodegeneration. These include FUS as well as the secreted growth factor progranulin, hemizygous mutations in which cause FTL [133, 134]. TDP-43 binds to introns 6 and 7 and the 3'UTR of FUS mRNA to enhance its expression, whereas TDP-43 binding to the 3'UTR of progranulin mRNA was associated with reduced expression [130]. Additionally, Tau and ataxin-1 and -2 were also identified as TDP-43 target mRNAs [123], though the functional implication of these interactions is not yet clear.

TDP-43 also negatively regulates its own expression by binding to the 3'UTR [116, 123, 135]. Ectopic expression of TDP-43 represses the expression of endogenous TDP-43, potentially through an alternative splicing event that produces a variant TDP-43 mRNA that is eliminated through nonsense mediated mRNA decay [130]. However, another report suggested that TDP-43 autoinhibition occurred independent of splicing [116]. Disruption of TDP-43 autoinhibition could lead to feed-forward mechanisms of TDP-43 proteinopathy, in which accumulation of aggregated cytosolic TDP-43 reduces TDP-43 splicing, leading to increased cytosolic mRNA translation, and further TDP-43 aggregation. Such a mechanism plausibly explains the nuclear clearing of TDP-43 that is observed in motoneurons of ALS

patients and animal models [136]. Future studies will likely focus on the role of TDP-43 autoinhibition in ALS, as well as the effects of ALS-associated mutations on TDP-43 splicing activity.

3.4 **Discovery of C9ORF72 mutations.**

The identification of aberrant GGGGCC (G4C2) intronic repeat expansions in the *C9ORF72* gene as the most common genetic cause of ALS and FTLD has reinforced the relation between ALS and FTLD [110, 111, 137, 138]. In normal individuals the number of repeat expansion were found to range from two to twenty three, whereas *C9ORF72* patients carried from sixty to hundreds of G4C2 repeats [138, 139]. Observations of population frequencies of the expansion are consistent with a common founder effect. In Finland *C9ORF72* expansions were found in 61% of patients with FALS (familial ALS) and in 19% of patients with SALS (sporadic ALS) [138]; however, further away from Scandinavia the expansion frequency decreases. In northern England *C9ORF72* expansions are present in 43% of patients with ALS with an identifiable family history and in 7% of apparently sporadic cases [140]. In Germany 22% of patients with FALS (familial ALS) carry the expansion [138], but in Japan the equivalent figure is only 3.4% [141, 142]. In North America the frequency of the *C9ORF72* expansion appears to be comparable with European populations: It is reported that 36% of patients with FALS and 6% of patients with SALS carry the expansion [138]. It is not new that repeat expansion cause hereditary diseases [143], but present research evidence has not provided a clear correlation of disease onset with G4C2 repeat expansion.

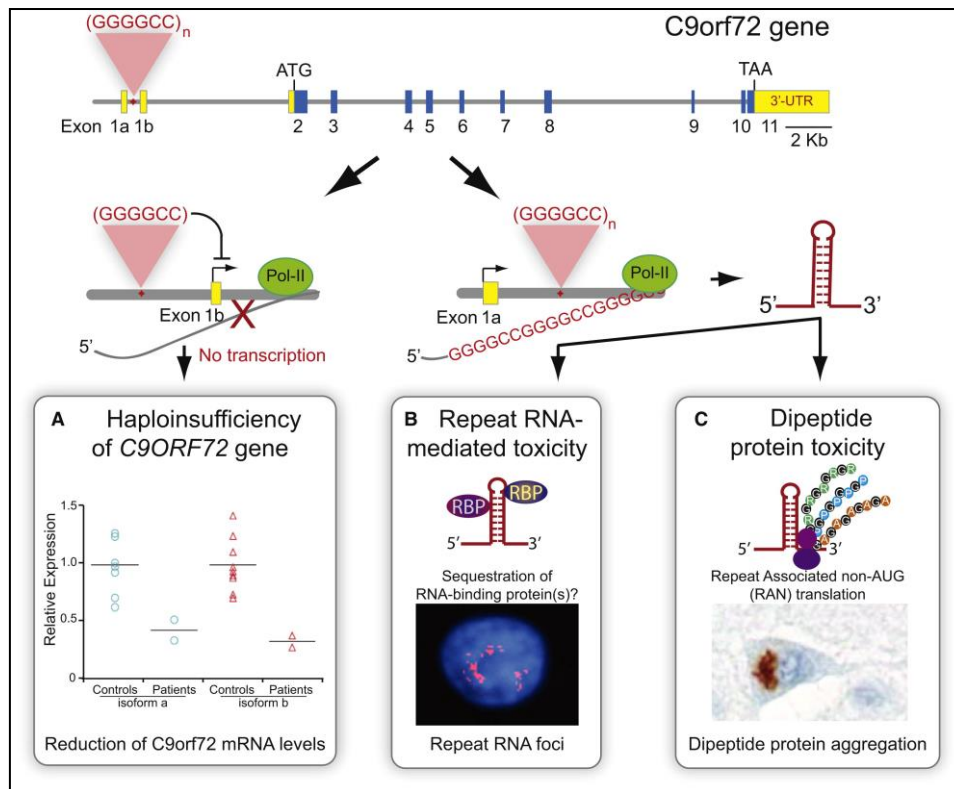


Figure 4: Pathogenic mechanisms for G4C2 repeat expansion.

Top: Schematic representation of the human C9ORF72 gene (yellow, UTRs; blue, coding exons). The hexanucleotide (GGGGCC) repeat expansion is located between alternative exons 1a and 1b. At least three mechanisms may contribute to disease pathogenesis: (A) GGGGCC repeat expansions may lead to reduced expression of the allele containing the repeat expansion (haploinsufficiency); (B) RNA foci containing transcribed GGGGCC repeats may sequester RNA-binding protein(s); or (C) repeat associated non-AUG (RAN) translation of GGGGCC repeat-containing RNA produces toxic polypeptides in each of three reading frames. The image was taken from [144].

3.5 Pathogenic mechanism of the C9ORF72 repeat expansion.

Recent studies have shown that stabilized RNA foci are formed from transcription of GGGGCC repeats in the sense and the antisense direction [145-147]. The relative importance of sense and antisense species for the pathophysiology of neuronal injury remains to be determined. The observations of transcribed repeats have a bearing on the formation of dipeptide repeat proteins (DPRs), as this requires inappropriate nuclear export to allow the RNA to access the translation machinery. Indeed, cytoplasmic RNA foci have been observed in CNS neuronal populations, including motoneurons [146, 148]. It has been shown that sense-RNA foci interact directly with export adaptors, including Aly/REF export factor (ALYREF) [148], which might help in the repeat RNA for export to the cytoplasm. If DPRs are toxic, this represents an attractive therapeutic target.

Considering the possibility that RNA species transcribed from hexanucleotide repeat are toxic, it has been suggested that the sense and antisense transcripts might form inappropriate double-stranded species, which could initiate apoptosis [149]. Recent data suggest that denaturation and renaturation of the GGGGCC repeats in the presence of its antisense complementary sequence produces a relatively small proportion of double-stranded RNA [150]. This study reports observations on the formation by the GGGGCC repeat sequence of unimolecular stabilized G-quadruplexes where bases are not readily available for Watson–Crick pairing. These observations were supported by other studies suggesting that the sense RNA exists in equilibrium between 2 possible conformations: a hairpin loop and a G-quadruplex [147, 151].

The second hypothesis inferred from other repeats expansion disorders [152, 153] led to the search for and the discovery of dipeptide repeat proteins (DPRs) in *C9ORF72* disease [154]. The long repeat is translated into protein in all three possible reading frames of the RNA, poly-(Gly-Ala), poly-(Gly-Pro), and poly-(Gly-Arg). Following the description of antisense transcription of the repeat sequence two distinct further proteins were identified corresponding to the three antisense reading frames, poly-(Ala-Pro) and poly-(Pro-Arg) [155]. It is proposed that translation is initiated directly by the repeat expansion, as has previously been observed by non-ATG translation (RAN translation) [153]. It was shown in spinocerebellar ataxia 8, a disorder caused by a CAG repeat expansion of the ataxin 8 gene, that translation of the repeat sequence occurred independently of the presence of an ATG site [153]. These dipeptide repeat proteins aggregate and form preferentially in affected brain regions [154]. DPRs appear to be toxic in cell and animal models [156-158].

C9ORF72-related ALS is a TDP-43 proteinopathy, which is common with most other subtypes of ALS, with the exception of *SOD1*-related ALS [159]. What is currently unclear is how the mislocalization of TDP-43 from the nucleus to the cytoplasm in all these cases contributes to motoneuron death. However, evidence suggests that the toxicity is most likely due to dysregulation of RNA processing and protein homeostasis, specifically impairment of the ubiquitin proteasome system, the unfolded protein response, and autophagy, rather than TDP-43 aggregates themselves being toxic [160]. Interestingly, p62, which is an autophagy receptor protein encoded by *SQSTM1*, not only co-localizes with TDP-43 aggregates in the brain and spinal cord of *C9ORF72*-related cases, but also with the TDP-43 negative, ubiquitin-positive inclusions, which have been observed to contain DPRs, in the extra motor

regions of the brain [161]. Thus, dysregulated protein homeostasis appears to be a common feature of *C9ORF72*-related ALS and other subtypes of ALS.

Another hypothesis is that the expansion of repeats leads to haploinsufficiency of *C9ORF72* expression. Reduced expression of *C9ORF72* mRNA has been reported in the presence of the expansion [110]. A study using a newly generated *C9ORF72* antibody suggests that there is reduced expression of the *C9ORF72* protein in the frontal cortex, but not in the cerebellar cortex of *C9ORF72* expansion carriers [162]. It has been observed that small expansions of approximately 50 repeats do not reduce *C9ORF72* transcription [163], possibly because smaller expansions do not lead to hypermethylation of a CpG island 5' to the repeat sequence in the promoter region [164, 165]. A number of other mechanisms have been proposed for haploinsufficiency: Trimethylation of histones H3 and H4 has been reported in *C9ORF72* expansion carriers and linked to increased binding of these histones to the repeat sequence with consequent reduced expression of *C9ORF72* [166]. Finally, biochemical analysis has suggested that formation of expanded *C9ORF72* DNA and RNA into hybrid R loops may also contribute to abortive transcription [147].

As all three hypotheses are supported by strong scientific evidence, it is unclear whether the mutation leads to partial loss of function, a gain of function or both. It has to be noted that *C9ORF72* patients with repeat expansion show 50% reduction in mRNA level in both long and short forms of the transcript [110, 137]. With these observations one could conclude that basic information on the actual function of the protein is very vital.

3.6 Current model systems to study *C9ORF72* functions.

Recent publications show that reduction of *C9ORF72* levels in both cortical and motoneurons does not affect neuronal survival *in vitro* [167] and *in vivo* [168] but causes reduced axon length of motoneurons and locomotion defect in zebrafish by antisense oligonucleotide-mediated reduction of *C9ORF72* protein [139]. In contrast to the results in *C. elegans* and zebrafish, studies in mouse have so far not supported a role for *C9ORF72* loss of function as a cause of FTL/ALS. Administering antisense oligonucleotides (ASOs) targeting mouse *C9ORF72* by stereotactic intracerebroventricular (ICV) injection reduced *C9ORF72* mRNA levels to 30-40% of control levels in the spinal cord and brain [145]. This effect appeared long-lived and *C9ORF72* levels remained lowered even several months after the initial ASO injection. *C9ORF72* depletion in these mice was well tolerated and did not result

in any behavioural or motor impairment. Cytoplasmic aggregation of ubiquitinated TDP-43 is the hallmark pathological feature of FTLD and ALS, including c9FTLD/ALS. TDP-43 remained nuclear in brain and spinal cord sections and ubiquitinated aggregates were not detected in mice with C9ORF72 depletion [145]. Thus, reducing C9ORF72 levels by over 50% in the nervous system for several months does not result in neuropathological or behavioral phenotypes. A conditional allele of C9ORF72 was generated using the Cre/loxP system. These mice were crossed to Nestin-Cre mice, which express Cre recombinase in neurons and glia starting at E10.5 and continuing into adulthood [169]. Cre-mediated inactivation of C9ORF72 in neurons and glia did not cause loss of motoneurons or motor function, including motor performance and grip strength [170]. Hallmark ALS pathologies, including ubiquitinated TDP-43 aggregates and gliosis were not detected either. There was no effect on survival even after 24 months. Thus, in two different mouse models, loss of C9ORF72 function is not sufficient to cause neurodegeneration and FTLD/ALS-related phenotypes.

Two studies of human c9FTLD/ALS have provided evidence arguing against a loss of function disease mechanism. First, if hexanucleotide repeat expansion mutations in C9ORF72 cause FTLD/ALS by a loss of function mechanism, then other ways to disable C9ORF72 function could also be a cause of disease. However, an analysis of the *C9ORF72* gene in several hundred ALS patients did not identify deleterious mutations in the coding region of C9ORF72 (including nonsense and frame shift mutations) [171]. Second, since a heterozygous C9ORF72 mutation is sufficient to cause FTLD/ALS, homozygous mutations might be predicted to cause a more severe form of the disease or even a different clinical presentation. However, an analysis of a patient homozygous for the C9ORF72 hexanucleotide repeats expansion revealed severe clinical and pathological features that were in the normal disease spectrum seen in heterozygous patients [172]. These two studies, while certainly not definitive, are not consistent with a loss-of-function mechanism.

Finally, studies in patient cells have provided somewhat of a formal test for the loss-of-function vs. gain-of-function hypotheses. Several studies have used RNA profiling to characterize gene expression changes associated with C9ORF72 mutations. These studies have included fibroblasts [145], iPS-derived neurons [173], iPS-derived motoneurons [174], and human brain tissue samples [175]. Each study uncovered a mutant-specific RNA signature in C9ORF72 mutant carriers which was not present in healthy controls. If these alterations in gene expression were caused by a loss of C9ORF72 function, then lowering

levels of C9ORF72 (e.g., by targeting expression with ASOs) would be predicted to either worsen or have no effect on the RNA signature. However, the studies in iPS neurons and the iPS-derived motoneurons revealed that targeting C9ORF72 with ASOs actually improved the signature rather than worsening it [173, 174]. Further, lowering C9ORF72 in control cells did not recapitulate the RNA signature [145, 174]. These results are not consistent with C9ORF72 mutations causing a loss of function. Lowering levels of C9ORF72 in *C. elegans* and zebrafish appears deleterious, whereas conditional inactivation of the gene specifically in motoneurons and glia in mouse does not affect motoneuron function or survival. Several additional studies will be useful to help resolve these discrepancies. The nestin-Cre deletion of murine *C9orf72* may not have removed the gene in a sufficient number of cells or in all of relevant cells and tissues. Indeed, both human C9ORF72 and the mouse homolog (*3110043O21Rik*) are expressed most highly in microglia and macrophages in the brain [176, 177]. Thus, it will be important also to consider potential non-cell-autonomous mechanisms of neurodegeneration.

A germline knockout of C9ORF72 would allow for the analysis of heterozygous and homozygous mutant animals constitutively lacking C9ORF72 expression. Mice have been generated in which the β -galactosidase gene replaces exons 2–6 of one of the C9ORF72 alleles [178]. Recent study have used gene targeting to generate homozygous mutant mice and extensively analysed them for any effects on survival and cognitive or motor behavioural impairments [179, 180]. These mice did not develop motoneuron disease but instead developed splenomegaly and several other peripheral pathologies, including marked expansion of myeloid cells and deficits in immune responses and microglial function [179, 180]. The neuroinflammation seen in these mice is reminiscent of that in human patient tissue. Thus, while these data suggest that loss of C9ORF72 function per se is unlikely sufficient to cause motoneuron disease, its requirement for proper microglia function could suggest a possible way that its loss could contribute to disease progression, similar to what is seen in mouse models of familial ALS caused by SOD1 mutations [181, 182].

The use of viral-mediated and BAC transgenic c9FTLD/ALS models [180, 183, 184] as another formal test of loss- vs. gain-of-function involves the use of C9ORF72 knockout mice. These models employ expression of human C9ORF72 transgenes harbouring various GGGGCC repeat lengths either via adeno-associated virus mediated somatic transgenesis [183] or in transgenic mice generated from a bacterial artificial chromosomes (BAC) that expresses a fragment of human C9ORF72 containing an expanded hexanucleotide repeat

[184] or the full length C9ORF72 gene harboring an expanded repeat [180]. These mice exhibit various phenotypes and pathological features reminiscent of c9FTLD/ALS [180, 183, 184]. Breeding these mice to C9ORF72 knockout mice (heterozygous and homozygous) or injecting the C9ORF72 transgene into the central nervous system of the knockout animals will help to obtain information on whether disease features occur or are delayed by the reduction of wild type C9ORF72. Similar approaches have been used to support a gain-of-function toxicity mechanism caused by SOD1 mutations in familial ALS [185].

3.7 The current state of knowledge on the function of C9ORF72.

The normal function of C9ORF72 still remains poorly understood. Experiments to define this function will facilitate the study of how alterations in that function might contribute to disease. C9ORF72 protein has homology to the Differentially Expressed in Normal and Neoplasia (DENN) protein family, which function as guanine nucleotide exchange factors (GEFs) to regulate Rab GTPase activity [186, 187]. Rab GTPases act as molecular switches to orchestrate multiple steps of membrane trafficking within cells [188]. It will be important to define which type of Rab C9ORF72 regulates since this will provide insight into the particular trafficking step and cellular location (e.g., endosomes, lysosomes, Golgi, etc.) where it likely functions.

Assays to measure these trafficking steps in cells from c9FTLD/ALS patients will help to test for C9ORF72 loss of function effects. Rab GTPases regulate several steps of membrane trafficking within the cell, and Rab GEFs, by facilitating the exchange of GDP with GTP, activate their Rab targets [189]. In Neuro2a cells, SH-SY5Y cells, and mouse primary cortical neurons, C9ORF72 was reported to show a diffuse nuclear localization with a punctate cytoplasmic pattern reminiscent of vesicles. These presumed vesicles were also detected in spinal motoneurons of healthy individuals and C9-ALS cases, supporting a role for C9ORF72 in membrane trafficking [190]. Indeed, C9ORF72 was found to co-localize and immunoprecipitate with several Rabs, including the endocytic Rab5 and Rab7, and the autophagy-related Rab1 and Rab11, in both cultured neuronal cell lines and primary cortical neurons [190]. Co-localization of C9ORF72 with Rab7 and Rab11 was also seen in human spinal motoneurons from healthy subjects [190], and this co-localization was seen in an increased proportion of cells in the spinal cord of a repeat expansion-positive ALS patient, although the meaning of this finding is unclear.

The knockdown of C9ORF72 by siRNA in neuronal cell lines resulted in a decrease in endocytic trafficking, as well as a disruption in autophagosome formation [190]. Therefore, although additional studies are needed to verify that C9ORF72 is indeed a Rab GEF, these data strongly support the hypothesis that C9ORF72 plays a role in endosomal and autophagy-related trafficking. Interestingly, mutations in Rab7 are associated with Charcot- Marie-Tooth disease [191], a motor and sensory neuropathy, and the gene mutated in ALS2, a recessive juvenile form of ALS, encodes a Rab5 GEF [192]. Together, these findings implicate a defect in endosomal and autophagy- endolysosomal trafficking in motoneuron disease and suggest that if a decrease in C9ORF72 expression dysregulates these cellular pathways, it could perhaps contribute to or modulate pathology in C9-FTLD/ALS. More detailed future studies could elucidate this possibility.

A new direction in our understanding of C9ORF72 nucleotide repeat expansion pathophysiology came from four independent studies [193-196] that implicated dysfunctional nucleocytoplasmic trafficking as a key event in C9ORF72 ALS/FTLD (Figure 5). In the first study, a large interactome screen showed that (G4C2) RNA interacts with RanGAP1, a GTPase-activating protein that stimulates the hydrolysis of RanGTPase (Ran) [173, 195].

Ran is necessary for the active transport of proteins that contain a classical nuclear localization sequence. RanGAP1 was shown to be a potent genetic modifier (suppressor) of a neurodegenerative phenotype (rough eye) in (G4C2)₃₀-expressing *D. melanogaster* [195]. C9ORF72 ALS iPSC-derived neurons and *D. melanogaster* C9ORF72 nucleotide repeat expansion models exhibited a disrupted Ran gradient [195] and showed reduced localization or sluggish fluorescent recovery after photobleaching (FRAP) for nuclear localization sequence containing reporter molecules, implying that there are deficits in nuclear protein import [195] and disruption of functional nucleocytoplasmic transport. Indeed, TDP43, which contains a classical nuclear localization sequence, was slightly enriched in the cytoplasm of C9 ALS iPSC neurons [195]. Genetic crosses and therapeutics designed to modify nucleocytoplasmic trafficking and enhance protein import or reduce nuclear export rescued the (G4C2)-mediated rough eye phenotype [195]. ASOs targeting the NRE sense strand rescued the nuclear transport deficits and were neuroprotective against the rough eye phenotype in the *D. melanogaster* model and rescued the Ran gradient and reduced cytoplasmic TDP43 localization in ALS iPSC neurons [195]. Notably, in these studies, the flies expressed only the sense strand RNAs and DPRs were undetectable during the time of neurodegeneration, suggesting that the observed deficits were primarily caused by nucleotide repeat expansion sense strand (G4C2) RNA.

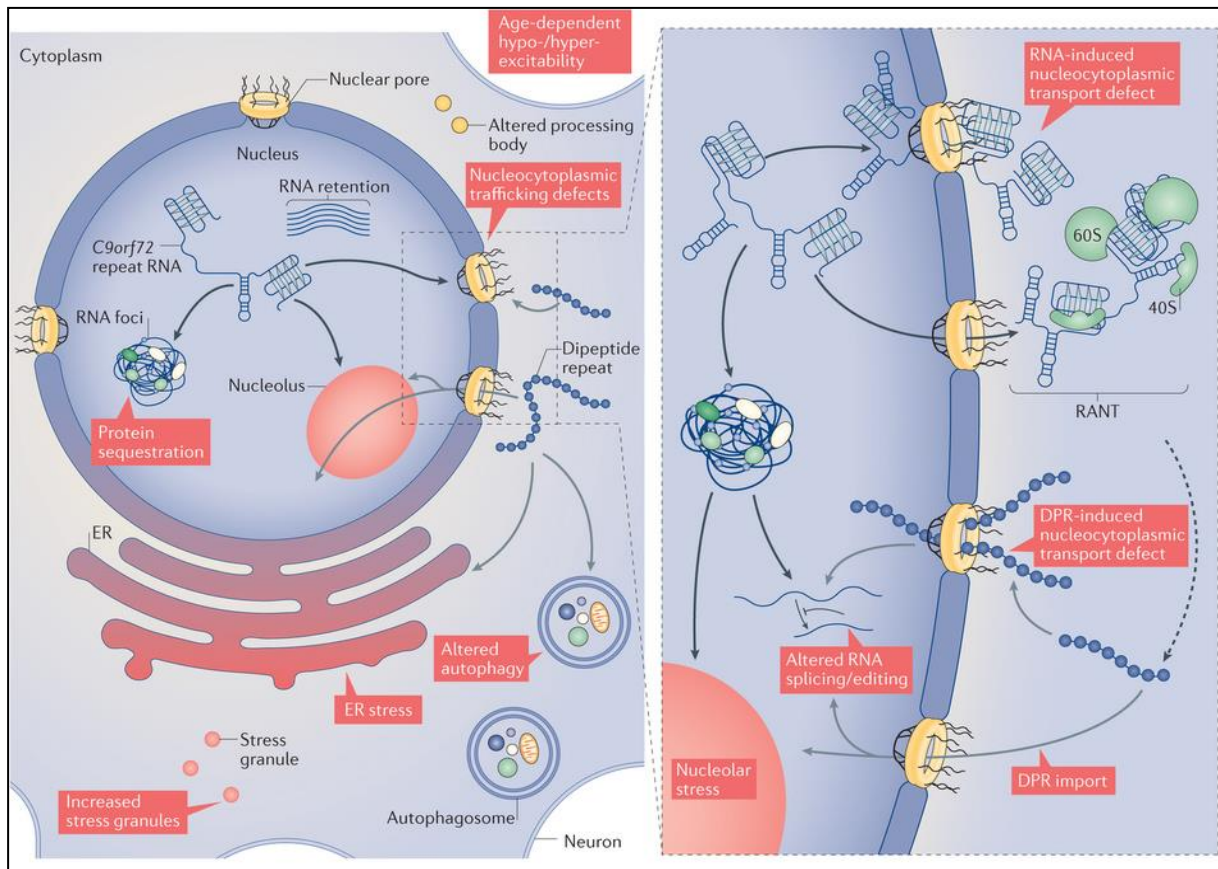


Figure 5: Cellular processes impaired by the C9ORF72 nucleotide repeat expansion.

Cellular features and pathways that are altered by the RNA and/or dipeptide repeat proteins (DPRs) generated from the chromosome 9 open reading frame (C9ORF72) nucleotide repeat expansion (NRE) mutation are shown. Black and grey arrows indicate pathological features linked to the C9ORF72 RNA or DPRs, respectively. The repeat-containing RNA, which forms RNA foci, has been implicated in sequestering key RNA-binding proteins (RBPs). This process may lead directly to altered nucleolar function, changes in RNA processing or maturation and nucleocytoplasmic transport defects. As shown in the right part of the image, RNA and DPRs generated from the *C9orf72* NRE mutation converge on pathways driving nucleocytoplasmic trafficking defects, including altered nuclear pore complex dynamics, import factors and nucleolar stress. *C9orf72* RNA can sequester nucleolar proteins, leading to nucleolar stress, or bind to nuclear pore complex proteins and disrupt nucleocytoplasmic trafficking. The image was taken from [197].

4. MATERIALS.

4.1. Cell lines.

Table 2: cell lines and primary culture used in the study.

Cell lines	Features	Origin	Source/Donor
HeLa 229	Cervical adenocarcinoma	Human	ATCC CCL-2.1
NSC-34	Mouse	Mouse	Biozol, Eching, Germany, ED-CLU140
HEK-293	Embryonic kidney	Human	CRL-1573
HEK293T	Embryonic kidney	Human	
Primary Moto-neurons	Mouse motoneurons	Mouse	CD1 E13.5 mouse

4.2 Bacterial strains.

Table 3: Bacterial strains used.

Bacteria	Genotype	Source/Donor
BL-21	<i>E. coli</i> B F ⁻ dcm ompT hsdS(rB ⁻ mB ⁻) gal λ(DE3)	Novagen
BL-21 Rosetta	F ⁻ <i>ompT hsdS_B(rB⁻ mB⁻) gal dcm</i> (DE3) pLysSRARE2 (Cam ^R)	Novagen
TOP 10	F ⁻ mcrA Δ(mrr-hsdRMS-mcrBC) φ80lacZΔM15 ΔlacX74 recA1 araD139 Δ(araleu) 7697 galU galK rpsL (Str ^R) endA1 nupG	Invitrogen

Table 4: Antibiotics used for bacterial culture.

Antibiotic	Working Concentration
Ampicillin	100µg/ml
Chloramphenicol	33µg/ml
Kanamycin	30µg/ml

4.3 Primary mouse motoneuron culture.

Table 5: Requirements for mouse motoneuronal culture.

Number	Name	
1.	Neurobasal	Gibco-cat. no. 21103-041. opened bottles should be used within 4 weeks.
2.	Horse serum	Linaris-cat. no. SHD3250ZK Thaw at 4 °C overnight, aliquot into 5 ml and heat-inactivation at 55 °C for 30 min, store inactivated aliquots at -20 °C and thaw directly only before use at room temperature (20-24°C). Do not freeze again. The batch of horse serum has to be tested for compatibility with motoneuron culture (see [198]).
3.	50x B27-Supplement	Gibco-cat. no. 17504-044. store 1ml aliquots at -20°C
4.	Glutamax	Gibco-cat. no. 35050-038), 100x (i.e., 200 mM).

5.	β -mercaptoethanol	Sigma-cat. no. M7522. Stock solution 100 μ M in sterile cell-culture tested water should be stored in the dark at room temperature.
6	Trypsin TRL3	Worthington-cat. no.LS003707. for trypsinization of cell aggregates; 1 g trypsin in 100 ml HBSS; store at -20 $^{\circ}$ C after thawing at 4 $^{\circ}$ C; use within 2 weeks.
7	Trypsin-Inhibitor	Sigma, cat. no. T-6522. Add 1 g to 98 ml HBSS and 2 ml of 1 M
8	HEPES pH 7,4	1 ml aliquots should be stored at 4 $^{\circ}$ C
9	150 mM borate buffer pH 8.35;	store aliquots at -20 $^{\circ}$ C
10	Poly-DL-ornithine hydrobromide (PORN)	Sigma cat. no. P8638) dissolve 50 mg in 1 ml. PORN working solution of 0.5 mg / ml Poly-DL-ornithine hydrobromide in 150 mM borate buffer pH 8.35.
11	Laminin	Invitrogen, cat. no. 23017-015, working concentration 2.5 μ g / ml in HBSS; store aliquots at -20 $^{\circ}$ C
12	Depolarization solution	Sterile filtered solution of 30 mM potassium chloride, 0.8 % (w/v) sodium chloride and 2 mM calcium chloride in water. Store at room

temperature.

13	p75 Antibody		MLR2, Biosensis, cat. no. M-009-100)
14	p75-antibody solution	dilution	Prepare 10 mM Tris/HCl pH 9.5. Store at room temperature.
14	Motoneuron medium.	culture	Neurobasal full medium: Neurobasal supplemented with 10 % horse serum, 1 x Glutamax, 1% B27 supplement.

4.4 Buffers for Immunofluorescence.

Table 6: Buffers for Immunofluorescence.

Buffer	Ingredients
PBS (1x) (/L)	8 g NaCl, 0.2 g KCl, 2.68 g Na ₂ HPO ₄ (1xH ₂ O), 0.24g KH ₂ PO ₄ , adjust to pH 7.4
Fixing buffer (/L)	1x PBS + 4% (w/v) PFA, adjust to pH 7.2
Permeabilization buffer	1x PBS + 0.2% (v/v) Triton-X 100
Blocking buffer	1x PBS + 10% (v/v) FCS
Mowiol mounting medium	2.4 g Mowiol 4-88, 6 g glycerol, 6 ml H ₂ O, 12 ml 0.2 M Tris/HCl adjust to pH 8.5

4.5 Buffers for Western blotting.

Table 7: Buffers for Western blotting.

Buffer	Ingredients
10 x SDS buffer (/L)	30.275 g Tris base, 144 g glycine, 10 g SDS
10x Semi dry buffer (/L)	24 g Tris, 113 g glycine, 2 g SDS
1x Semi dry transfer buffer	1x semi dry buffer + 20% (v/v) methanol
10x TBS (/L)	61g Tris base, 90 g NaCl, adjust to pH 7.5 with HCl
TBST	1 x TBS + 0.5% (v/v) Tween20
Blocking solution	TBST20 + 5% (w/v) dry milk powder or BSA
Stripping buffer (500 ml)	7.5 g glycine, 0.5 g SDS, 1.54 g DTT, 5 ml Tween20, Adjust to pH 2.2
2x Laemmli buffer	100 mM Tris/HCl [pH 6.8], 20% (v/v) glycerol, 4% (w/v) SDS, 1.5% (v/v) 2-mercaptoethanol, dash bromophenol blue
Lysis buffer For Cytosolic fraction	
1.5 M Tris-HCL pH 8.8	18.15g Tris-HCl for 100ml, adjust pH to 8.8 with 6N HCL
1M Tris-HCL pH 6.8	12.114g for 100ml, adjust pH to 6.8 with 6N HCl.
10 % APS	10g APS for 10ml
10% SDS	20g SDS for 10ml
20% SDS	20g SDS for 10ml
TEMED	Use under airflow hood
Bromophenol blue 1%	0.1g for 10ml

4.6 Commercial kits and molecular ladders.

Table 8: Commercial kits and molecular ladders.

Name of kit	Company/Donor
Plasmid purification Kit	QIAGEN (Cat No./ID: 12162)
Minipräp Plasmid Kit	MACHEREY-NAGEL GmbH & Co. KG (740588.10)
QIAquick PCR Purification Kit	QIAGEN (28104)
RNA purification Kit	QIAGEN (959034)
SuperScript First-Strand Synthesis System for RT-PCR	Invitrogen (11904018)
LightCycler FastStart DNA Master SYBR Green I	Roche (03003230001)
QIAEx II Gel Extraction Kit	QIAGEN (20021)
Invitro transcription Kit	Ambion (AM1334)
Topo cloning Kit	Invitrogen (C404003)
Big dye terminator Kit	Fermentas (4337455)
100bp ladder	Fermentas (SM0321)
1Kb ladder	Fermentas (SM0311)
Prestained protein ladder	Fermentas (26616)

4.7 Stock buffers for protein purification.

Table 9: Stock buffers for protein purification.

Buffer	Ingredients
1M Tris-HCl buffer	Merck
5M NaCl	Merck
3M Imidazole	Merck
1 M HEPES	Merck
1M MgCl ₂	Merck
β-mecaptoethanol	Sigma 14.7 M stock solution
Glycerol	Merck

1 M NiSO ₄	Merck
1 M NaOH	Merck
Isopropanol	Sigma

4.7.1 Buffers for purification of hnRNP R.

E. coli Culture Medium: prepare 5 l of LB (Invitrogen) according to the manufacturer's instructions (20g /1L).

Lysis buffer: 500 mM NaCl, 20 mM Imidazole, 50 mM Tris-HCl buffer pH 7.5, 1 mM DTT, 1 mM EDTA, 1 tablet of Protease Inhibitor, 50 µl Benzonase, Lysozyme.

Buffer A (binding buffer): Prepare fresh from stock solutions directly before use 500 mM NaCl, 20 mM Imidazole, 50 mM Tris-HCl buffer pH 7.5, 1 mM DTT.

Buffer B (elution buffer): Prepare fresh from stock solutions directly before use 250 mM NaCl, 500 mM Imidazole, 50 mM Tris-HCl buffer pH 7.5

Buffer E (Gel purification): Prepare fresh from stock solutions directly before use 100 mM NaCl, 50 mM Tris-HCl buffer pH 7.5, 1 mM DTT.

4.7.2 Buffers for purification of SMN.

E. coli Culture Medium: Prepare 5 l of LB (Invitrogen) according to the manufacturer's instructions (20g /1L).

Lysis buffer: 500 mM NaCl, 30 mM Imidazole, 50 mM HEPES buffer pH 7.4, 5 mM MgCl₂, 5 mM β-mercaptoethanol, 10% glycerol, 1 tablet of Protease Inhibitor, 50 µl Benzonase, Lysozyme:

Buffer A (binding buffer): Prepare fresh from stock solutions directly before use 500 mM NaCl, 30 mM Imidazole, 50 mM HEPES buffer pH 7.4, 5 mM MgCl₂, 5 mM β-mercaptoethanol, 10% glycerol, 1 tablet of Protease Inhibitor

Buffer B (elution buffer): Prepare fresh from stock solutions directly before use 250 mM NaCl, 500 mM Imidazole, 50 mM HEPES buffer pH 7.4, 5 mM MgCl₂, 5 mM β-mercaptoethanol, 20% glycerol, 1 tablet of Protease Inhibitor

Buffer E (Gel purification): Prepare fresh from stock solutions directly before use 100 mM NaCl, 50 mM Tris-HCl buffer pH 7.5, 1mM DTT.

4.7.3 Buffers for purification of TDP-43.

E. coli Culture Medium: prepare 5 l of LB (Invitrogen) according to the manufacturer's instructions (20g /1L).

Lysis buffer: 250 mM NaCl, 30 mM Imidazole, 50 mM HEPES buffer pH 7.4, 5 mM MgCl₂, 5 mM β-mercaptoethanol 10% glycerol, 1 tablet of Protease Inhibitor, 50 μl Benzonase, Lysozyme.

Buffer A (binding buffer): Prepare fresh from stock solutions directly before use 250 mM NaCl, 30 mM Imidazole, 50 mM HEPES buffer pH 7.4, 5 mM MgCl₂, 5 mM β-mercaptoethanol 10% glycerol, 1 tablet of Protease Inhibitor. Filtered and degassed.

Buffer B (elution buffer): Prepare fresh from stock solutions directly before use 150 mM NaCl, 500 mM Imidazole, 50 mM HEPES buffer pH 7.4, 5 mM MgCl₂, 5 mM β-mercaptoethanol 20% glycerol, 1 tablet of Protease Inhibitor. Filtered and degassed.

Buffer E (Gel purification): Prepare fresh from stock solutions directly before use 100 mM NaCl, 50 mM Tris-HCl buffer pH 7.5, 1mM DTT. Filtered and degassed

4.7.4 Buffers for His-Trap HP column stripping and cleaning.

Striping buffer: 20 mM sodium phosphate, 0.5 M NaCl, 50 mM EDTA, pH 7.4, filtered and degassed

Recharging buffer: 0.1 M NiSO₄ made from 1M Stock solution, double filter before use

Remove ionically bound proteins: 1.5 M NaCl

Remove precipitated proteins: 1 M NaOH

Remove hydrophobically bound proteins, lipoproteins, and lipids: 30% isopropanol

4.7.5 Columns used for protein purification.

Table 10: Columns used for protein purification.

Columns	Application	Company
1ml His Trap	His Tag protein purification	Ge life science (29-0510-21)
5ml His Trap	His Tag protein purification	Ge life science (17-5248-01)
1ml Hi Tap Q	IEX purification	Ge life science (17-1153-01)
1ml Hi Trao sp	IEX purification	Ge life science (17-1151-01)
Desalting column	Desalting	Ge life science (17-5087-01)
Superdex column	Gel purification	Ge life science (28989336)

4.8 Antibodies.

Table 11: Primary antibodies used for Western blotting (WB), immunofluorescence (IF)

Name	Source	Company	Dilution	Application
β -Actin	ms	Gentex (GTX 26276)	1:3000	IB
Tdp-43	Rb	Cell signaling (E1014)	1:3000	IB
Tdp-43	Rb	Abcam (ab50930)	1:4000	IB/IF
Tdp-43	Rb	Abcam (Ab41972)	1:350	IB/IF
Tdp-43	ms	EnCor (Ab41972)	1:250	IB/IP
hnRNP R	Rb	Abcam (Ab30930)	1:3000	IB

hnRNP R	Rb	Abcam (ab83272)	1:3000	IB
SMN	Rb	BD Bioscience (610646)	1:3000	IB/IP
Calnexin	Rb	SICGEN (AB0037-200)	1:5000	IF
C9ORF72	Rb	Santacruz (sc138763)	1:3000	IB
C9orf72	M	Proteintech	1:3000	IB
GFP	Rb	Santacruz (Sc- 8334)	1:5000	IB
FLAG M5	Ms	Sigma (F4042)	1:5000	IB
FLAG M2	Ms	Sigma (F1804)	1:5000	IB/IP
GAPDH	Rb	Calbiochem (CB1001)	1:5000	IB
Histone	rb	Abcam (ab1791)	1:20000	IB
Fus/TLS	rb	Santa Cruz (Sc-47711)	1:1000	IB/IF
Tubulin	Rb	Sigma	1:5000	IB
p-cofilin	rb	Cell Signaling (3311)	1:2000	IB
Cofilin	rb	Cell Signaling (5175)	1:5000	IB

Table 12: Secondary antibodies used for immunofluorescence.

Name	Source	Company	Dilution	Application
Alexa Fluor 488, anti-rat IgG.	Donkey	Jackson Immuno Research , 712-542-150	1:800	IF
Alexa Fluor	Donkey	Jackson Immuno	1:800	IF

488 anti-rabbit IgG Affi-pure.		Research , 711-545-152		
Cy3 anti-rabbit IgG Affi-pure.	Donkey	Jackson Immuno Research , 711-165-152	1:800	IF
Cy3 anti-mouse IgG Affi-pure.	Donkey	Jackson Immuno Research , 715-505-150	1:800	IF
phalloidin cross-linked with a 555 nm fluorochrome.	Toxin	Cytoskeleton, PHDH1	100 nM	IF
phalloidin cross-linked with 670 nm fluorochrome.	Toxin	Cytoskeleton, PHDN1	200 nM	IF
Anti-rat IgG affiniPure.	Goat	Rockland, 612-103-120	1:5000	WB
Anti-Mouse IgG affiniPure (H+L).	Goat	Jackson, 115-035-003	1:5000	WB
Affinity Pure Anti-Mouse IgG light chain specific.	Goat	Jackson, 115-055-174	1:2000	WB
AffiniPure Anti-Rabbit IgG (H+L).	Goat	Jackson, 111-035-003	1:5000	WB
Anti-Rabbit IgG, Light Chain Specific	Mouse	Jackson, 211-032-171	1:2000	WB

4.9 EMSA buffers.

Table 13: Buffers used for EMSA.

EMSA	Menge	Stoff
10 x TBE	890 mM	Tris Base
	890 mM	Boric acid
	20 mM	EDTA
20 x SSC	3 M	NaCl
	300 mM	Trisodium citrate
5 x Shift buffer	125-250 mM	Tris/HCl (pH 8,0)
	500 mM	NaCl
	15 mM	MgCl
	0,5 mM	EDTA
	2,5 mM	DTT
	2,5%	Tween
Loading dye	50%	Glycerin
	1mM	EDTA
	0,4%	Bromphenol blue

4.10 Instruments used.

- Leica SP5 confocal microscope equipped with 488,561,649 and UV laser with 50mWatt power for illumination.
- Roche real time light cycler PCR machine (Roche)
- Eppendorf gradient master cycler instrument
- FPLC System (GE Life Science)
- Ultra centrifuge (Beckmann)

- Bacterial shaker
- Nikon TE2000 Microscope with autofocus system for life imaging, equipped with ... camera

4.11 Software used.

Windows XP, Microsoft Office 2007, EndNote X5, Adobe Photoshop CS4, Corel Draw X4, LAS AF confocal microscopy software, ImageJ, Graphpad Prism (6).

5. METHODS

5.1 Animals and ethics statement.

CD-1 mice were kept at the animal facilities of the Institute of Clinical Neurobiology at the University Hospital of Wuerzburg providing controlled conditions such as food and water in abundant supply, 20-22°C, a 12 hours light/dark cycle, and 55-65% humidity, respectively. Each experiment was performed strictly following the regulations on animal protection of the German federal law, the Association for Assessment and Accreditation of Laboratory Animal Care and of the University of Wuerzburg, in agreement with and under control of the local veterinary authority and Committee on the Ethics of Animal Experiments, i.e. Regierung von Unterfranken, Wuerzburg (License numbers 566/200-244/13 and 55.2-2531.01-08/14). This study was approved by the local veterinary authority (Veterinaeramt der Stadt Wuerzburg) and Committee on the Ethics of Animal Experiments, i.e. Regierung von Unterfranken, Wuerzburg (License numbers 566/200-244/13 and 55.2-2531.01-08/14).

5.2 Cell Culture.

All dividing cells (HEK293, HEK293T and NSC-34) were cultured and maintained in a humidified incubator (Thermo) at 37°C with 5 % CO₂. Trypsin-EDTA was used for splitting the cells upon confluence. The adherent epithelial cells were washed with sterile PBS (GIBCO, Invitrogen) once and detached by incubation with 1 ml Trypsin/EDTA (GIBCO, Invitrogen) per flask. Trypsinization was stopped after 3-5 minutes by re- suspending the cells in FCS containing medium. A centrifugation step 400xg was done (which centrifuge, which time, which rotor, how many g) to removed Trypsin-EDTA solution and a defined part of the cell solution was transferred into a new cell culture flask with fresh culture medium. The cells were in culture until sixty passages in DMEM + 10% FBS+1%penstrp.

5.3 Cryo stocking of cell lines.

For long term storage, and as the cells (HEK293, HEK293T and NSC-34) were maintained for no more than fifty passages the 70% confluent cells were processed for trypsinization to detach cells from cell culture plates, transferred to a 15 ml tube (Greiner) with 5 ml DMEM + 10% FBS. After centrifugation at 400xg (Eppendorf) for 5 min, the cell pellet was resolved in 3 ml DMEM + 20% FBS with 10% DMSO (cryoprotectant) and aliquoted into 1 ml per cryo tube, gradually cooled to -80°C in isopropanol after which the cryo tubes were transferred to liquid nitrogen tank where the temperature is -186°C. For

thawing of cell stocks, frozen cells were rapidly thawed at 37°C and immediately transferred into pre-warmed medium for re-culture. Cells are usually seeded into plates one night before performing experiments.

5.4 Transfection of HEK-293, HeLa and NSC-34 cell.

Cell for transfection was done with 1:3 ratios of DNA (μg) and LipofectamineTM 2000 (μl , Invitrogen, 11668019). One day before transfection, cells were seeded into the required plates to gain 70% confluence. For optimum transfection the transfection mixture was prepared by adding required amount of DNA and LipofectamineTM2000 in separate tubes with OptiMEM media (Invitrogen, 31985070) and incubated for 5 min at RT before mixing them together. After mixing the transfection mixes together the mixture was incubated for 10min at RT and added dropwise to the appropriate cell (HEK-293, HeLa and NSC-34 cell). The volume of the plates was then increased to the required volume with DMEM+10% FCS medium without antibiotics. This medium was removed and replaced with DMEM+10% FCS media after 4-6 hours of transfection.

5.5 Primary motoneuron culturing.

The technique of dissecting out lumbar spinal cord and preparing a motoneuron culture was performed according to [198]. Plates and dishes were coated with sufficient PORN solution overnight at 4°C. On the next day the plates were washed three times with water and covered with air-dry coverslips. Laminin aliquots were thawed at 4°C and 2.5 μg / ml laminin solution in HBSS prepared. The surface of PORN coated plates or plates containing coverslips were cotted with laminin. These were then incubated overnight at 4°C or at least for 2 h at room temperature; laminin coated coverslips can be stored at 4°C and used within 1 week.

For the preparation of panning plates p75 antibody was diluted 1 to 5000 in sterile antibody dilution solution. The surface of a culture dish used for panning was covered with sufficient antibody solution over night at 4°C or for minimum of 2 hours at room temperature. Before dishes can be used for panning they should be washed 3 times with HBSS and covered with pre-warmed Neurobasal medium containing GlutaMAX (Gibco). Store panning plate at room temperature until use.

To isolate spinal motoneurons, pregnant mice with fourteen day old embryos were sacrificed by cervical dislocation. Lumbar spinal cord was isolated from the embryos and these tissues preserved in ice cold HBSS solution. For subsequent genotyping of embryos, the tail was dissected and placed in 400 ml of lysis buffer. Isolated spinal cords were trypsinized by the addition of 20 μ l of 1% trypsin solution to each Eppendorf tube containing a dissected spinal cord in 180 μ l ice-cold HBSS. Trypsinization was performed for 15 min at 37°C. To stop the process of trypsinization, 20ml of 1% trypsin inhibitor was added to the Eppendorf tubes and then the tissue aggregates were mechanically triturated. The cells were now enriched from the triturated cells on a 10 cm panning plate that was previously coated with an antibody against the p75NTR receptor (1.8 ng/ml). The cells were incubated on the panning dish and allowed to settle down for a period of 35 minutes after which they were washed three times with room temperature warm Neurobasal medium in order to eliminate the p75NTR negative cells. The settled cells were depolarized with 30mM potassium chloride and then transferred to Neurobasal medium containing B27 supplement and 10% heat inactivated horse serum. Cells were counted on haemocytometer and plated at a density of 1500-2000 cells/coverslips for neurite length measurements and 25,000 cells on 12 mm coverslips for calcium imaging experiments. The neurotrophic factor BDNF was added to the medium at a final concentration of 10 ng/ml. Motoneurons were treated with fresh medium within 24 hours after plating and further-on after every alternate day till day seven.

5.6 Overexpression and knockdown of C9ORF72 by shRNA in cultured mouse motoneurons.

To knockdown of C9ORF72 in cultured mouse motoneurons, we chose the target sequence 5'-GGTCCTAGAGTAAGGCATATT-3' in the C9ORF72 coding sequence and cloned the corresponding short hairpin construct into the EcoRI / BamHI site of a modified pSIH-H1 shRNA vector (System Bioscience), where the CMV promoter driven copGFP was replaced by the EGFP cassette (Stratagene): The following oligonucleotides were used:

C9ORF72	shRNA	forward-oligo	(5'-
GATCCGGTCCTAGAGTAAGGCATATTTCAAGAGAATATGCCTTACTCTAGGACCT			
TTTTG	-3'),	and	reverse-oligo
AATTCCAAAAAGGTCCTAGAGTAAGGCATATTCTCTTGAAATATGCCTTACTCTA			(5'-
GGACCG,	control	scrambled	forward-oligo
GATCCGTAAGCGTTAATTGGCTACATTCAAGAGATGTAGCCAATTAACGCTTACT			(5'-

TTTTG -3') and reverse-oligo (5'-AATTCCAAAAAGTAAGCGTTAATTGGCTACATCTCTTGAATGTAGCCAATTAACGCTTACG -3') The construct for overexpressing C9ORF72 fused with an C-terminal HA-tag was created using PCR primers specific for human C9ORF72 from human cDNA and subcloned into a pCR4-TOPO vector (Invitrogen) using the following primer: forward (5'-GGTACCGCCATGTCGACTCTTTGCCACCG -3', start codon of C9ORF72 in bold) and reverse (5'-CTCGAGTTAAGCGTAATCTGGAACATCGTATGGGTAAAAAGTCATTAGAACATCCGTTCTTGC -3', HA-tag sequence in bold). This human C9ORF72 – HA cassette was then cloned via BamHI and XhoI into a modified FuGW vector system 4driven by a ubiquitin promoter, where the GFP was replaced by a multiple cloning site. Integrity of all clones used was checked with sequencing and analysis of restriction patterns.

Lentiviral knockdown or overexpression virus was prepared as described previously [3]. Cultures of mouse motoneurons were infected in suspension before being plated and harvested after 5 or 7 DIV. Cell lysates were analyzed by western blot analysis or processed for immunostaining.

5.7 Standardization of lentiviral concentration on NSC-34 cells.

Lentiviral concentration was determined both by immunochemistry for HA tagged overexpression protein and immunofluorescence for knockdown constructs. Increasing volumes of virus starting from 1µl, 2µl, 5µl and 10µl volume were added to equal numbers of cells. The cells with virus were incubated at RT for 10 minutes and plated to individual wells of a 12 well dish with appropriate volume. The cells were fixed 3 days after the infection to determine the viral titer.

5.8 Sample preparation for LC-MS analysis using NSC-34 cells.

NSC-34 cells were cultured in Dulbecco's DMEM (DMEM, Gibco) supplemented with 10% FBS and 1% Penicillin/Streptomycin under standard culture conditions. Control cells and cells for overexpressing hC9ORF72-HA were split and seeded at equal density on a 6 well dish. The cells were maintained in the same media without Penicillin/Streptomycin and transfected with the overexpression plasmid the next day. The cells were collected at day 4 after transfection and processed for immunoprecipitation experiments. The cells were lysed (25 mM Tris-HCl pH 7.5, 150 mM NaCl, 2 mM EDTA, 2 mM EGTA, 10% glycerol (vol/vol), 1% NP-40 (vol/vol), 2 mM Na₃VO₄, 50 mM NaF) for immunoprecipitation with

protease and phosphatase inhibitors added freshly. The lysate was scraped off and collected in a 1.5ml centrifuge tube and centrifuged at 10,000xg for 5 min. The supernatant was collected and preincubated with Sepharose 6 Fast Flow (GE, 17-0969-01) for 1h at 4°C. Protein pulldown was performed using 30µl HA antibody coupled beads (Covance, AFC-101P-1000) at 4 °C for 6hr. The sedimented complex was washed 3 times with the lysis buffer and three times with PBS. After washing, the samples were stored at -80°C. For proteolytic digestion, the samples were resuspended in 8 M Urea (20 mM Hepes, pH 8). Proteins were reduced with 10 mM DTT for 30 min followed by alkylation of cysteins with 55 mM iodoacetamid for 45 min. We added 1 µg of Lys-C protease and digestion of proteins was carried out for 3 hours at room temperature. The urea was diluted by factor five with 50 mM ammonium bicarbonate and the mixture was digested overnight with 1 µg trypsin.

5.9 LC-MS data acquisition and analysis.

These experiments were performed by our collaboration partner Daniel Hornberg, Felix Meissner and Matthias Mann at the Max Planck Institute of Biochemistry, Martinsried, Germany. Samples were desalted via C18 StageTips 6. We used liquid chromatography (Thermo Scientific EASY-nLC 1000 HPLC) with in- house packed columns (75 µm inner diameter, 20 cm length, 1.9 µm C18 particles (Dr. Maisch GmbH, Germany). Peptides were separated at 50°C in a 102 min gradient from 98% buffer A (0.5% formic acid) and 5% buffer B (0.5% formic acid to 80% acetonitrile) to 60 % buffer B at 250 nl/min. The LC was directly coupled to an Orbitrap mass spectrometer (Orbitrap Elite7, Thermo Fisher Scientific) via nano electrospray source. The mass spectrometer was operated in a data dependent acquisition mode. Following a survey scan (MS1, 300 to 1.650 m/z) at a resolution of 120,000 up to the 10 most abundant isotope patterns (charge ≥ 2) were subjected to collision-induced dissociation (isolation window of 2 Th, normalized collision energy of 35). Isotope patterns that had been subjected to fragmentation were excluded for the subsequent cycles (30s) in order to reduce resequencing. Xcalibur software (Thermo Scientific) was employed to record the data.

5.10 Data analysis.

The data obtained from LC-MS was processed by searching against the UniProtKB mouse FASTA database (06/2012) with the MaxQuant software⁸ (v 1.3.8.2) and Andromeda search engine⁹ using standard settings. Carbamidomethylation of cysteine residues was set as

fixed modification. We set enzyme specificity to trypsin allowing cleavage N-terminal to proline and up to two miscleavages. A 1% false discovery rate (FDR) cut-off on the level of peptides and proteins was used. After nonlinear retention time calibration identifications were matched to unidentified MS 1 features across the samples within a 0.5 min time window (MaxQuant 'matching between runs' algorithms). For quantification we used MaxLFQ label free algorithms [10]. Before statistical analysis we strictly excluded potential contaminants (n=247) and proteins only identified with site modifications. Statistical analysis was performed in PERSEUS (which is part of the MaxQuant framework) and R. Data were filtered for at least 2 valid values in at least one condition and remaining missing values were imputed with a normal distribution based on the whole data set (width = 0.3; shift = 1.8). We determined significant outlier with t-test statistics (permutation-based false discovery rate of 5% and S_0 of 0.1). To assess the interactome on cellular pathway level we performed an 1D annotation enrichment on the t-test difference. For the enrichment analysis we applied a Benjamini-Hochberg FDR at 2% (Figure 33)

5.11 Immunofluorescence analysis of primary mouse motoneurons and cell lines.

Cells were seeded on laminin-coated glass coverslips as described earlier [198]. After three washings with PBS, cells were fixed for 10 minutes with 37°C pre-warmed 4% paraformaldehyde. Cells were permeabilized with 0.3% Triton-X 100 in PBS for 20 minutes and blocking was performed with 15% goat serum in PBST (PBS with 0.5% Tween20). First antibody was incubated overnight at 4°C in 5% goat serum in PBST, and after three washes with PBST incubated at room temperature for 1 hour with appropriate fluorescence labelled secondary antibodies raised in goat (Jackson ImmunoResearch). Cells were washed and incubated for 5 minutes with DAPI-solution and then coverslips were mounted with Mowiol. Cells were investigated with a confocal microscope (SP2, Leica). Images were processed with ImageJ and Photoshop 7.0 (Adobe).

5.12 Lentivirus Production.

A HIV based lentiviral expression system has been used in my studies [199]. The $\Delta 8.9$ and VSVG vectors were used as helper plasmid for packaging FuVal expression vector. HEK293T cells were used for packaging. The cells were propagated in DEMEM + 10%FCS in 3, 125 cm flasks up to 90% confluency. On the day of packaging, the following reaction was set up in two 50ml reaction tubes.

Table 14: Plasmid concentration required for lentivirus production.

Tube A			Tube B		
	Components	Volume		Components	Volume
	Opti-MEM	9ml		Opti-MEM	9ml
	Δ8.9	45μg		Lipofectamin	216μl
	VSVG	30μg			
	Expression plasmid	18μg			

The above reaction was incubated for 5min and then the two reactions were mixed and incubated for 30min. The cells were washed with 10ml PBS and the cells were harvested by trypsination with 0.1% trypsin. The cells were incubated for 10min at 37°C and then centrifuged at 300xg for 5min, and the pelleted cells were resuspended in 30ml optimum transfection medium with 10% FCS. This was then mixed with the transfection mix making the volume to 48ml. This was then distributed in 6 10cm petri dishes with 8ml each and incubated in the cell culture incubator overnight.

The cells were washed with PBS and the mediums were changed to Neurobasal with 1% glutamax and 2% B27 packaging medium (12 ml in each petri dish) and were incubated for 48 hours. The transfection efficiency was estimated by microscopic examination. For harvesting the virus, the supernatant medium was collected and centrifuged at 5000 rpm for 15min at room temperature and filtered with a 0.2μm filter. The supernatant was then layered on 10% sterile sucrose solution and centrifuged with ultra-centrifuged at 250000rpm (Beckman ultracentrifuge) for 1.5 hr at 4°C using a swing bucket rotor (SW28). The pellet was then slowly re-suspended in 100μl of TBS buffer overnight on ice. The suspension was then gently mixed by pipetting up and down and 10μl aliquots were prepared and stored at -80°C until further use.

5.13 Protein Purification.

5.13.1 Preparation of bacterial lysates for recombinant protein purification.

His-tagged proteins were expressed in *E. coli* after cloning corresponding cDNA constructs into the corresponding vector system. These proteins were purified using His-Trap HP 1 ml and Superdex 10/300 gel filtration columns (GE Healthcare). Fresh transformed vector in *E. coli* strain BL21 was used each time for making starter cultures. The overnight starter culture was inoculated in a 1:100 dilution with the appropriate antibiotic selection in a 5L culture LB media and incubated at 37°C. The protein production was induced at OD ~0.5 with 0.1M IPTG. After the induction the incubator temperature was reduced to 20°C and protein production was continued for 18hr.

Bacterial pellets were lysed with the appropriate lysis buffer for the protein in a French press lysis machine at a pressure of 1.5Pa. The lysed suspension was centrifuged at 20,000xg for 20min. the supernatant was collected and filtered through a 0.4µm filter and degassed before pumping into the FPLC.

5.13.2 Setup of FPLC for purification and maintenance.

All buffers used for running the FPLC had to be filtered and degassed before use. Before starting the FPLC, the inlet connector was placed in fresh distilled water. After switching ON the FPLC and the auto calibration of the pumps, both pump A and B were cleaned by pump washing command. After the pump washing the system wash was executed and the system brought to a flow rate of 1ml/min. The valve position was changed to the required column position at a steady flow rate. The required column was then connected to the appropriate valve. After running 5 column volumes (CV) of distilled water, the column was equilibrated with 5CV of appropriate buffer and the system was ready for protein purification. After each purification, the FPLC system was cleaned with 0.5 M NaOH on both pumps and a subsequent system wash with distilled water, finally with 20% Ethanol.

5.13.3 Chromatography.

Proteins were purified using a series of chromatography steps starting with an affinity chromatography as a first capture step. The purification of the protein ended with a gel

filtration step was performed to remove contaminating proteins but also to separate different oligomeric states of the protein.

5.13.4 Immobilized metal affinity chromatography (IMAC)

Hexahistidin (His₆)-tags has a strong affinity to Ni²⁺-ions, which can be chelated by iminodiacetic acid (IDA) groups. Proteins containing a His₆-tag thus can be bound to the column and eluted by the addition of the competitor imidazole, which is chemically and structurally similar to histidine residues.

The supernatant of a His-tag containing cleared cell lysate was loaded on a pre-equilibrated Ni-MAC column (Column volume (CV) = the size of the column used for purification; GE-Lifesciences) with a flow rate of 1 ml/min on the FPLC System. Both the protein sample and the binding buffer IMAC-A were supplemented with appropriate amount of imidazole (10mM to 40mM) to prevent unspecific binding. The column was washed with approximately 20 column volumes binding buffer to remove unbound sample until a stable baseline of the UV-absorption was achieved. The desired protein was then eluted by a step gradient up to 500 mM imidazole.

5.13.5 Chitin-Intein system

The IMPACTTM system (New England Biolabs) provides expression vectors to generate fusion proteins consisting of the desired protein and an intein-tag including a chitin-binding domain. This chitin-binding domain specifically binds to chitin beads. Thiols such as DTT induce the autocatalytic activity of inteins to cleave themselves from the target protein, which is thereby eluted from the chromatography column whereas the intein-chitin-tag stays bound on the chitin beads [200]

5.13.6 Ion exchange chromatography.

The net charge of a protein at a certain pH is exploited in ion exchange chromatography. The pH at which the protein stays neutral is called the isoelectric pH. At basic pH, proteins with a positive net charge ionically interact with cation exchange chromatography columns. The protein can be eluted by changing the pH or by increasing the salt concentration. IEX purification is usually used as a step after affinity purification.

The affinity purified protein was diluted with binding buffer to achieve a salt concentration of (normally 60 mM NaCl) and subsequently loaded onto appropriate HiTrap IEX exchange

column (column volume 1 ml; GE Healthcare) with a flow rate of 1 ml/min. The column was washed with approximately 20 column volumes binding buffer to remove unbound proteins. The target protein was then eluted by a gradient up to 1 M NaCl.

5.13.7 Size-exclusion chromatography.

Size-exclusion chromatography was performed as a final purification step. The column consists of a spherical composite of cross-linked agarose and dextran matrix, which allows the separation of molecules with a molecular weight of 10-600 kDa. Thus, aggregates as well as higher oligomers can be separated from monomeric protein.

The concentrated protein sample was applied to a pre-equilibrated HiLoad™ 26/60 Superdex™ 200 column pg (column volume 330 ml, respectively; GE Healthcare) and isocratically eluted with buffer. The presence and purity of the target protein in the elution fractions was analyzed by SDS-PAGE. Protein concentrations were determined by UV-spectrophotometry at 280 nm.

Eluted protein samples were then concentrated using Centricon® concentrators (Millipore) with suitable molecular cut-offs, split in 25-50 µl aliquots, frozen in liquid nitrogen and stored at -80 °C until use.

5.14 Co-immunoprecipitations of recombinant proteins.

The association between recombinant proteins was analyzed by co-immunoprecipitations using GammaBind Plus Sepharose beads (GE Healthcare, 17088601). Different varying concentrations of protein were incubated together in binding buffer and incubated for 1hr at room temperature.

Table 15: Recombinant protein binding buffer

HEPES	20 mM
NaCl	150 mM
NP-40	0.1 %
MgCl ₂	2.5mM

After mixing the proteins with 20 μ l GammaBind Plus Sepharose beads and 1 μ g antibodies against the specific protein or IgG control, the mix was incubated for 1 h at room temperature. The resin was washed 5 times with binding buffer to remove unbound proteins. For elution, beads were boiled in 2 x Laemmli buffer at 95 °C for 5 minutes. The eluted proteins were then analyzed by Western blotting using specific antibodies against each protein. Pictures were contrast optimized by AIDA Analysis Software (Version 3.52). Image processing was carried out with Photoshop 7.0 (Adobe).

5.15 Electrophoretic Mobility Shift Assay (EMSA).

Murine full length β -actin 3'UTR was produced from the plasmid pTZ19 that had been linearised by *EcoRI* digestion and transcription was started using the MEGAscript® T7 Kit (Ambion) with P³² alpha CTPs. To the 5 x EMSA binding reaction mixture 1.25 mg / ml bacterial tRNA and 1.25 mg / ml BSA were added to avoid unspecific protein / mRNA binding. Different amounts of recombinant hnRNP R, TDP-43 or rSMN were incubated with 0.45 pM radioactively labeled probe for 20 minutes. For the competition experiments an unlabeled 23nt U-rich RNA Oligo (5'-ACAAAACCUAUUUUUUGUUUUGU-3') at increasing concentrations was added. Protein / mRNA complexes were resolved at room temperature on a 1.2 % agarose gel in 0.5 x Tris-borate-EDTA running buffer at 70 V. The gel was blotted onto a Hybond N+ membrane (GE Healthcare) in 20 x SSC overnight and exposed in a phosphorimager (Fuji) for band visualization. Pictures were contrast optimized by AIDA Analysis Software (Version 3.52). Image processing was carried out with Photoshop 7.0 (Adobe).

Table 16: EMSA reaction setup.

	10 μ L preparation	15 μ L preparation
Shift buffer	2 μ L	3 μ L
Purified protein	0-6 μ L	0-10 μ L
labelled RNA	2 μ L	2 μ L
add H ₂ O	10 μ L	15 μ L

5.15.1 Linearisation of beta-actin 3'UTR cDNA (vector)

Table 17: Linearisation of beta-actin plasmid

Tango buffer (Thermo Scientific, BY5)	50 μ L
Plasmid (5 μ g/ μ L)	25 μ L
Eco R1 (10 u/ μ L)	8 μ L
add H ₂ O	500 μ L

Linearised plasmid was purified by QIAquick PCR Purification Kit (Cat No./ID: 28106).

5.15.2. Radiolabeling beta-actin 3'UTR mRNA using MEGAscript Transcription kit (Ambion).

Table 18: Radiolabeling beta-actin 3'UTR mRNA

ATP solution	5 μ L
CTP solution	3 μ L
GTP solution	5 μ L
UTP solution	5 μ L
10 x reaction buffer	5 μ L
DNA Template	1.3 μ g
α - ³² P-CTP	19 μ L
Enzyme Mix	5 μ L
add H ₂ O	50 μ L

The mixture was incubated for 9 h at 37°C (in radioactive lab). Digestion of DNA template was done with 2.5 μ L TURBO DNase at 37°C for 15 min. Discarding of non-incorporated

nucleotides was performed by using a G50-coloums (GE Healthcare). The freshly equilibrated columns were treated with the radiolabeled probe and centrifuged at 800xg for 2min. The eluted supernatant was captured in the collection tube and 10 μ L of RNase Inhibitor (40 u/ μ L, Fermentas, EO0381) was added to prevent RNA degradation. The probe was aliquoted to 10 μ L samples each, and stored at -20°C for up to 1-2 weeks.

5.16 Cytosolic and nuclear fractionation.

The cells for fractionation were washed with ice cold 1X PBS three times. Required amount of lysis buffer was added according to the cell number.

Table 19: Cytosolic fractionation buffer:

Tris, pH 7.4,	50 mM
NaCl,	150mM
NP40,	0.1%
1x Complete Protease Inhibitor (Roche)	1 tablet for 10 ml

The cells were lysed for 10min on ice with shaking. The lysate was collected in a centrifuge tube and centrifuged for 10min at 1000xg. The supernatant was collected, which was the cytosolic fraction and the pellet fraction being the nuclear fraction.

Table 20: Nuclear fractionation buffer.

HEPES	20mM
NaCl	400mM
Glycerol	2.5%
EDTA	1mM
NaF	0.5mM
DTT	0.5mM
CHAPS	0.6%

Benzonase	2 unit
1x Complete Protease Inhibitor (Roche)	1 tablet for 10 ml

The nuclear fraction was washed two times with ice cold cytosolic buffer, then lysed with nuclear lysis buffer. The lysate was suspended 20 times with a pipette and centrifuged at 10,000g for 10min. The supernatant was used as nuclear fraction. The lysis condition was analysed by SDS-PAGE. After Western blotting the blot was probed with anti-histone (Rb Abcam) as a nuclear marker and anti-GAPDH (Rb, Santacruz) or β III-tubulin (M, Boehringer Mannheim) as a cytosolic marker.

5.17 Immunoprecipitations from cultured mouse motoneurons and cells.

After 7 days in culture plates were washed three times with PBS and cells were lysed as per the cytosolic and nuclear fraction protocol. Lysate collected was pre-cleaned on GammaBind sepharose beads and used as input. First antibody was added to the lysate and the mixture was rotated for 5 hr at 4 °C. Beads were added and the mixture was rotated for 1 hour at 4 °C. After three rounds of washing in lysis buffer beads were incubated in SDS-loading buffer at 95 °C for 5 minutes. After centrifugation at 1000g for 5min supernatants were collected and run on a SDS-PAGE. After Western blotting the proteins were detected with the same primary antibodies and appropriate horseradish peroxidase coupled secondary antibodies and visualized with ECL reagent (GE Healthcare) on a LAS reader (Fuji). Images were analysed with AIDA software (Version 3.52).

5.18 Live cell imaging of actin dynamics.

A GFP-tagged cytoplasmic actin construct was prepared using plasmids carrying the β -actin cDNA under the control of a CMV promoter as described [201]. The GFP coding region of the pSIH-H1 shRNA vector (System Bioscience) containing scrambled or C9ORF72 shRNA was fused in frame to the actin coding cDNA to obtain a construct coding β -actin with an N-terminally fused GFP followed by an 11 amino acid linker sequence. The lentivirus produced from the vector was always quantified and equal ratios of cells to virus were used in all experiments. Actin dynamics were analysed in transduced cultured motoneurons at 5 DIV with GFP-actin scrambled shRNA or GFP-actin C9ORF72 shRNA seeded in μ -dish (35mm high) at a density of 10,000 cell plated on laminin221. The motoneurons used for live cell

imaging were washed three times with 37°C neurobasal medium and then incubated with fresh neurobasal medium with BDNF (5ng/ml) for 30 min at 37°C at 5% CO₂. Imaging was performed using the Eclipse TE2000 microscope from Nikon equipped with a 60× Plan Apochromat NA 1.4 immersion objective combined with Perfect Focus System (Nikon) and a top stage incubation chamber and objective heater (Tokai Hit). The microscope was setup for the experiment 1hr before the start to attain optimal temperature and CO₂ conditions. GFP-actin expressing cells were identified by excitation with a CoolLED pE-100 470nm system. Emission was filtered through a 493/574-nm dual-band beam splitter and recorded with an Orca Flash 4.0 (Hamamatsu) camera. Cells were imaged for 1350 sec at 15-sec intervals with an exposure time of 400msec with 2X2 binning. Kymographs were generated and analysed using the ImageJ Kymograph plugin. Velocity of actin dynamics was calculated as the total track distance divided by the total time (1350sec) from each kymograph.

5.19 G/F-actin ratio measurement.

The cells for G/F-actin ratio measurements were washed three times in 37°C PBS before lysis with actin stabilization buffer. The lysates were kept on ice for 10 minutes. Cells were dislodged by scraping and the entire extract centrifuged at 4°C for 75 minutes in a tabletop centrifuge at 100.000 g. The supernatant containing G-actin was recovered and the pellet containing F-actin separated.

Table 21: G-actin stabilization buffer.

PIPES, pH 6.9	0.1 M
Glycerol	30%
DMSO	5%
MgSO ₄	1 mM
EGTA	1 mM
TX-100	1%
ATP	1 mM
1x Complete Protease Inhibitor (Roche)	1 tablet for 10 ml

Table 22: F-actin depolymerization buffer.

PIPES, pH 6.9	0.1 M
CaCl ₂	10 mM
cytochalasin D	5 μM
MgSO ₄	1 mM

The F-actin was solubilised with actin depolymerization buffer. Aliquots of supernatant and pellet fractions were separated on 12% SDS-PAGE gels and then western blotted with monoclonal anti-β-actin antibody. Signal was detected by ECL in a digital dark room and integrated optical band density was used to estimate the cellular F/G-actin ratio.

5.20 SDS-PAGE and Western blotting.

Protein levels or posttranslational modifications such as phosphorylation were detected using the sodiumdodecylsulfate polyacrylamide electrophoresis (SDS-PAGE). Gels of different density were prepared according to the table below.

Table 23: Resolving Gel

Gel Percentage	8%	10%	12%	15%
30% Polyacrylamide (ml)	4	5	6	7.5
1.5 M Tris-HCl (pH: 8.8) (ml)	3.75	3.75	3.75	3.75
10% SDS (μl)	150	150	150	150
10% APS (μl)	150	150	150	150
TEMED (μl)	9	6	6	6
Water (ml)	6.95	5.95	4.95	3.45
Total Volume (ml)	15	15	15	15

Table 24: Stacking Gel

Gel Percentage	4%
30% Polyacrylamide (ml)	1.7
1.0 M Tris-HCl(pH: 6.8) (ml)	1.25
10% SDS (μ l)	100
10% APS (μ l)	100
TEMED (μ l)	10
Water (ml)	6.8
Total Volume (ml)	10

The proteins migrate in an electric field and are separated according to their size because SDS provides a uniform negative charge to the proteins. Gels of different percentage were used depending on the size of protein to be separated.

Protein lysates were heated to 95°C for 5 min and stored at -20°C until used. Denatured protein lysates were loaded onto the gels, besides the pre-stained protein ladder (Fermentas, #SM0671). Gels were subjected to 80 volt for about 10-15 minutes until the proteins move into the separating gel, followed by a complete run at 120 volt for about 45-50 minutes. Subsequently, proteins were transferred to a methanol activated PVDF membrane (Whatman) in a semidry electro blotting system (Thermo Fisher Scientific) with a current of 1.0 mA per cm² membrane for 2 hours.

Table 25: Blot size for protein blotting.

Gel size	Voltage and current	time
12cmX5cm(Biometra)	120mA current constant	1.5hr
7cmX8.4cm(Biorad)	120mA	1.3hr

Membranes were rinsed in 1X TBST for 1 min before blocking the membrane for 1 h in blocking buffer to reduce unspecific binding of the antibody. The membrane was incubated with the respective primary antibodies overnight at 4°C. After washing the membrane three times for 10 min in TBST, antibody antigen complexes were detected by respective HRP linked donkey anti rabbit or sheep anti mouse secondary antibodies. Then the blot was washed three times 10 min each in TBST, incubated in ECL solution before

exposure to x-ray film (Konica Minolta) and subsequent development or direct imaging (ChemoCam Imager INTAS). For reprobing with other antibodies, membranes were reactivated with 100% methanol and incubated in stripping buffer for 30 min at RT (room temperature), after which the membrane was blocked for 1 h and then taken up for primary and secondary antibody for detection (as described above).

5.21 Coomassie staining for protein gels.

The SDS-PAGE gel was removed from the glass and rinsed once in ddH₂O in a suitable container with a lid. The gel was fixed with a fixing solution of 30min. Coomassie stain was added to the fixed gel such that it covered the gel and placed in a microwave oven on high power for 40seconds to 1 minute (until the Coomassie stain boiled). The gel was then incubated at room temperature for 5 to 10 minutes on a rocking table. The stain was poured off and rinsed twice in ddH₂O. Destain solution was added to cover the gel. Kimwipes were added to absorb the stain. The gel was again placed in a microwave oven on high power for 40 seconds to 1 minute (until the destain solution boiled), and then incubated for 10 minutes on a rocking table. The former detaining step was repeated till the expected staining was obtained.

Table 26: Gel fixing solution:

o-Phosphoric acid 85 %	1 ml
Methanol	20 ml
Water	79 ml

Table 27: Coomassie stain.

Water	500ml
Glacial acetic acid	100 ml
Methanol	400 ml
Coomassie R250	1 g
Total volume	1 liter

Table 28: Destain solution.

Water	700ml
Glacial acetic acid	100 ml
Methanol	200 ml
Total volume	1 liter

5.22 Cloning.

5.22.1 Polymerase chain reaction (PCR).

For amplification of the required open reading frame into a plasmid cDNA was used as a template. A standard PCR reaction was performed as following:

25ng DNA, 1.5 µl each of forward and reverse primer (10pmole), 5 µl 3prime PCR buffer, 1 µl *pfu* (proof reading DNA polymerase selfmade in lab from addgene Plasmid number #12509), 1 µl 10mM dNTPs and H₂O to fill up the volume to 50µl. The amplified product was analysed by gel electrophoresis.

Table 29: PCR cycling conditions.

Cycle condtions	Time	Temperature
Denaturing	5min	95°C
Anealing	30 sec	95°C
Extension	30 sec	Primer specific
Extension	2.5min	72°C X 32 cycles
Final Extension	7min	72°C
Hold		2°C

5.22.2 Restriction enzyme digestion and analysis of DNA fragments.

Cloning was done using protocols of the standard laboratory manual of Sambrook et al. For restriction digestion of plasmids for cloning, 2.0µg DNA was used with 2-5 units of

restriction enzyme and appropriate buffer depending on the restriction enzyme used. The reaction volume was 50µl. For the cloning of PCR products, the entire volume of the PCR (50µl) was purified using PCR purification kit (Qiagen) and used for the restriction digestion. The reaction was incubated at 37°C for 2-6 hours and analyzed by gel electrophoresis on 0.8% to 2% agarose gel in 1X TAE buffer depending on the size of the expected DNA fragments which were visualized using a UV detector.

5.22.3 Ligation of restricted fragment into vector.

The vector backbone and the insert after restriction was analysed on an agarose gel and the concentration of the DNA estimated with the help of the marker. The ligation ratio of insert to vector is 1:5; i.e. for 1 part of vector we take 5 parts of fragment.

$$\text{Fragment (ng)} = 125\text{ng} \times \text{length of fragment (bp)} \div \text{length of vector (bp)}$$

$$(125\text{ng} = 50\text{ng of vector} \times 5)$$

Table 30: Ligation reaction setup.

10X ligation buffer	2 µl
T4-DNA-ligases	2µl
Insert	5 times of insert
vector	50ng
Water	Make up to total
Total volume	20µl

At the same time a parallel control only containing vector DNA and no insert was prepared to test the vector re-ligation. The reactions were incubated overnight at 16°C.

5.22.4 Sequencing.

Sequencing of DNA was performed by Sanger sequencing [202] using terminator dye (Applied Biosystems). The terminator dye help in the incorporation of the four used dideoxynucleotides (ddNTP), lacking the 3'-OH group and labeled with a different fluorescent dye. The fragments of the PCR reaction thus generated are of various lengths depending upon the incorporation of the dideoxynucleotides. These fragments were separated by size capillary electrophoresis. At the end scanning the fluorescent signals of chains separated by size identified the sequence. The sequencing was done by following protocol.

PCR reaction for Plasmid:

DNA	-500ng
Terminator mix	-2 μ l
5X Sequencing Buffer	-4 μ l
Primer	- 15pmole

fill up to a total volume of 20 μ l with HPLC water

PCR reaction for PCR product:

DNA	-150ng
Terminator mix	-1 μ l
5X Sequencing Buffer	-4 μ l
Primer	- 15pmole

fill up to a total volume of 20 μ l with HPLC water

Cycling conditions

10 sec	95°C	
4 min	60°C	} X25
5 min	60°C	
hold	22°C	

The PCR product was precipitated by adding 50µl of 100% ethanol and 2µl of 3M sodium acetate. The DNA was pelleted by centrifugation at 14,000rpm for 20min at 4°C, the pellet was washed twice with 70% ethanol, air dried and dissolved in 20µl of Hi-Di formamide and used for sequencing.

5.22.5 Transformation of chemical competent *E.coli*.

Either TOP10 or BL21 chemically competent *E.coli* cells were used for the transformation of the ligated DNA. 2-5µl ligation reactions was added to 50µl of competent cells and incubated on ice for 30min. The cells were given a temperature shock by incubating them at 42°C in water bath for 90sec or 40°C in thermoshaker for 90sec and then transferred to ice for 2mins. Prewarmed 180µl of SOB medium was added and bacteria were allowed to recover for 60min at 37°C. 100µl of the transformed bacteria were plated on LB-agar plates with appropriate antibiotic as a selection marker, incubated overnight and colonies were selected and grown in 5ml LB medium with antibiotics overnight and DNA was isolated by mini prep to screen for positive clones. Mini preps were performed by alkali lysis method using SeqLab Miniprep plasmid kit. The resultant DNA was screened by restriction digestion profile followed by sequencing of the clone to confirm the identity of the positive clone.

5.22.6 Easy prep plasmid purification.

Easy prep plasmid purification was used for screening large number of clones. It is an easy and cheap method.

Table 31: Lysis buffer for plasmid purification.

Solution constituents	For 50ml lysis buffer
10mM Tris-HCl pH 8.0	500µl from 1M stock solution
1mM EDTA	100µl from 0.5M stock solution
15% Sucrose	7.5g
0.4mg/ml RNase	2ml from 10mg/ml stock
2mg/ml lysozyme	100mg
0.1mg/ml BSA	5mg

Clones were picked and incubated overnight in 1.5ml starter culture. The overnight cultures were centrifuged at 6000xg for 30 sec., the supernatant sucked off completely with a vacuum pump sucker. The dry pellets were resuspended with 50µl lysis buffer. The mixture was incubated in room temperature for 5min. This mixture was boiled for 2min at 99°C in a thermoshaker or 30sec at 100°C in a water bath. The mixture was immediately incubated on ice for 60sec and centrifuged at 20000xg for 20min. After centrifugation 5µl of the supernatant was used for restriction digestion. The purification can only be used for restriction digestion analysis and cannot be used for sequencing reactions. Strains that have a *recA*-insert such as JM105, JM109, and XL-1 Blue cannot be processed with this method.

5.23 Cross linking antibody to beads for LC-MS analysis.

Crosslinking enables elution of protein with little antibody contamination. The beads in use (based on the affinity to the antibody employed) were washed with PBS at 4°C overnight. The overnight washed beads are separated from the PBS by centrifugation. The washed beads are incubated for 10min with dilution buffer at 4°C. During the incubation time the required antibody for the pull down and IgG control was mixed in dilution buffer. The beads after incubation were separated from the buffer and mixed with the antibody containing dilution buffer and incubated at 4°C overnight in a rotating shaker. The beads after overnight incubation were separated from the supernatant and washed with fresh dilution buffer and then with PBS. The beads were mixed with freshly prepared crosslinking solution and were allowed to rotate in a rotating shaker for 30min. The beads were washed with washing buffer and again the crosslinking solution was added as of the previous step for three times. After the crosslinking step the beads were then quenched with quenching buffer for 5min in a rotating shaker, then washed with PBS. The quenching step was repeated as of the previous step and washed with PBS. The excess unlinked antibody in the beads was removed by washing with 1 M glycine pH 3.0 for 10min in a rotating shaker, and then the beads were cleaned with PBS three times and stored in 4°C till use.

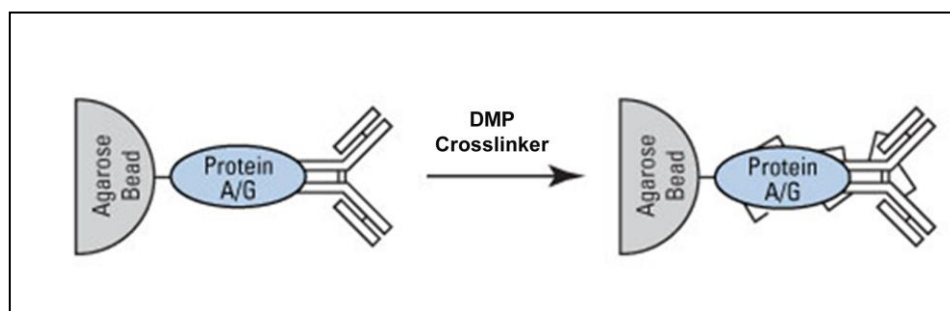


Figure 6: Crossling of beads with antibody.

Table 32: Table of affinity of protein A and protein G coupled beads to mouse and rabbit antibody.

Antibody	Protein A	Protein G
Mouse IgG ₁	+	++++
Mouse IgG _{2a}	++++	++++
Mouse IgG _{2b}	+++	+++
Mouse IgG ₃	++	+++
Rabbit	++++	+++

5.24 Quantitative PCR.

To quantify the amount of specific mRNA populations, qRT-PCR was performed. Amplification of cDNA and quantification of amplicates were performed by using the Roche SYBR green system. The primer specific optimisation was done for the MgCl₂ condensation.

MgCl ₂ concentration	1mM	2mM	3mM	4mM	5mM
MgCl ₂ (μl)	0.4	0.8	1.2	1.6	2.0
H ₂ O (μl)	16.6	16.2	15.8	15.4	15

The light cycle program for faststart DNA Master SYBR Green 1 kit

Reaction		Temperature	Time (min:Sec)
		95°C	10:00
45 Cycle	Denaturation	95°C	00:10
	Annealing	55°C	00:10
	Elongation	72°C	00:05

Recording melting curve	95°C	00:00
	60°C	00:15
	0.1°Cs ⁻¹ to 95°C	
Cool	40°C	

5.25 Immunoprecipitation of protein-RNA complexes.

The protein-RNA complexes were pulled down from the cytosolic fraction as per the immunoprecipitation protocol mentioned in method (5.16). Before harvesting, the cells were washed three times with ice cold PBS. Freshly prepared cytoplasmic lysis buffer was used for each lysis. The lysis buffer was added to the cell culture plate and incubated on a shaker for 10min on ice. The lysate was collected in a fresh 1.5 ml centrifuge tube and centrifuged at 5000g for 5min. The collected supernatant contained the cytosolic extract, which then could be used for subsequent experiments.

The supernatant was mixed with pre-cleaned beads and was incubated in a rotatory shaker for 1hr. The pre-cleaned lysates were collected for each condition and divided into 2 parts. One part was mixed with RNase at 100µg/ml and the other part kept without RNase. The divided fraction was incubated HA crossed linked beads and the corresponding IgG control and incubated for 6hr at 4°C. The resin was washed 5 times with binding buffer to remove unbound proteins. For elution, beads were boiled in 2 x Laemmli buffer at 95 °C for 5 minutes. The eluted proteins were then analyzed by Western blotting using specific antibodies against each protein.

For the isolation of RNA that was bound to proteins, the beads were washed again three times with lysis buffer containing 1M urea. This step was added to remove any secondary interacting protein from the complex. The beads were then lysed with lysis buffer with 0.1% SDS, 30µg proteinase K and DNases. This sample was then incubated in a heating block at 50°C for 30min. After the incubation 100µl of Phenol:Chloroform:Isoamyl Alcohol (25:24:1) was added and mixed by vortexing. The water phase (upper) was removed after a quick 1min centrifugation. To precipitate the RNA from the water phase 12µl of 3M sodium acetate, 250µl ethanol (100%) and 1µl Glycogen Blue was added for 100µL collected water phase. This sample was incubated overnight at -20°C. The overnight-incubated samples were

centrifuged at 16,000xg for 20min. The supernatant was completely removed and the pellet was air-dried. The pellet was used directly for cDNA synthesis.

cDNA synthesis mix:

Random primer (50ng/ μ l)	1 μ l
dNTP mix (10mM)	1 μ l
water	12 μ l
total volume	13 μ l

The cDNA mix was directly added to the pellet and incubated at 65°C for 5min. Then the mix was incubated on ice for 1min after a short spin. The first strand synthesis mix was added to the mixture.

5X First strand buffer	4 μ l
DTT	1 μ l
Rnase out	1 μ l
Super script III	1 μ l
Total	7 μ l

The mixture was mixed by pipetting and incubated for 25°C for 5min, then incubated for 60min at 50°C. The reaction was inactivated by incubating at 70°C for 15min. The sample was analysed by quantitative PCR.

5.26 Statistical analysis.

Sample size was chosen according to standard practice in the field, taking into account available numbers of cells per *in vitro* experiment. At least three independent experiments were performed for statistical analysis. Data are expressed as mean \pm standard error of the mean (SEM). ‘n’ indicates the total number of analyzed specimens, e.g. axons or growth cones. Student's unpaired t test was performed for comparison between two groups (GraphPad

Prism4). One-way analysis of variance (ANOVA) with Bonferroni's tests was used for data analysis of more than two groups (GraphPad Prism4). Densitometric intensities of bands from western blots were normalized to loading controls or total protein levels. Values from control conditions in each independent experiment were set as 1. One-sample t test was used to compare the means to this reference value. Values from at least three independent experiments were pooled, and results were expressed as the mean \pm s.e.m. and applied for statistical analysis using GraphPad Prism4 software.

6. RESULTS

6.1 Protein purification of murine recombinant hnRNP R and SMN.

According to an already established protocol for the purification of His tagged hnRNP R [45] the hnRNP R full length protein, a construct for the 1-430 amino acid N-terminal fragment of hnRNP R and the C-terminal fragment (431 to 632 amino acids) was also cloned into a pETM11 vector system that contains a Tev cleavage site at the N-terminal part. The constructs for pETM11::hnRNP R, pET 28 A::hnRNP R, pETM11::N-terminal hnRNP R and pETM11::C-terminal fragment were transformed into *E. coli* BL21- DE3 (NOVAGEN). In each case a single colony was used to inoculate a 100 ml LB Kam/Amp pre-culture. Bacteria were transferred into LB Kam/Amp and grown at 37°C and 200 rpm until the optical density (oD600) reached 0.5. Expression was induced by the addition of 0.1 mM IPTG and continued for 20 h at 20°C.

Bacteria were harvested by centrifugation and lysed with lysis buffer by the use of a cell disruptor system. The lysate was cleared by centrifugation and the supernatant was then incubated with pre-equilibrated HisTap 1ml column. The column was washed with 40CV (column volume) washing buffer till a stable base line was obtained. The protein was eluted with a step elution from 10%, 20%, 40%, 60%, 80%, and 100% with 3CV elution each. The peak fractions were analyzed by SDS-PAGE.

The elution fractions 60% to 100% were subjected to size-exclusion chromatography using a HiLoad™ 26/60 Superdex™ 200 pg column with gel purification buffer. The eluted proteins were analyzed by SDS-PAGE and concentrated in centrifuge concentrators (MW cutoff: 10,000 Da). The protein concentration was determined spectrophotometrically (hnRNP R: MW=70.88, $\epsilon_{280} = 87350 \text{ M}^{-1} \text{ cm}^{-1}$, N-terminal hnRNP R: MW=48.36, $\epsilon_{280} = 34630 \text{ M}^{-1} \text{ cm}^{-1}$, C-terminal hnRNP R: MW=22.54, $\epsilon_{280} = 52720 \text{ M}^{-1} \text{ cm}^{-1}$). The samples were flash frozen with liquid nitrogen and stored at -80°C

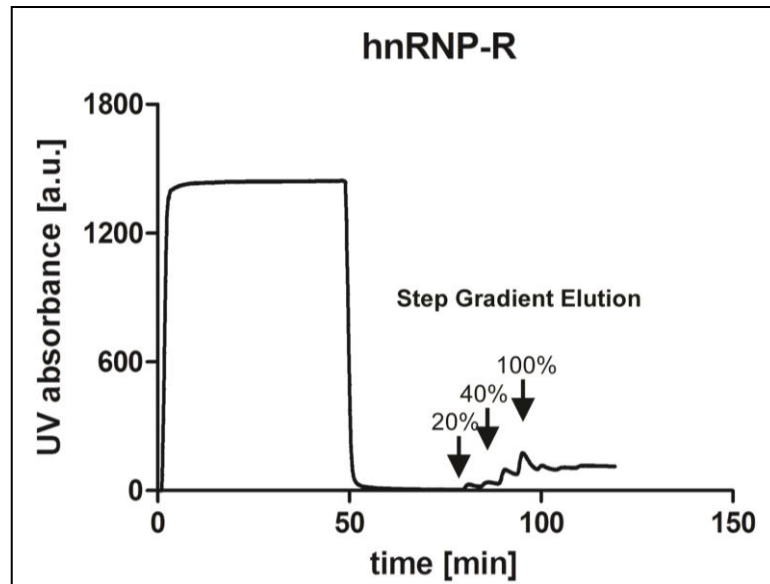


Figure 7: Purification scheme of recombinant hnRNP R expressed as His-tagged protein in *E. coli* strain BL21. (Dombert, Sivadasan et al. 2014. PLoS One 9(10): e110846)

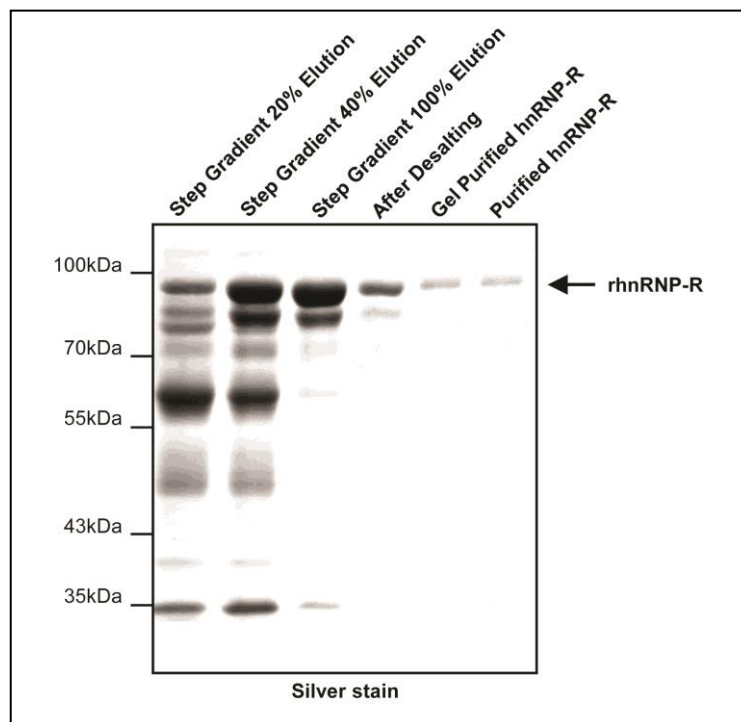


Figure 8: Affinity purification profile on a fast protein liquid chromatography (FPLC) of hnRNP R and SDS-PAGE of recombinant hnRNP R purification steps visualized by silver staining. (Dombert, Sivadasan et al. 2014. PLoS One 9(10): e110846)

A construct encoding SMN was cloned into a pET32A vector system. The Pet 32A vector adds an extra trxA tag (18 kDa) to the protein. The pET32A::SMN construct was transformed into *E. coli* BL21- DE3 cells. A single colony was used to inoculate a 100 ml LB_{Amp} pre-culture. Bacteria were transferred into 2 L LB_{Kam/Amp} and grown at 37°C and 200

rpm until the optical density (oD600) reached 0.5. Expression was induced by the addition of 0.1 mM IPTG and continued for 20 h at 18°C.

Bacteria were harvested and SMN protein was affinity purified as described above for hnRNP R. The protein concentration was determined spectrophotometrically (SMN: MW=49.8 kDa, $\epsilon_{280} = 87350 \text{ M}^{-1} \text{ cm}^{-1}$). The samples were flash frozen with liquid nitrogen and stored at -80°C.

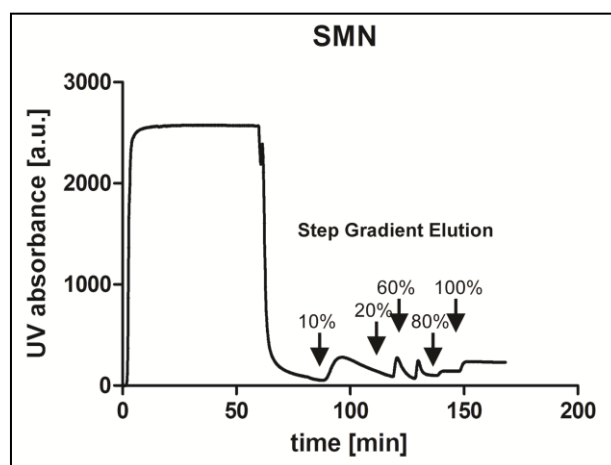


Figure 9: Purification scheme of recombinant SMN expressed as His-tagged protein in *E. coli* strain BL21. (Dombert, Sivadasan et al. 2014. PLoS One 9(10): e110846)

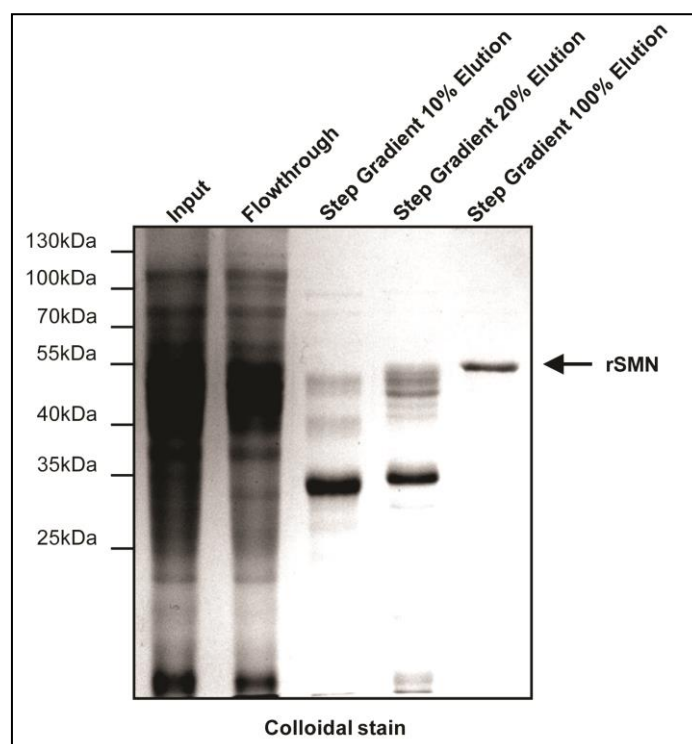


Figure 10: Affinity purification profile on a FPLC of SMN and SDS-PAGE of recombinant SMN purification steps visualized by colloidal staining. (Dombert, Sivadasan et al. 2014. PLoS One 9(10): e110846)

6.2 Protein purification of murine recombinant TDP-43.

Constructs encoding the full length TDP-43, its fragments and mutant isoforms (Figure 11 and 12) were cloned in the pET32A vector and pETM11 Vector systems. The clones were transformed into *E. coli* BL21- DE3 cells. A single colony was used to inoculate a 100 ml LB_{Amp} pre-culture. Bacteria were transferred into 2L LB_{Kam/Amp} and grown at 37 °C and 200 rpm until the optical density (oD600) reached 0.5. Expression was induced by the addition of 0.1 mM IPTG and continued for 20 h at 15°C.

Bacteria were harvested by centrifugation and lysed with lysis buffer by the use of a cell disruptor system. The lysate was cleared by centrifugation and the supernatant was then incubated with pre-equilibrated HisTap 1ml column. The column was washed with 40CV washing buffer till a stable base line was obtained. The protein was eluted with 100% elution buffer with 10CV elution volumes. The peak fractions were analyzed by SDS-PAGE. The Affinity purified proteins were dialysed with the IEX buffer with a HiPrep 26/10 desalting column (CV 53 ml). The desalted eluted peak was passed through a cation-exchange column and washed with 20 CV of IEX buffer. The protein was eluted by a gradient up to 1 M NaCl.

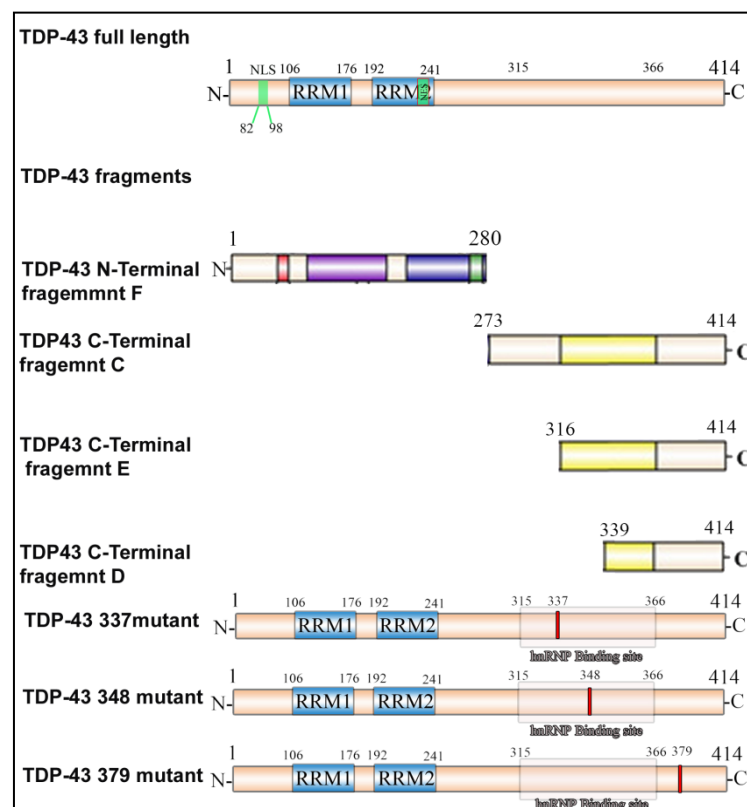


Figure 11: TDP-43 Full length, fragments and mutants.

The IEX purified samples were used for size-exclusion chromatography using a HiLoad™ 26/60 Superdex™ 200 pg column with gel purification buffer. The eluted proteins were analyzed by SDS-PAGE and concentrated in centrifuge concentrators (MW cutoff: 10,000 Da). The protein concentration was determined spectrophotometrically (TDP-43: MW=64.3 kDa, $\epsilon_{280} = 45295 \text{ M}^{-1} \text{ cm}^{-1}$, TDP-43 N-terminal MW=kDa, $\epsilon_{280} = 27305 \text{ M}^{-1} \text{ cm}^{-1}$, TDP-43 C-terminal fragment MW=kDa, $\epsilon_{280} = 17990 \text{ M}^{-1} \text{ cm}^{-1}$). The samples were flash frozen with liquid nitrogen and stored at -80°C .

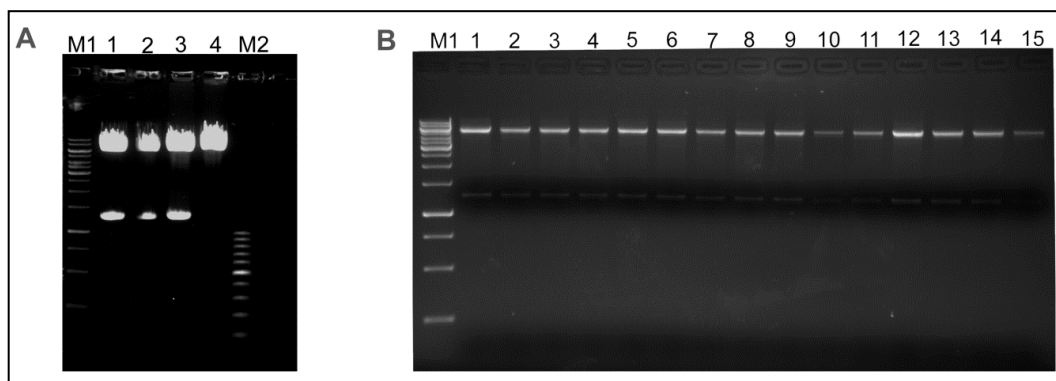


Figure 12: Cloning of TDP-43 mutants.

A) M1-Marker 1Kb, 1. TDP-43 337, 2. TDP-43 348, 3. TDP-43 379, 4. Empty vector, and M2 100Bp Marker. B) Restriction digestion of pETM-11 TDP43 mutant positive clones.

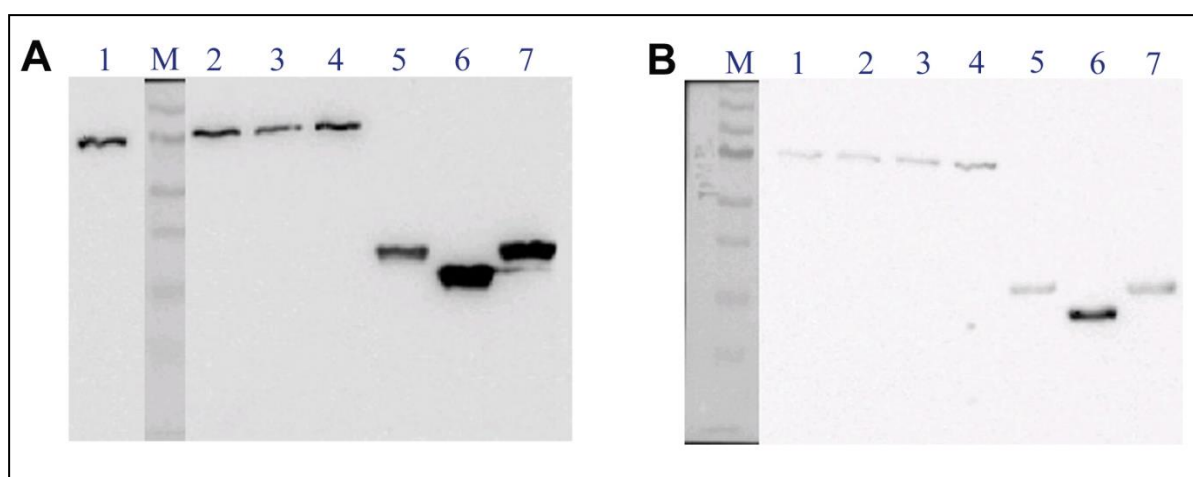


Figure 13: Western blot for TDP43, mutants and fragments.

(A) Western blot developed with TDP-43 antibody, (B) Western blot developed with His antibody. 1. TDP-43 WT, M. Marker 2. TDP-43 337, 3. TDP-43 348, 4. TDP-43 379, 5. C-terminal fragment TDP-43, 6. Fragment E of C-terminal TDP-43 and 7. C-terminal fragment TDP-43.

6.3 HnRNP R interaction with SMN in motoneurons.

Previous studies have shown the interaction of hnRNP R and SMN [45, 47] by a yeast two-hybrid (Y2H) screen using a mouse brain library and over expression system in cell lines. In order to investigate the cellular compartment for interaction in detail, immunoprecipitation of pure nuclear and cytosolic fractions was done from cultured motoneurons, spinal cord tissue of E18 mouse embryos, and cultured HEK293T cells. Pure motoneurons were cultured for 7DIV on laminin-111 since the relative proportion of cytosolic hnRNP R and the degree of overlap with SMN protein in distinct compartments was highest at this time point. A single E18 spinal cord from a mouse embryo was used for each fractionation. The fractionation of nuclear and cytosolic parts was controlled with antibodies against histone H3 used as a marker for the nuclear fraction and β III tubulin and GAPDH as markers for the cytosolic fraction. As expected hnRNP R was found in both nuclear and cytosolic fraction of all three-cell types.

Intriguingly, an interaction of SMN and hnRNP R was predominantly detected in cytosolic compartments of cultured motoneurons (Figure 14 A) and spinal cord tissue (Figure 14 B). Pulldown of hnRNP R clearly co-precipitated SMN and *vice versa*. Surprisingly, the nuclear fraction did not show any interaction of SMN and hnRNP R. It needs to be considered that the nuclear fraction contained only the soluble nuclear fraction. As the nuclear lysis buffer does not contain any harsh detergents or high salt concentration, the Cajal bodies/Gems (Cajal/Gems) where SMN is found [203, 204] are not dissolved. HEK293T cells differ from primary motoneurons and spinal cord extracts by showing much higher nuclear SMN levels which can be detected in soluble fractions together with hnRNP R (Figure 14 C). Also in these cells, no interaction of SMN and hnRNP R was found by co-immunoprecipitation, neither in the cytosol nor in the nucleus, suggesting that this interaction is cell type and possibly also compartment specific (Figure 14 C).

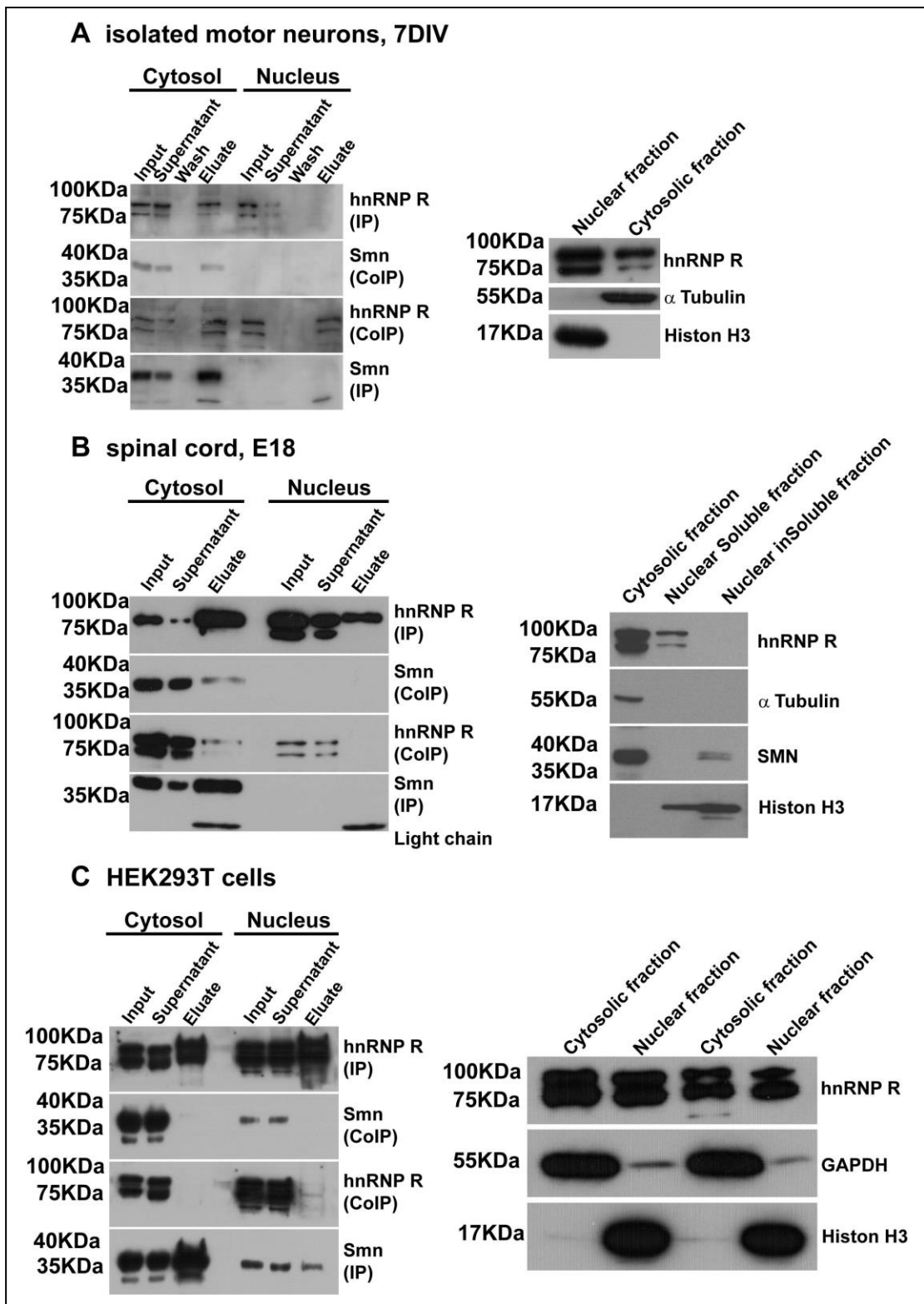


Figure 14: Coimmunoprecipitation of SMN and hnRNP R in primary motoneurons, native spinal cord and HEK293T cells.

(A) 1,000,000 primary motoneurons were cultured for 7DIV on laminin-111. Cytosolic and soluble nuclear fractions were subjected to a pull-down with either SMN or hnRNP R antibodies, respectively. Coprecipitation of hnRNP R or SMN, respectively, was determined revealing an interaction of SMN and hnRNP R, particularly in the cytosolic fraction of embryonic mouse motoneurons (eluate lane). SMN was not detectable in the soluble nuclear

fraction of motoneurons. HnRNP R was found both in nuclear and cytosolic extracts. For immunoprecipitation experiments an antibody directed against the C-terminus of hnRNP R (Abcam) was used. Supernatants after IP still contained some SMN or hnRNP R protein, respectively, suggesting that the interaction appears not to be exclusive as demonstrated by immunofluorescence colocalization analysis. No signal was obtained in the washing solution. Successful fractionation was controlled by alpha tubulin (cytosol) and histone H3 (nucleus) (right panel). (B) Fractionation of spinal cord tissue from E18 mouse embryos revealed a similar result as shown in (A). In the cytosolic fraction hnRNP R IP pulled-down SMN protein and *vice versa*. Nuclear SMN was not detected in the soluble, but in the corresponding insoluble nuclear fraction (right panel, lower blot). In contrast, nuclear hnRNP R was not found in the insoluble nuclear fraction. Cytosolic and nuclear extracts were validated by alpha tubulin and histone H3. (C) HEK293T cells were cultured and cytosolic and soluble nuclear fractions were prepared. SMN and hnRNP R were detected in cytosolic extracts as well as in soluble nuclear fractions. The pull down of SMN and hnRNP R, respectively, was successful (eluate lane, IP), but hnRNP R or SMN, respectively, could not be coprecipitated, neither from cytosolic nor from nuclear extracts. Successful fractionation was verified by anti-GAPDH (cytosolic) and anti-histone H3 (nucleus) antibodies (Dombert, Sivadasan et al. 2014. PLoS One 9(10): e110846).

6.4 Direct SMN interaction with hnRNP R modulates affinity of hnRNP R.

The direct association between hnRNP R and SMN was analyzed by co-immunoprecipitations of recombinant proteins. Two different concentrations were used to check the interaction of SMN to hnRNP R as shown below.

	SMN Concentration ratio	hnRNP R Concentration ratio
1.	1	1
2.	1	2

Different concentrations of bacterially expressed SMN or hnRNP R protein were dialyzed separately in binding buffer (20 mM HEPES (pH 7.0), 10% glycerol, 150 mM NaCl and 0.02 % Tween, 2.5mM MgCl₂). The dialyzed proteins were incubated together with binding buffer for 1hr at room temperature. The protein mixture was then incubated with 20 µl beads and 1 µg antibodies against hnRNP R, SMN or IgG control, respectively, for 1 h at room temperature. The resin was washed 5 times with binding buffer to remove unbound proteins. For elution, beads were boiled in 2 x Laemmli buffer at 95 °C for 5 minutes. The

eluted proteins were then analyzed by Western blotting using specific antibodies against each protein.

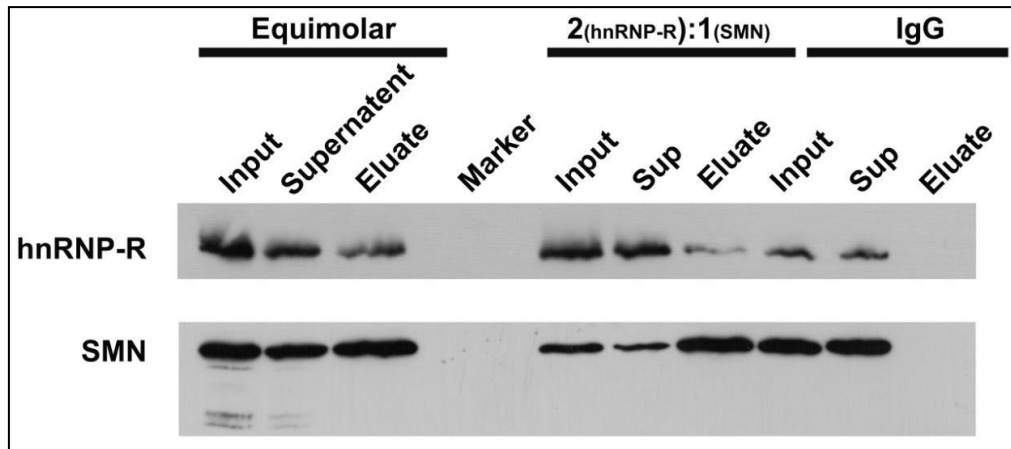


Figure 15: SMN immunoprecipitations from recombinant proteins and co-immunoprecipitations of hnRNP R. The blot indicate that at equimolar or 2:1 ratio, the two recombinant proteins can interact directly *in vitro* and the interaction can be efficiently pulled down with antibodies against hnRNP R.

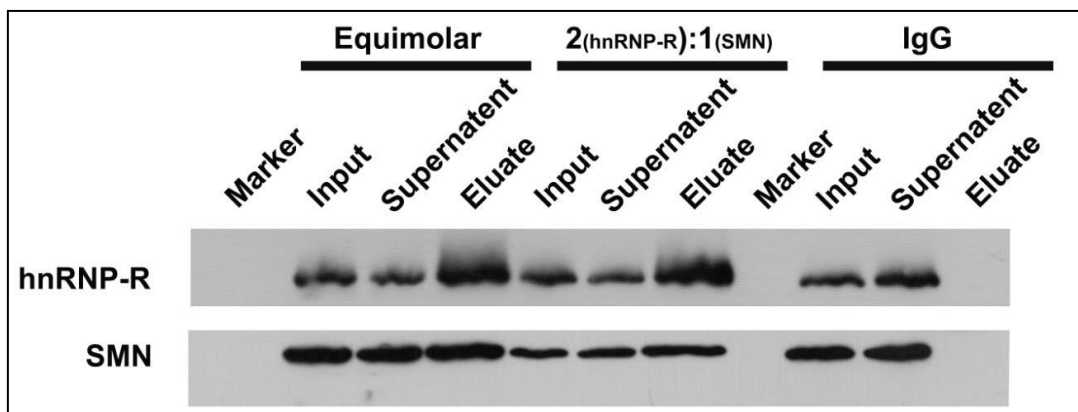


Figure 16: Recombinant hnRNP R immunoprecipitations and co-immunoprecipitations of SMN. The blot indicate that at equimolar or 2:1 ratio, the two recombinant proteins can interact directly *in vitro* and the interaction can be efficiently pulled down with antibodies against SMN.

Immunoprecipitation of recombinant protein by SMN and hnRNP R antibodies revealed distinct interactions with hnRNP R (Figure 15) and vice versa (Figure 16). SMN and hnRNP R could be precipitated with antibodies against either protein at different concentrations. These data indicate that SMN and hnRNP R can interact with each other and that other binding partners are not necessary for this interaction. HnRNPs are known to form homomeric interactions [205]. In order to test whether the formation of hnRNP R dimers

influences binding to SMN, we doubled the amount of recombinant hnRNP R in this assay. When SMN was now pulled down, less hnRNP R was co-immunoprecipitated and vice versa, whereas the efficacy of the immunoprecipitation itself was comparable between both experimental conditions (Figure 15 and 16). The IgG control was negative thus validating the specificity of the detected interaction (Figure 15 and 16). From this data we can conclude that hnRNP R and SMN can interact directly without the help of another interacting protein.

6.5 Depletion of SMN alters the subcellular distribution of hnRNP R in motoneurons.

In order to determine the functional influence of SMN on the subcellular distribution of the hnRNP R protein and vice versa in motoneurons, a lentiviral construct was created to knockdown SMN and hnRNP R proteins. The hnRNP R knockdown construct was created to down regulate all three isoforms of hnRNP R (Figure 17 B) [206]. Western Blot analysis verified the specificity of the applied hnRNP R and SMN antibodies (Figure 17 A and C). The depletion of hnRNP R did not alter total protein levels of SMN in motoneurons (Figure 17 A).

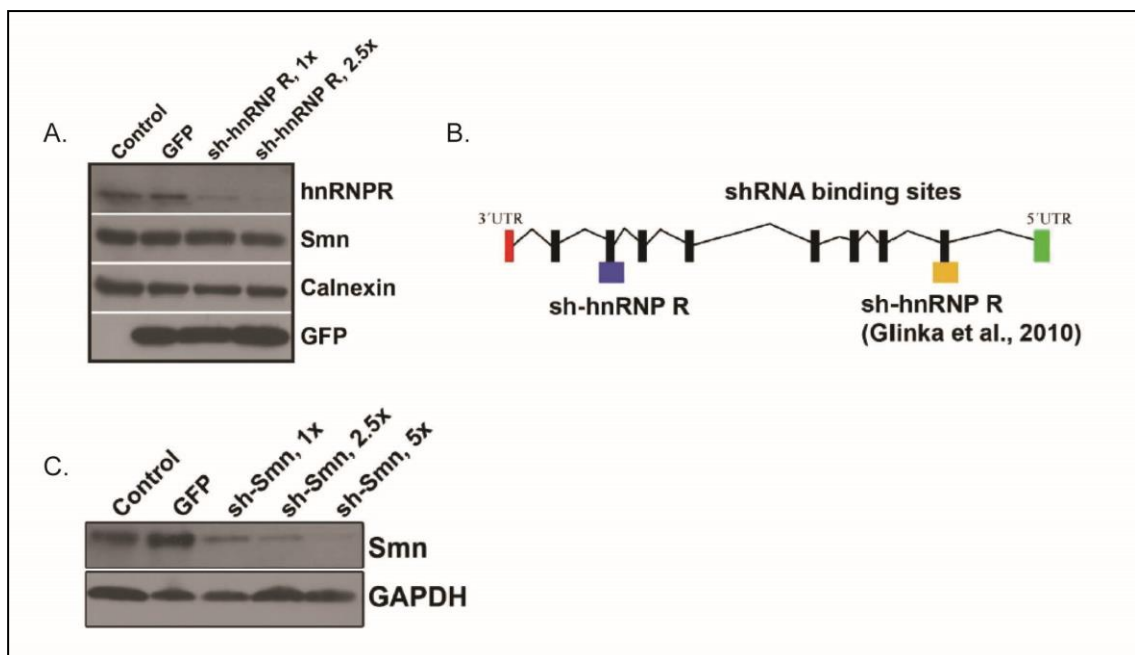


Figure 17: Lentiviral knockdown of hnRNP R and SMN in motoneurons.

(A) Motoneurons showed reduced hnRNP R protein levels upon lentiviral knockdown. Uninfected or GFP-infected mouse embryonic motoneurons were used as controls. Levels of calnexin and SMN were not affected. (B) Two shRNA binding sites were designed to deplete hnRNP R protein. In this study, the one near the 3'UTR was used since it affects all predicted hnRNP R isoforms identified by database research. The other lentiviral construct was applied and verified as previously reported [45]. (C) Lentiviral knockdown of SMN led to a dose-

dependent reduction of SMN levels. GAPDH protein was not altered significantly. (Dombert, Sivadasan et al. 2014. PLoS One 9(10): e110846)

The distribution of hnRNP R between nucleus and cytoplasm after SMN depletion was investigated by subcellular fractions of motoneurons followed by Western Blot analyses (Figure 18 A-B). Antibodies against histone (H3) were used as a marker for nuclear fractions and β III-tubulin or GAPDH as markers for cytosolic fractions. SMN levels in soluble nuclear fractions were below the detection limit (Figure 18 A). Cytoplasmic SMN was highly reduced by 89% ($p=0.0053$) after lentiviral knockdown (Figure 18 B). In comparison to GFP control levels, cytoplasmic hnRNP R was decreased by 38% (non-significant, $p=0.1299$), whereas hnRNP R levels in the nucleus remained unchanged with a small non-significant increase by 15% ($p=0.45$) (Figure 17 B). Normalizing hnRNP R signals of nuclear or cytosolic fractions against histone or tubulin, respectively, compared signal intensities. Statistical analysis of the relative ratio between cytosolic and nuclear content revealed a significant drop of this ratio by 47% ($p=0.0256$) after SMN knockdown (Figure 17-B left). Interestingly, the effect on hnRNP R translocation strongly relied on the efficacy of the performed knockdown. When the remaining SMN levels were higher than 40% of control levels no shift in hnRNP R translocation was observed.

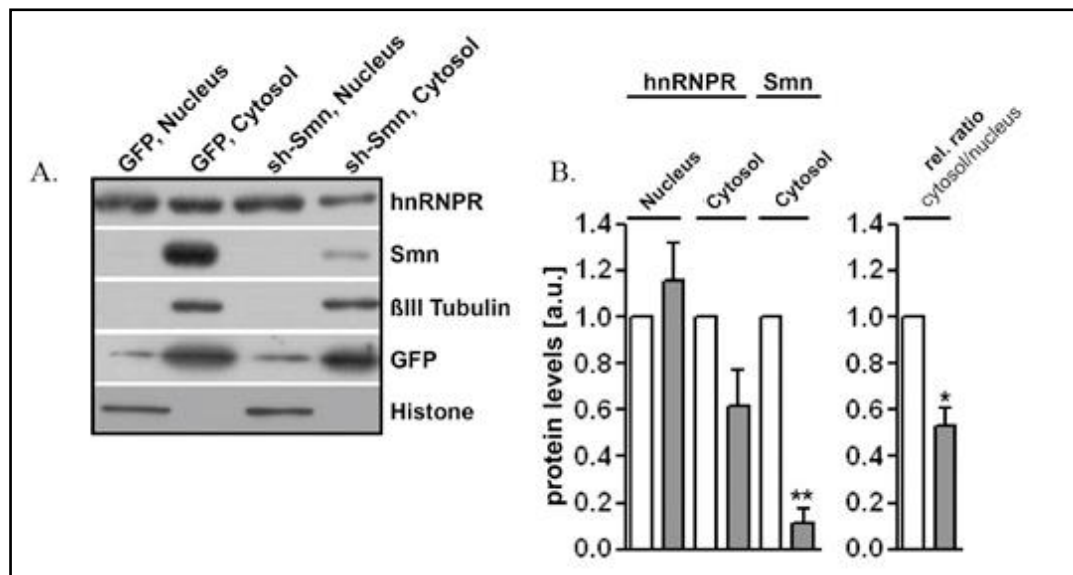


Figure 18: Subcellular distribution of SMN and hnRNP R protein in primary mouse motoneurons.

(A) Cytosolic and nuclear fractions were prepared from GFP- and sh-SMN-infected motoneurons cultured for 7DIV on laminin-111. One representative Western Blot is shown. Successful fractionation was controlled by β III-tubulin and histone-3, which additionally

served as normalization proteins for quantification. GFP expression was comparable in both conditions. (B) After SMN knockdown cytosolic SMN protein levels were profoundly decreased by 89% (mean \pm SEM of sh-SMN cells 0.11 ± 0.06 , N=3; P=0.0053, t=13.74, DF=2). Nuclear or cytosolic hnRNP R were not significantly altered (mean \pm SEM for sh-SMN cells 1.15 ± 0.17 , N=3; p=0.4513, t=0.9281, DF=2 and 0.62 ± 0.15 , N=3; P=0.1299, t=2.497, DF=2, respectively). In comparison to GFP-infected control motoneurons the relative ratio between cytosolic and nuclear hnRNP R was significantly reduced in sh-SMN-infected cells (mean \pm SEM of sh-SMN cells 0.53 ± 0.08 , N=3; P=0.0256, t=6.127, DF=2). All signals were normalized to their respective GFP controls, which were set to '1'. For statistical analysis one-sample t-tests were performed.

Similar to the above knockdown experiments, hnRNP R levels of primary motoneurons isolated from SMA type I (*Smn*^{-/-};*SMN2tg*) mouse embryos (E13.5) were investigated. Quantitative Western blot analysis after fractionation of these primary motoneurons showed that SMN protein levels were reduced by 78% (p=0.0072) (Figure 19 B). In comparison to *Smn*^{+/+};*SMN2tg* controls, nuclear hnRNP R levels were similar in *Smn*^{-/-};*SMN2tg* motoneurons (1.2, p=0.6317), whereas the cytosolic content was significantly reduced by 56% (p=0.0472) (Figure 19 B). Strikingly, the relative ratio between cytosolic and nuclear hnRNP R levels revealed a strong reduction of 64% (p=0.0012) in SMA type I motoneurons (Figure 19 C). Interestingly, hnRNP R protein levels from total lysates were comparable in *Smn*^{+/+};*SMN2tg* and *Smn*^{-/-};*SMN2tg* motoneurons, highlighting a defective hnRNP R translocation upon SMN deficiency.

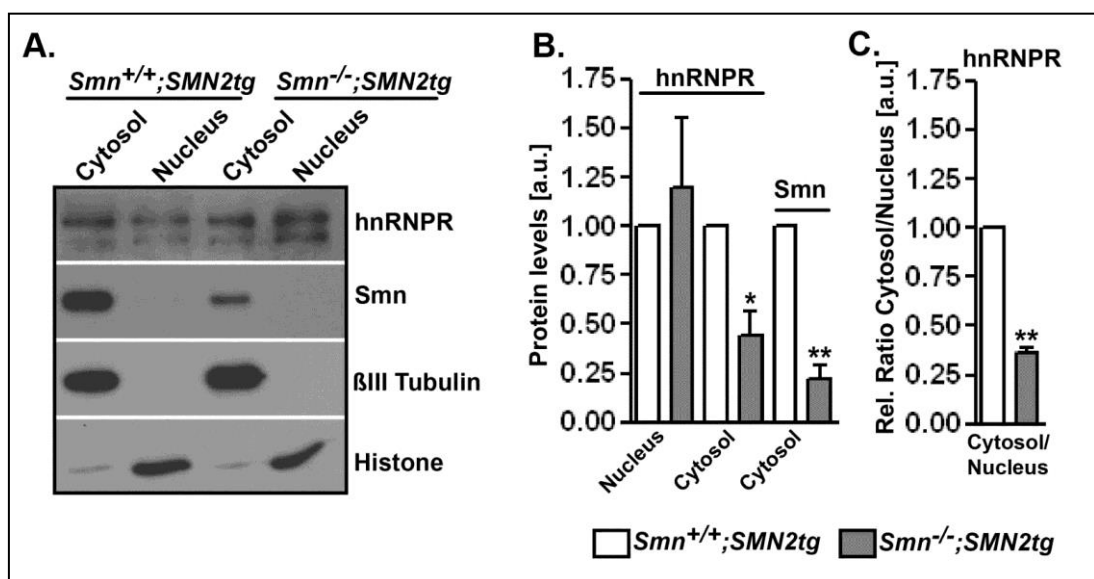


Figure 19: Subcellular distribution of hnRNP R is altered in SMA type I primary motoneurons.

(A) Cytosolic and nuclear fractions were analysed in three independent experiments from control and SMA type I motoneurons. One representative Western Blot is shown in (A). β III tubulin and histone-3 served as control for successful fractionation and as standards for quantification. For probing of hnRNP R an antibody raised against the C-terminus (Abcam) was applied. (B) In SMA type I motoneurons cytosolic SMN protein levels were strongly reduced by 78% (mean \pm SEM of SMA type I cells 0.22 ± 0.07 , N=3; $p=0.0072$, $t=11.71$, DF=2). Cytosolic hnRNP R was significantly decreased by 56% (mean \pm SEM of SMA type I cells 0.44 ± 0.13 , N=3; $P=0.0472$, $t=4.436$, DF=2) in SMN deficient motoneurons. (C) The relative ratio of cytosolic and nuclear hnRNP R content was significantly reduced by 64% in SMN deficient cells (mean \pm SEM of SMA type I cells 0.36 ± 0.02 , N=3; $p=0.0012$, $t=29.13$, DF=2). Values for $Smn^{+/+};SMN2tg$ control motoneurons were always set as '1'. For statistical analysis one-sample t-tests were performed.

To test whether the altered distribution of hnRNP R is also observed *in vivo* we isolated spinal cords from E18 control and $Smn^{-/-};SMN2tg$ mice and performed nuclear and cytosolic fractionations followed by Western blot analysis (Figure 20 A). By calculating the relative ratio of cytosolic and nuclear hnRNP R, we detected a decrease by 20% ($p=0.0146$) in SMA type I tissue homogenate, thus confirming the *in vitro* results from cultured embryonic mouse motoneurons. In fractions from E18 spinal cord tissue higher protein levels were obtained. Relative levels of nuclear hnRNP R appeared to be more prominent than cytosolic levels since axonal projections that significantly contribute to cytosolic content are cut off by isolating spinal cord tissue. SMN was detectable both in cytoplasmic and nuclear fractions. In SMA type I spinal cord tissue nuclear and cytosolic SMN levels were significantly reduced by 86% ($p<0.0001$) and 64% ($p<0.0001$), respectively (Figure 19-B, C). In comparison to control spinal cord extracts nuclear hnRNP R was not altered in SMA type I spinal cords (1.03, $p=0.7636$), whereas cytosolic hnRNP R was significantly reduced by 54% ($p=0.0003$) (Figure 19-B,C). The relative ratio between cytosolic and nuclear hnRNP R content revealed a robust reduction of 52% ($p=0.0009$) (Figure 20 C). Again, nuclear and cytosolic levels of hnRNP R had been normalized against histone and tubulin, respectively. hnRNP R protein levels from total spinal cord lysates were comparable between $Smn^{+/+};SMN2tg$ and $Smn^{-/-};SMN2tg$, indicating that SMN protein is necessary for cytoplasmic and axonal translocation of hnRNP R, and thus also for cytoplasmic/axonal translocation of hnRNP R bound proteins and mRNAs.

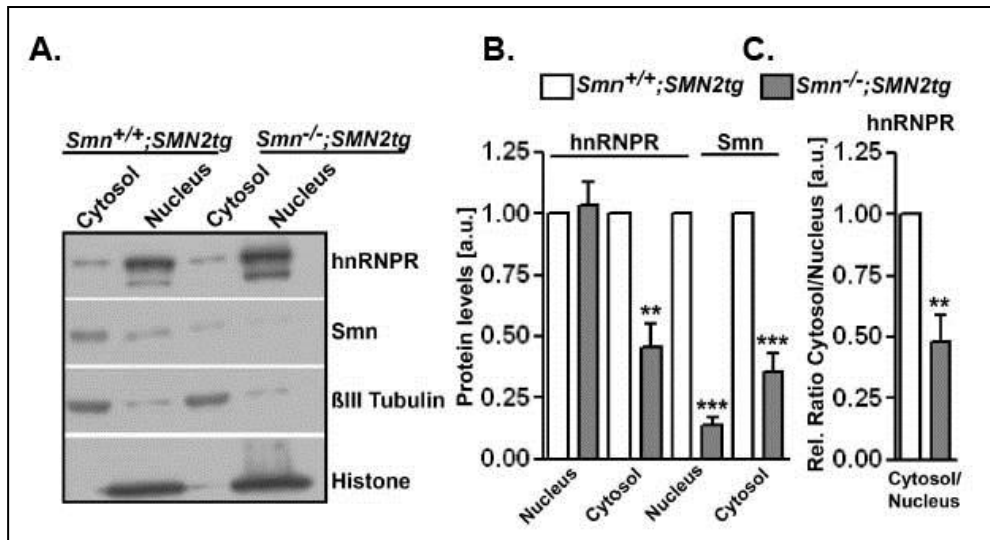


Figure 20: Cytoplasmic hnRNP R is reduced in SMA type I E18 spinal cord.

(A) Cytosolic and nuclear fractions were analyzed from 4 E18 control and 4 E18 SMA type I spinal cords from independent litters. One representative Western Blot of these fractionations is shown. For Western Blot analysis a C-terminal hnRNP R antibody was used. βIII-tubulin and histone-3 served as control for fractionation and for normalization of signals. (B) Nuclear hnRNP R was not altered in SMN deficient spinal cord (mean ± SEM of SMA type I spinal cords 1.03 ± 0.10 , $n=10$; $p=0.7636$, $t=0.3101$, $DF=9$), whereas cytosolic hnRNP R protein was significantly reduced (mean ± SEM of SMA type I spinal cords 0.46 ± 0.10 , $N=10$; $P=0.0003$, $t=5.598$, $DF=9$). (C) The relative ratio between cytosolic and nuclear hnRNP R was profoundly decreased in SMA type I spinal cords by 52% (mean ± SEM of SMA type I spinal cords 0.48 ± 0.11 , $n=10$; $p=0.0009$, $t=4.868$, $DF=9$, one-sample t-test) (Dombert, Sivadasan et al. 2014. PLoS One 9(10): e110846)

6.6 TDP-43 interaction with SMN and hnRNP R influenced by the mutation.

A major breakthrough occurred in 2006 with the observation that TDP-43 is a component of cellular inclusions in FTL-D-U [103]. TDP-43 was also identified as the main constituent protein of cellular ubiquitin-positive skein-like inclusions and round inclusions, which are pathologic hallmarks characteristic of ALS in the spinal anterior horn motoneurons. The relationship between these diseases has been verified by genetic approaches as well. Several groups detected TDP-43 mutations in familial ALS [207-209]. Recent studies have shown the interaction of TDP-43 with heterogeneous nuclear ribonucleoprotein family proteins like hnRNP R and with RNA processing biogenesis proteins like SMN [131, 210]. We therefore wanted to see if the mutations that were observed, especially the mutations located in the glycine region at point 337, 348 and 379, had any influence on the interactions of TDP-43 with proteins like hnRNP R, SMN and Fus/TLS [51, 210].

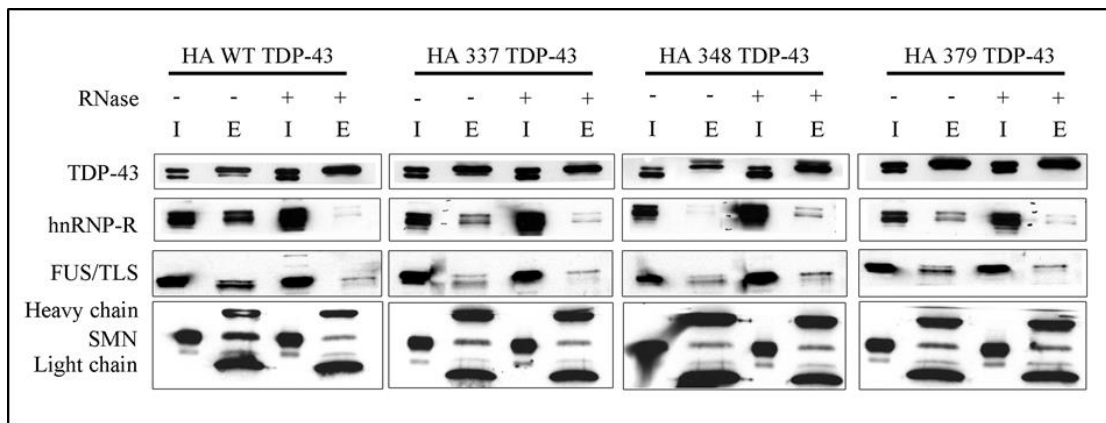


Figure 21: TDP-43 wildtype and mutant protein pull down from NSC-34 cells.

NSC-34 cells were transfected with HA-tag overexpression plasmid for TDP-43 WT and TDP-43 mutant with patient mutation at amino acid 337, 348 and 379. The pull-down was confirmed with IB with TDP-43 antibody, and co-immunoprecipitation was checked with hnRNP R, FUS/TLS, SMN.

As shown in Figure 21 the immunoprecipitation of overexpressed TDP-43 WT shows significant pull-down of SMN, hnRNP R and FUS/TLS [131]. Interestingly the mutations at the glycine rich domain of TDP-43 lead to a reduction in the binding of hnRNP R, SMN and FUS/TLS proteins compared to wildtype TDP-43 (quantified in Figure 22). The results also show that the treatment with RNase lead to a loss in the binding of the interacting protein, suggesting that the RNA binding proteins like hnRNP R and FUS/TLS are mostly co-precipitated because they may bind to the same RNAs as TDP-43. But it needs also be noted that even after complete removal of RNA there is coimmunoprecipitation of TDP-43 with SMN, hnRNP R and FUS/TLS. This suggests that some of the interactions can be a direct protein-protein interaction.

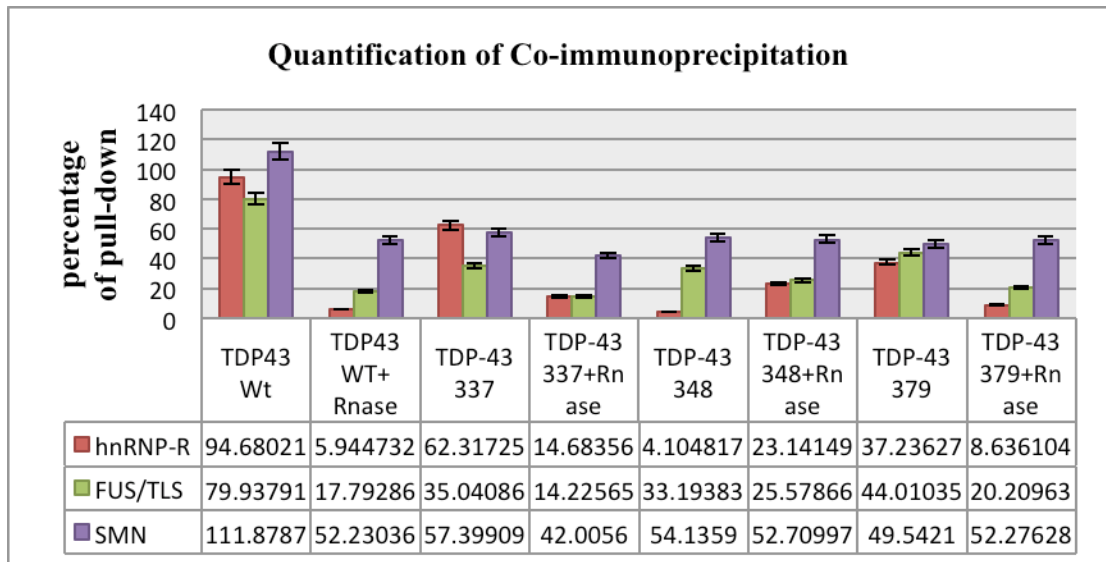


Figure 22: Quantification of pull-down of hnRNP R, FUS/TLS, and SMN by wildtype and mutant TDP-43 from NSC-34 cells.

6.7 Direct interaction of SMN with TDP-43.

To further confirm if there is a direct association of TDP-43 with SMN different concentrations of purified recombinant TDP-43 and SMN were dialyzed separately in binding buffer (20 mM HEPES (pH 7.0), 10% glycerol, 150 mM NaCl and 0.02 % Tween, 2.5mM MgCl₂). The dialyzed proteins were incubated together with binding buffer for 1hr at room temperature. The protein mixture was then incubated with 20 μ l of beads and 1 μ g antibodies against TDP-43, SMN or IgG control, respectively, for 1 h at room temperature. The resin was washed 5 times with binding buffer to remove unbound proteins. For elution, beads were boiled in 2 x Laemmli buffer at 95 °C for 5 minutes. The eluted proteins were then analyzed by Western blotting using specific antibodies against each protein.

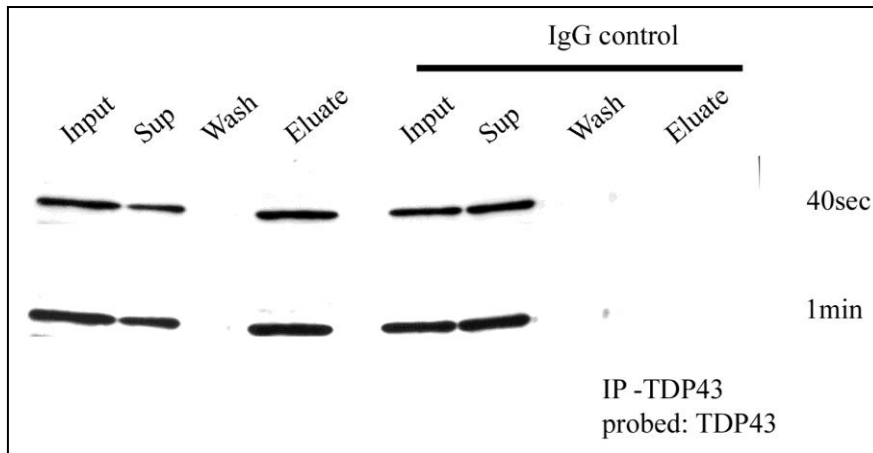


Figure 23: Recombinant TDP-43 immunoprecipitations.

The Western blot clearly shows the efficient pull-down of recombinant TDP-43 used to analysis the direct interaction with SMN.

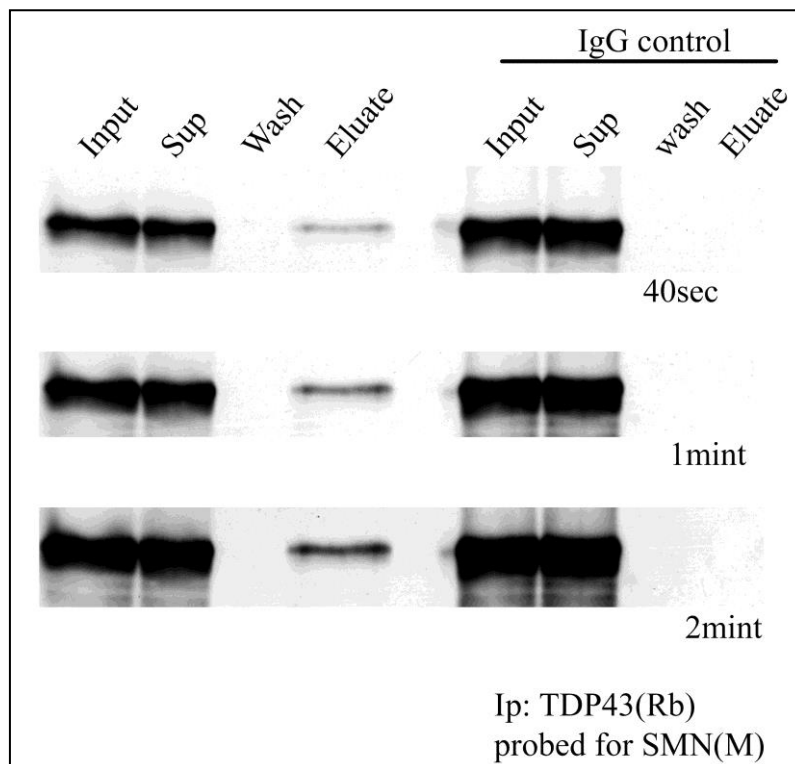


Figure 24: Co-immunoprecipitations of recombinant SMN by TDP-43 antibodies.

The blot clearly shows the direct interaction of recombinant TDP-43 and SMN when recombinant TDP-43 was pulled down.

The results clearly show that TDP-43 interacts directly with SMN. Interestingly, the interaction was only detectable with 1:2 ratio of TDP-43: SMN (Figures 23, 24). This proved

that immunoprecipitation with recombinant proteins of SMN and TDP-43 reveals a direct interaction of the proteins when they are present at a particular stoichiometric ratio.

6.8 HnRNP R SMN interaction enhance the binding of the 3'UTR of β -actin mRNA to the hnRNP R complex.

Earlier studies have shown that overexpression of hnRNP R and SMN enhances neurite growth in PC12 cells, and that this effect correlates with binding of the β -actin mRNA to the hnRNP R complex [47]. To investigate whether recombinant SMN modulates the binding affinity of β -actin mRNA to hnRNP R electrophoretic mobility shift assay (EMSA) experiments were done. Fresh purified and quantified SMN and hnRNP R was used for each experiment. The amount of protein that was required for the complete experiment was first dialysed for 1hr against PBS buffer. SMN and hnRNP R needed for each condition were mixed separately together at room temperature for 1hr. 2 μ l of radioactively labeled 3'UTR of β -actin mRNA were taken for quantification of the radioactive measurement with a Liquid scintillation counter. The probe was diluted to obtain 0.024 μ M to 0.36 μ M as proposed by [45]. The total reaction setup volume was 15 μ l. The reaction mixture was incubated on ice for 30min, mixed with 5 μ l loading dye and loaded on a 0.8% agarose gel which was run at 70V for 3hr. The gel after running was washed with 10X SCC buffer and was transferred to a nitrocellulose membrane overnight, which was developed with a phospho-film reader (Biorad, Personal Molecular Imager (PMI) System, 170-9400).

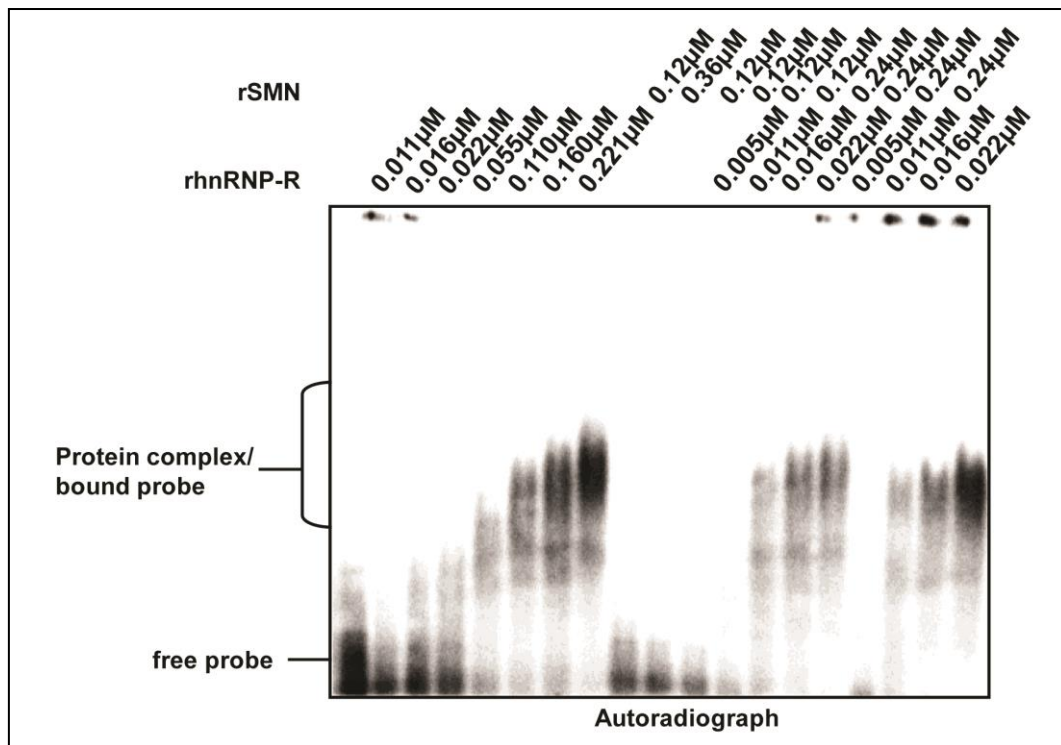


Figure 25: Electrophoretic mobility shift assay of radioactively labeled β -actin 3'UTR with recombinant hnRNP R and SMN.

Recombinant hnRNP R shifts radioactively labeled 3'UTR of β -actin mRNA at concentrations ranging from 0.011 μ M to 0.221 μ M. Recombinant SMN protein itself did not shift the β -actin mRNA at high concentrations (0.36 μ M). However, 0.12 μ M of SMN were sufficient to enhance the capacity of 0.005 μ M hnRNP R to shift β -actin mRNA to levels observed with 0.055 μ M ng hnRNP R alone. These data provide further evidence that hnRNP R interacts with the 3'UTR of β -actin, and they indicate that SMN potentiates this interaction. (Dombert, Sivadasan et al. 2014. PLoS One 9(10): e110846)

As shown in Figure 25 hnRNP R was able to bind to 3'UTR of β -actin mRNA. Recombinant SMN protein itself did not shift the β -actin mRNA at high concentrations (0.36 μ M, Figure 25), thus confirming earlier findings that SMN itself does not have RNA binding activity. However, 0.12 μ M of rSMN was sufficient to enhance the capacity of 0.022 μ M hnRNP R to shift β -actin mRNA to levels observed with 0.021 μ M hnRNP R alone (Figure 25). These data provide further evidence that hnRNP R interacts with the 3'UTR of β -actin mRNA, and they indicate that SMN potentiates this interaction by an order of magnitude in our assay.

6.9 TDP-43 binds to the 3'UTR of β -actin.

The preferential binding of TDP-43 to UG-rich sequences *in vivo* and the ability of TDP-43 to bind to 3'UTR in EMSA experiments were reported previously [123, 130, 211]. In order to examine if TDP-43 can bind to the 3'UTR of β -actin, electrophoretic mobility shift assays (EMSA) were done. Freshly purified and quantified hnRNP R, TDP-43, N-Terminal fragment of TDP-43 (amino acids 1-280), and C-terminal fragment of TDP-43 (amino acids 273-414) were used for the experiments. The N-terminal and C-terminal fragments of TDP-43 were used to confirm if the binding of the 3'UTR of β -actin was likely to be specific for the RNA binding motif (RRM) located in the N-terminal fragment of TDP-43.

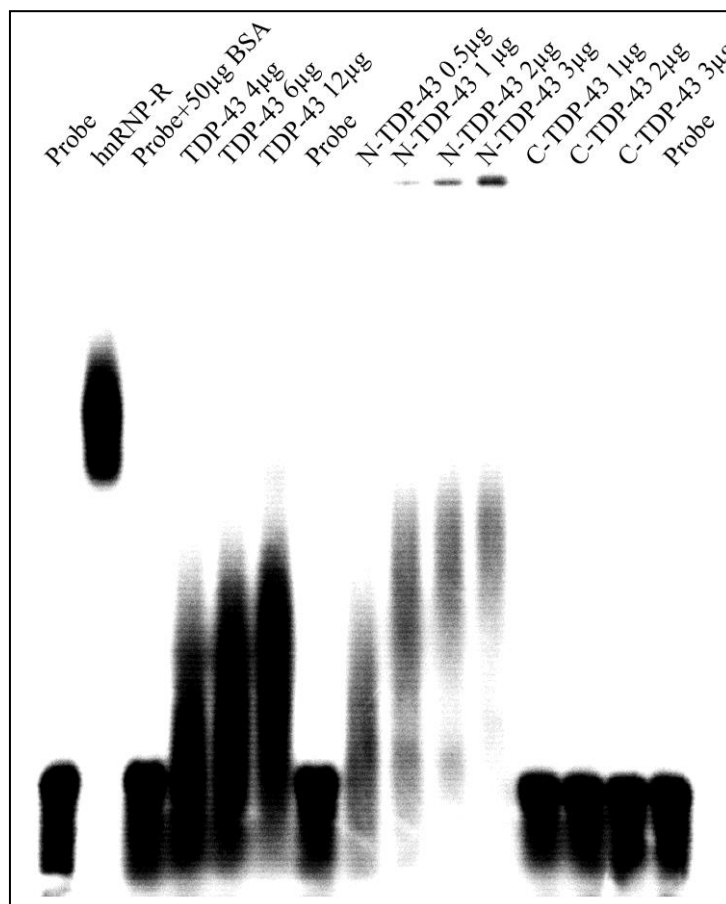


Figure 26: 3'UTR of β -actin interaction with TDP-43.

EMSA for β -actin 3'UTR interaction with TDP-43. The EMSA clearly shows that only the N-terminal TDP-43 fragment having the RRM is able to bind to β -actin 3'UTR, whereas the C-terminal fragment that contains only the glycine rich domain does not bind. Electrophoretic mobility shift assay of radioactively labelled β -actin 3'UTR with recombinant TDP-43. Recombinant hnRNP R shifts radioactively labelled 3'UTR of β -actin mRNA at concentrations ranging from 4 μ g to 12 μ g (positive control).

The amount of protein that was required for the complete experiment was first dialysed for 1hr against PBS buffer. HnRNP R, TDP-43 and TDP-43 fragments needed for each condition were mixed separately together and incubated at room temperature for 1hr. 2 μ l of radioactively labeled 3'UTR of β -actin mRNA was taken for quantification of the radioactive measurement with a liquid scintillation counter. The probe was diluted to get 0.024 μ M to 0.36 μ M which was as proposed [45]. The reaction setup was done in such a way that the total volume was 15 μ l. The reaction mixture was incubated on ice for 30min and mixed with 5 μ l loading dye and loaded on a 0.8% agarose gel which was run at 70V for 3hr. The gel was washed after running with 10X SCC buffer and was transferred to a nitrocellulose membrane overnight. The distribution of the labeled mRNA on the membrane was detected with an X-ray film.

As shown (Figure 26) TDP-43 is able to bind to the 3'UTR of β -actin at 6-12 μ g of recombinant protein. The binding of the 3'UTR to TDP-43 was specifically at the N-Terminal region of TDP-43 where the RNA binding motifs were present. The N-terminal TDP43 was able to make a shift at a lower concentration compared to the full TDP-43. This was due to the difference in molar concentration with respect to the fragment compared to the full-length form of the proteins. As shown in the electrophoretic mobility shift assay (EMSA) no shift was observed with the C-terminal fragment of TDP-43 that does not contain any RNA binding motifs. These data provide the first clear evidence that the 3'UTR of β -actin was able to bind to TDP-43 and that the binding site of the 3'UTR was likely to be at the RRM binding motif in TDP-43 that is located between 1-230 amino acid sequences for TDP-43. The binding of the 3'UTR was specific and no additional factor was required for such interaction.

6.10 TDP-43 SMN interaction enhanced the binding of the 3'UTR of β -actin mRNA to TDP-43.

To investigate whether SMN was able to modulate the binding affinity of β -actin mRNA to TDP-43 as was observed with hnRNP R, electrophoretic mobility shift assay (EMSA) experiments were again performed using equivalent experimental procedures as described above.

The EMSA results show (Figure 27) that 12 μ g of protein was required to produce a saturating shift with 3'UTR of β -actin. But when the same concentration of 3'UTR was used with half the concentration of TDP-43 that had been pre-incubated SMN the same shift was

observed. One observation that needs to be stressed was that only when the ratio of TDP-43: SMN was 1:2 this shift was observed. The reason being that a direct interaction of TDP-43 and SMN was observed when the ratio of TDP-43: SMN was 1:2. This is why no higher shift was observed with increased concentration i.e., 12 μ g TDP-43. These results confirm that SMN can modulate the binding of TDP-43 to the 3'UTR of β -actin.

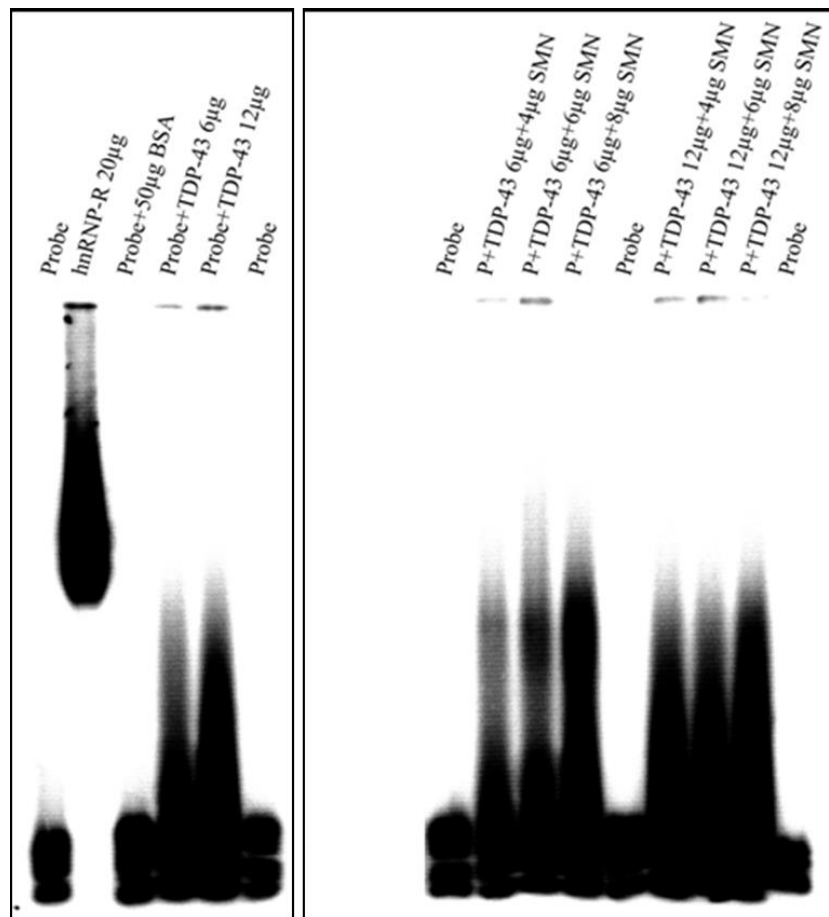


Figure 27: EMSA for TDP-43 interaction with the 3'UTR of β -actin and the influence of SMN enhancing the binding of the 3'UTR of β -actin to TDP-43.

6.11 TDP-43 mutations in the C-terminal region influence the binding of mRNA.

The RRM domains in TDP-43 are the major site of RNA and DNA binding [121]. This is supported by the EMSA (Figure 26) result showing the binding of the 3'UTR of β -actin only to the N-terminal part of TDP-43 and not to the C-terminal part containing only the glycine rich domain. The majority of mutations found in the *TDP-43* gene in patients were reported to alter the glycine rich domain region of TDP-43 [112] and just one reported mutation was located in the RRM1 domain at D169G [212]. To check if the mutations in the

glycine rich region influence the binding of RNA, immunoprecipitations of protein-RNA complexes of TDP-43 WT and mutants were performed [213].

NSC-34 cells were transfected with a HA-tag overexpression plasmid for TDP-43WT, 337, 348 and 379. The cultured cells were incubated after transfection for 48hr. The cell were collected and processed for immunoprecipitation. The supernatant was mixed with pre-cleaned beads and was incubated on a rotatory shaker for 1hr. The pre-cleaned lysates were collected for each condition and incubated with anti-HA cross-linked beads or the corresponding IgG control for 6hr at 4°C. The resin was washed 2 times with binding buffer to remove unbound proteins and 2 times with binding buffer with 1M urea. This is done to remove all co-interacting proteins. The urea-cleaned resin was precipitated with phenol chloroform to extract the total RNA from the protein. The purified RNA was quantified and equal amounts of RNA were used for c-DNA preparation.

Pre-mRNA specific primers against β -actin and TDP-43 [130, 214] were used for the analysis of the transcripts. This analysis showed that the mutation in the glycine rich domain of TDP-43 had influenced the binding of β -actin and TDP-43 RNA. The results show that mutated TDP-43 337 shows higher affinity for binding β -actin and TDP43 mRNA than wt-TDP-43 (Figure 28). This result indicates that this mutation in the glycine rich region of TDP-43 influences the stability of the protein, thereby helping the protein to bind to RNA better than the non-mutated TDP-43 protein.

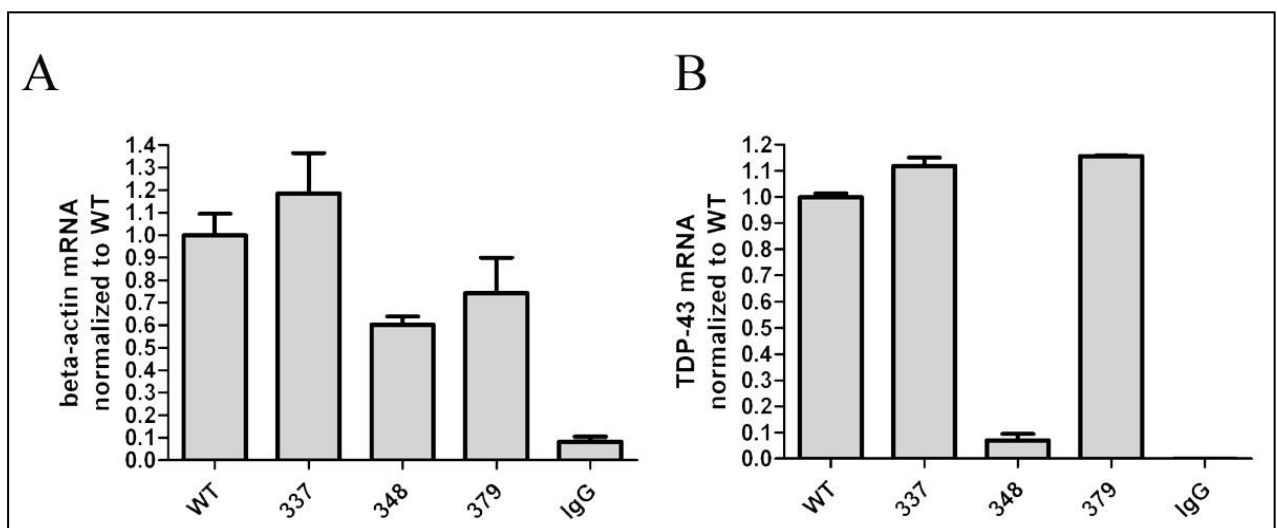


Figure 28: Quantification of RNA pull down of overexpressed HA-tagged TDP-43 and mutants in NSC-34.

(A.) Quantification of β -actin mRNA with respect to WT and mutants of TDP-43, (B.) Quantification of TDP-43 mRNA with respect to WT and mutants of TDP-43.

6.12 Cloning of plasmids for overexpression of C9ORF72 and shRNA for mouse C9ORF72.

One of the reasons for assuming common bases for ALS and FTLD came from genetic linkage studies that identified a locus on chromosome 9p21 in familial ALS-FTLD [215] and genome-wide association studies in sporadic ALS and FTLD [216]. The underlying mutation was subsequently shown to be an expansion of a GGGGCC (G4C2) repeat within intron 1 of C9ORF72 [110, 111]. This repeat expansion accounts for 20–80% of familial and 5–15% of sporadic ALS and FTLD in North American and European populations [110, 111, 138, 217]. The size of the repeat in ALS and FTLD cases has been estimated by Southern blotting to range between 700 and 1,600 repeats [110]. The mean number of G4C2 repeats in controls is two; 95% have less than eight repeats [217]. The mechanism by which the G4C2 intronic repeats cause neurodegeneration is still debated. The recent finding that G4C2 repeat expansions are potentially toxic, sequester RNA binding proteins, and may initiate neurodegeneration in mutant C9ORF72 ALS and FTLD with the help of RNA binding proteins SF2, SC35, and hnRNP-H have revealed important incitement to study these disease mechanisms [147, 218]. Specifically, such studies revealed the hnRNP-H capacity to directly bind to G4C2 RNA and localize closely with RNA foci in transfected cells and the brains of human C9ORF72 associated ALS and FTLD cases [218].

However, the questions about the endogenous function of C9ORF72 or whether C9ORF72 functionally interacts with RNPs like hnRNP R and TDP-43 remained open. Recent publications on the knockdown of C9ORF72 in Zebrafish and *C.elegans* have described effects ranging from axonal shortening to neuronal degradation [139, 167, 168]. One limitation of these studies is the low sequence similarity of mammalian C9ORF72 with their Zebrafish (76%) [139] and *C.elegans* (23%) homologues [168]. For this reason it was necessary to verify the results with other species like mouse which has 98% similarity to human C9ORF72. To address this, an overexpression and knockout lentiviral system for primary mouse motoneuron cell cultures was developed. Mouse C9ORF72 knockdown in cultured mouse motoneurons was done by shRNA designed in such a way that it can knockdown all splice isoforms (Figure 29). The target sequence 5'-GGTCCTAGAGTAAGGCATATT-3' for C9ORF72 was chosen and cloned into the pSIH-H1 shRNA vector (System Bioscience): C9ORF72 shRNA top-oligo (5'-gatccGGTCCTAGAGTAAGGCATATTTCAAGAGAATATGCCTTACTCTAGGACCTTttg -3'), and as control the scrambled-oligo (5'-

gatccGGTCCTAGAGTAAGGCATATTTCAAGAGAATATGCCTTACTCTAGGACCTTttt
g -3') was used.

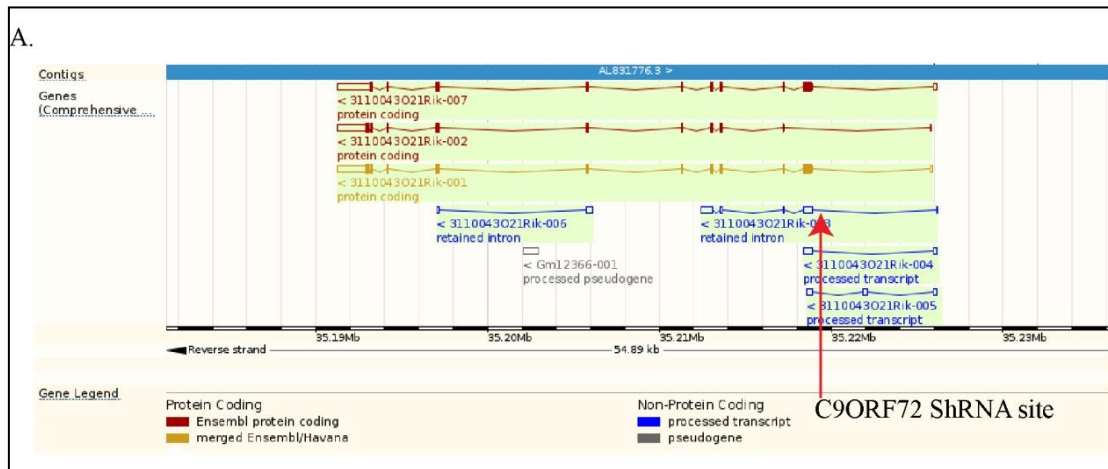


Figure 29: Localisation of shRNA site in the mouse *C9orf72* gene with its splice isoforms.

The constructs for overexpressing C9ORF72 fused with a C-terminal HA-tag were created using PCR primers specific for human or mouse *C9orf72* cDNA. The cloned fragments were subcloned into a pCR4-TOPO vector (Invitrogen) using the following primers: forward (5'- GGTACCGCCATGTCTGACTCTTTGCCACCG -3', start codon of C9ORF72 in bold) and reverse (5'- CTCGAGTTAAGCGTAATCTGGAACATCGTATGGGTAAAAGTCATTAGAACATCTCGTTCTTGC -3', HA-tag sequence in bold). This human C9ORF72–HA cassette was then cloned via BamHI and XhoI into a modified FuGW vector system driven by an ubiquitin promoter, where the GFP was replaced by a multiple cloning site. Integrity of all clones used was checked with sequencing and analysis of restriction patterns. For mouse *C9orf72* the following primers were used forward (5'- ggtaccgccATGTCTGACTAT-3') and reverse (5'- GGCGGATCCTTAAGCGTAATCTGGAACATCGTATGGGTAAAAGG-3', HA-tag sequence in bold). The mouse C9ORF72–HA cassette was then cloned via BamHI site. Cultures of mouse motoneurons were infected in suspension before being plated and harvested after 5 or 7 DIV. Cell lysates were analysed by western blots or processed for immunostaining (Figure 30).

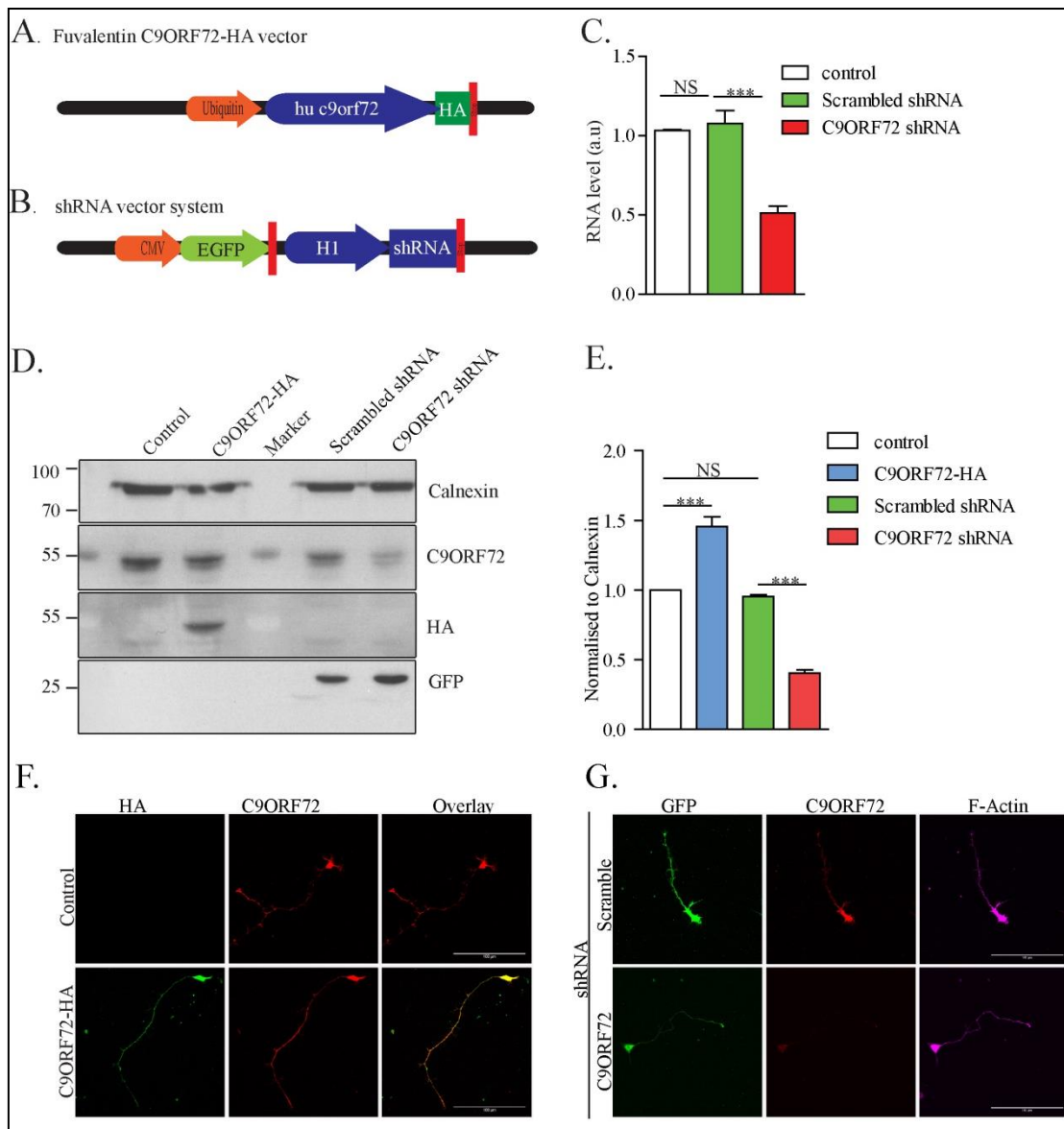


Figure 30: Confirmation of C9ORF72 overexpression and knockdown in cultured mouse motoneurons.

(A) Diagram of hu-C9ORF72 overexpression vector. (B) Diagram of C9ORF72 shRNA vector with coexpression of GFP under the CMV promoter. (C) Quantification of C9ORF72 RNA expression levels by qPCR in motoneurons infected with and without lentivirus with scrambled shRNA and C9ORF72 shRNA (ANOVA with Bonferroni posthoc test, mean \pm s.e.m., $P < 0.001$, $n = 4$ independent experiments) (D) Protein quantification of C9ORF72 protein levels in cultured motoneurons after overexpression or knockdown of C9ORF72. This figure shows one representative blot from $n = 5$ independent experiments. (E) Quantification of the Western blots, as shown in D. $n = 5$ independent experiments. $***$, $P < 0.001$; ANOVA with Student's t-test, mean \pm s.e.m. (F&G) Representative image of C9ORF72 overexpression and knockdown in 5DIV cultured motoneurons in the presence of BDNF stained for the representative protein. Bars, 100 μ m.

The knockdown efficiency of the construct was tested in 7 DIV cultured motoneurons. RNA levels (by qPCR), and protein level (by western blot analysis or immunostaining) showed a 50% reduction in the signal of mouse C9ORF72 (Figure 30 C, E).

6.13 C9ORF72 expression regulates axonal growth in cultured motoneurons.

To analyse the effect of overexpression or knockdown of C9ORF72 on cell survival, 7 DIV cultured motoneurons were infected with lentivirus for the knockdown of the endogenous C9ORF72 gene or for the overexpression of the human C9ORF72-HA construct, with and without brain derived neurotrophic factors (BDNF). Uninfected motoneurons and scrambled shRNA infection were used as controls. The results clearly show that the survival of 7 DIV cultured motoneurons was not affected by C9orf72 knockdown or overexpression, compared to their respective positive and negative controls (Figure 31 A) (data from n=5 independent experiments, 100 cells per condition assayed *, P < 0.05; **, P < 0.01; ***, P < 0.001; ANOVA with Kruskal-Wallis test, mean ± s.e.m.).

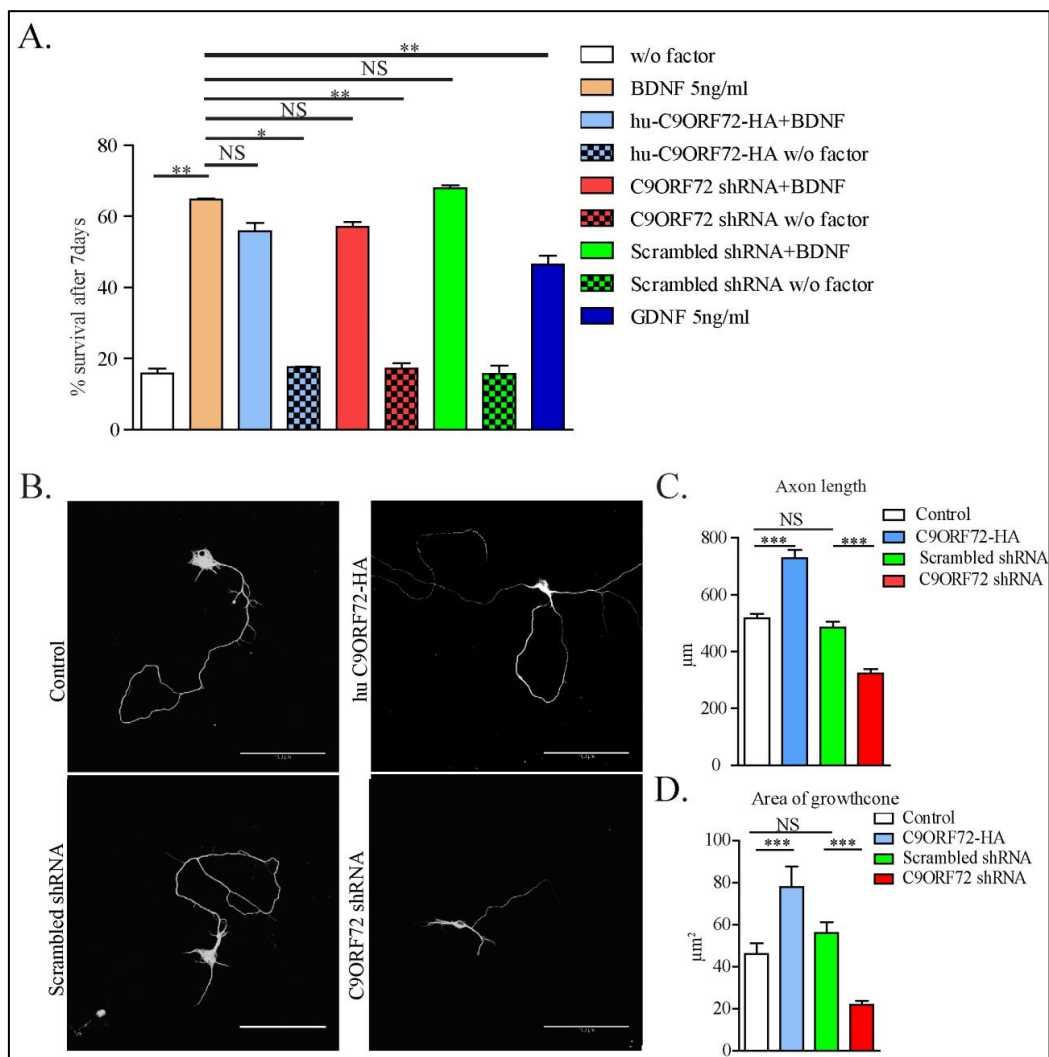


Figure 31: Altered C9ORF72 expression does not affect motoneuron survival but axonal length.

(A) Survival of cultured mouse motoneurons transduced with lentiviral vectors for C9ORF72 overexpression or knockdown as indicated. Cells were cultured with or without 5ng/ml BDNF, as indicated. GDNF was added as an alternative survival factor at 5ng/ml as a control. Graph shows data from n=5 independent experiments, 100 cells per condition assayed *, P <

0.05; **, $P < 0.01$; ***, $P < 0.001$; ANOVA with Kruskal-Wallis test, mean \pm s.e.m. (B) Representative image of control motoneurons or motoneurons after lentiviral hu-C9ORF72 overexpression or knockdown at 7DIV in the presence of BDNF, stained for tubulin to visualize processes. Bars, 100 μ m. (C) Effects of hu-C9ORF72 overexpression and knockdown on axon length after 7 DIV on laminin 221 matrixes. $n = 3$ independent experiments. (D) Effect of overexpression of C9ORF72 and knockdown on growth cones after 5DIV on laminin 221 matrixes. $n=3$ independent experiments. *, $P < 0.05$; **, $P < 0.01$; ***, $P < 0.001$; ANOVA with Bonferroni posthoc test.

This clearly showed that the knockdown of C9ORF72 or its overexpression did not interfere with survival signaling, which is in line with a previous publication [173]. Interestingly, when the axon length was analysed, there was a significant difference to controls. The overexpression of huC9ORF72-HA in motoneurons at 7 days in culture showed significant increases in axon length (Figure.29-B, C) compared to controls while knockdown of *C9orf72* led to significantly shorter axons compared to controls ($n = 3$ independent experiments. *, $P < 0.05$; **, $P < 0.01$; ***, $P < 0.001$; ANOVA with Bonferroni posthoc test) (Figure 31 B, C). To further analyse if the expression of *C9orf72* had an influence on the growth cone size, the area of growth cones was measured in 5 DIV cultured motoneurons grown on laminin 221. The results from $n=3$ independent experiments clearly showed that C9ORF72 overexpression led to increased growth cone size while knockdown led to reduced growth cone size compared to controls (Figure 31 D). These results indicate that C9ORF72 modulates axonal growth and growth cone size in spinal motoneurons.

6.14 Identification of the C9ORF72 interactome.

To investigate the mechanism by which C9ORF72 acts on axon growth and differentiation it was important to determine the interacting proteins of C9ORF72. Recent reports have suggested a role of C9ORF72 in protein trafficking [186, 187]. In line with these findings we collaborated with the group of Matthias Mann, Max-Planck-Institute for Biochemistry, Munich Martinsried to determine interacting proteins by mass spectrometry (MS)-based proteomics [219]. Due to the lack of suitable antibodies against mouse *C9orf72* protein, immunoprecipitation of endogenous protein was not possible and we overexpressed HA tagged human C9ORF72 protein. Immunoprecipitated interacting proteins from NSC-34 cells showed pulldown of the protein with HA antibody, and the pull-down efficiency was confirmed with C9ORF72 antibody (Figure 32 A, B). The interacting protein pull-down was

analysed by quantitative interaction proteomics by our collaboration partners as described [219, 220].

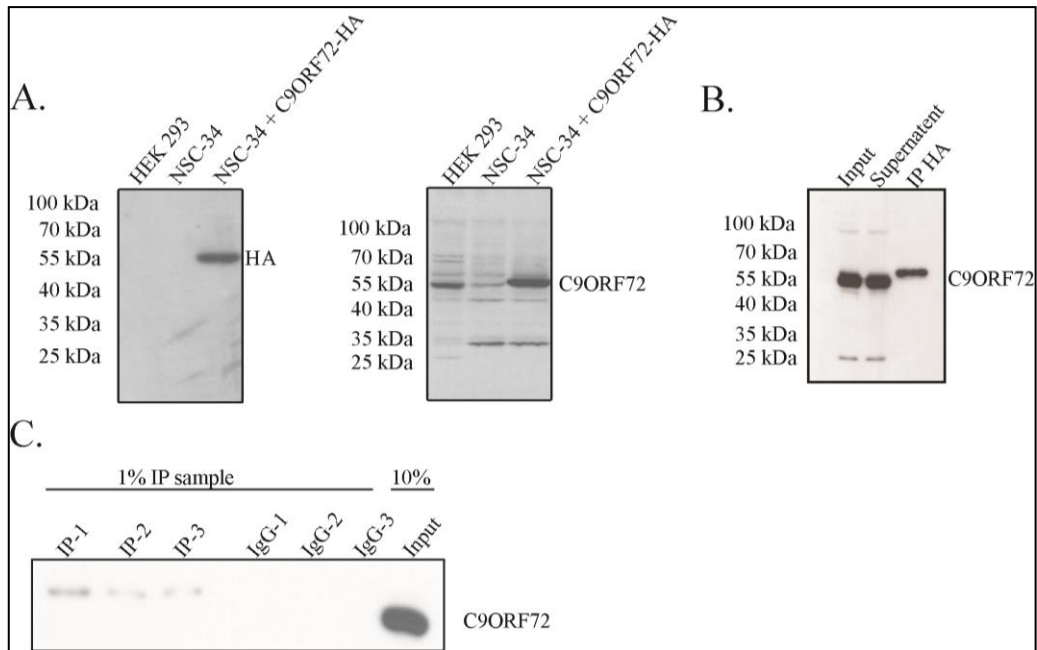


Figure 32: Interactome of C9ORF72 in NSC34 cells.

(A) Western blot analysis of HEK293 and NSC-34 cells overexpressing huC9ORF72-HA (B.) Western blot analysis of immunoprecipitates of huC9ORF72-HA protein. Transduced huC9ORF72 was precipitated with antibodies against HA, the resulting blots were stained with antibodies against huC9ORF72. (C) Confirmative blot for samples used for LC-MS analysis. Samples were pulled down with HA antibody and the blots were probed with C9ORF72 antibody. 1% of immunoprecipitation sample and 10% of input was used for the analysis.

The C9ORF72 interactors showed that the key proteins were actin dynamics regulating proteins such as Cofilin, Arp2/3 and Coronin (Figure 33). These regulatory proteins were significantly enriched in the interactome. Most of these regulatory proteins were important for actin dynamics. Our focus was mostly on cofilin, because we identified two family members of cofilin (Cfl1 and Cfl2) as significant C9ORF72 interactors. Cofilin plays a central role in the regulation of actin dynamics. Cofilins represent a family of actin-binding proteins, which disassemble actin filaments. Three highly conserved and highly (70-82%) identical genes belonging to this family have been described in humans and mice.

- CFL1, coding for cofilin 1 (non-muscle, or n-cofilin)
- CFL2, coding for cofilin 2 (found in muscle: m-cofilin)
- DSTN, coding for destrin, also known as ADF or actin depolymerizing factor

Actin-binding proteins regulate assembly and disassembly of actin filaments [221]. These proteins bind to actin monomers and filaments, G actin and F actin, respectively. Cofilin causes depolymerisation at the minus end of filaments, thereby preventing their reassembly. The protein is known to disassemble actin filaments by creating more positive ends on filament fragments. The importance of cofilin in the regulation of actin dynamics could be responsible for the reduced axon growth and the reduced size of axonal growth cones with the reduced expression of C9ORF72 in our shRNA experiments (Figure 31 and [222]).

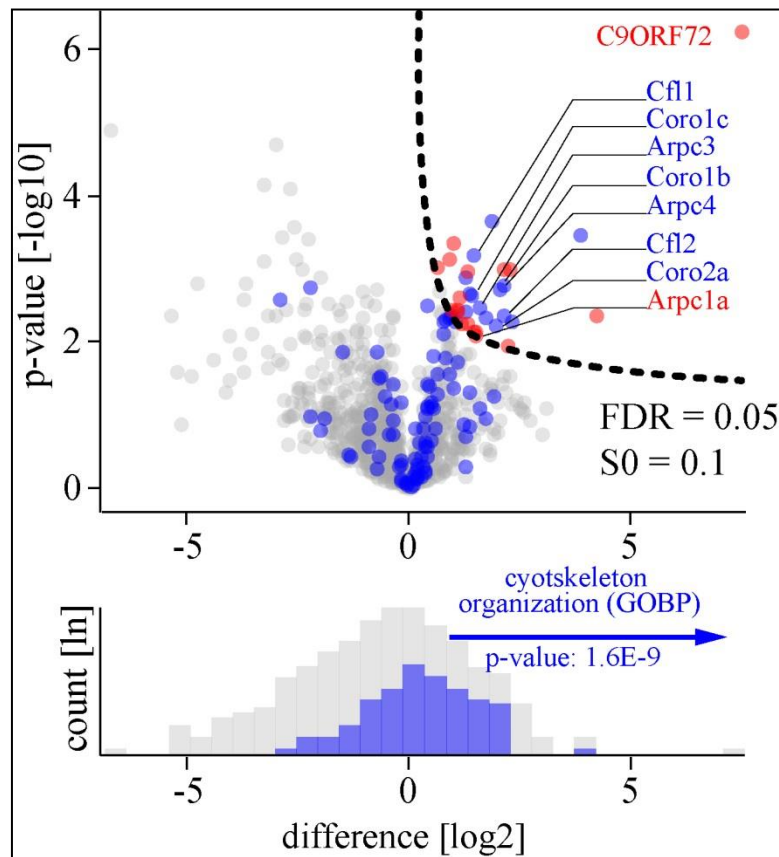


Figure 33: Interactome analysis of huC9ORF72 protein.

The upper panel shows a volcano plot with significantly enriched interacting proteins of C9ORF72 (dotted line) and proteins annotated in the GOBP for the GO term cytoskeleton organisation (blue). The lower panel depicts the significant shift of the GO term cytoskeleton organisation (blue) compared to the background (grey)

Immunostaining of primary motoneurons overexpressing HA-tagged C9ORF72 showed that cofilin and C9ORF72-HA colocalize in the cell body, in axons and axonal growth cones (Figure 34 A, B and C). Immunoprecipitation of C9ORF72-HA from primary mouse motoneurons confirmed the interaction with cofilin by immunoblot analysis (Figure

35A). Endogenous cofilin pulldown also revealed strong binding both of overexpressed C9ORF72-HA (Figure 35 C) and endogenous C9ORF72 (Figure 35 C, right panel).

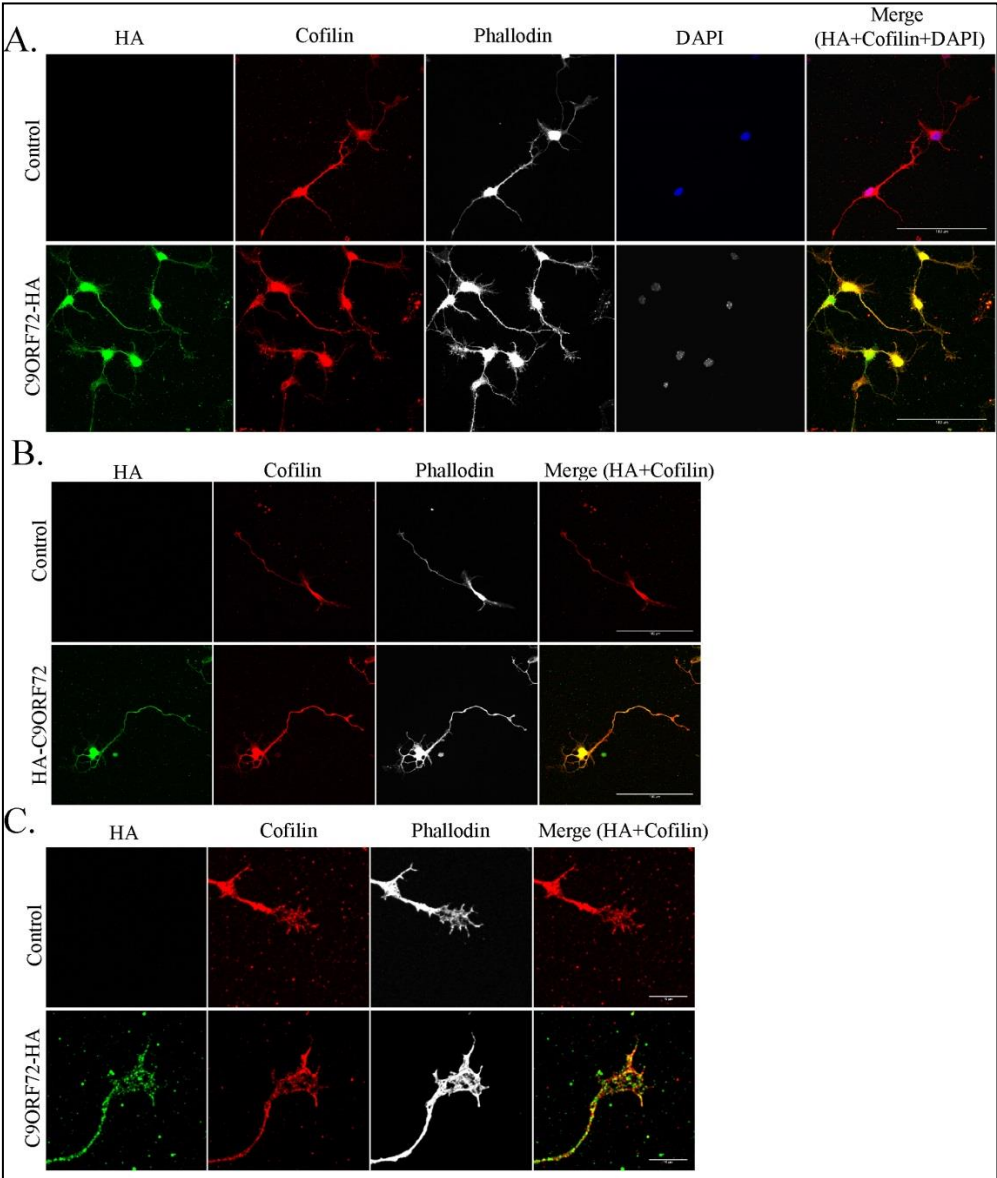


Figure 34: C9ORF72 colocalization with overexpressed huC9ORF72-HA at 5DIV cultured motoneurons.

(A&B) Motoneurons cultured for 5DIV show colocalization of huC9ORF72-HA with cofilin. Bar 100 μ m. (C) Colocalization of huC9ORF72-HA with cofilin in axonal growth cones. Bar 10 μ m

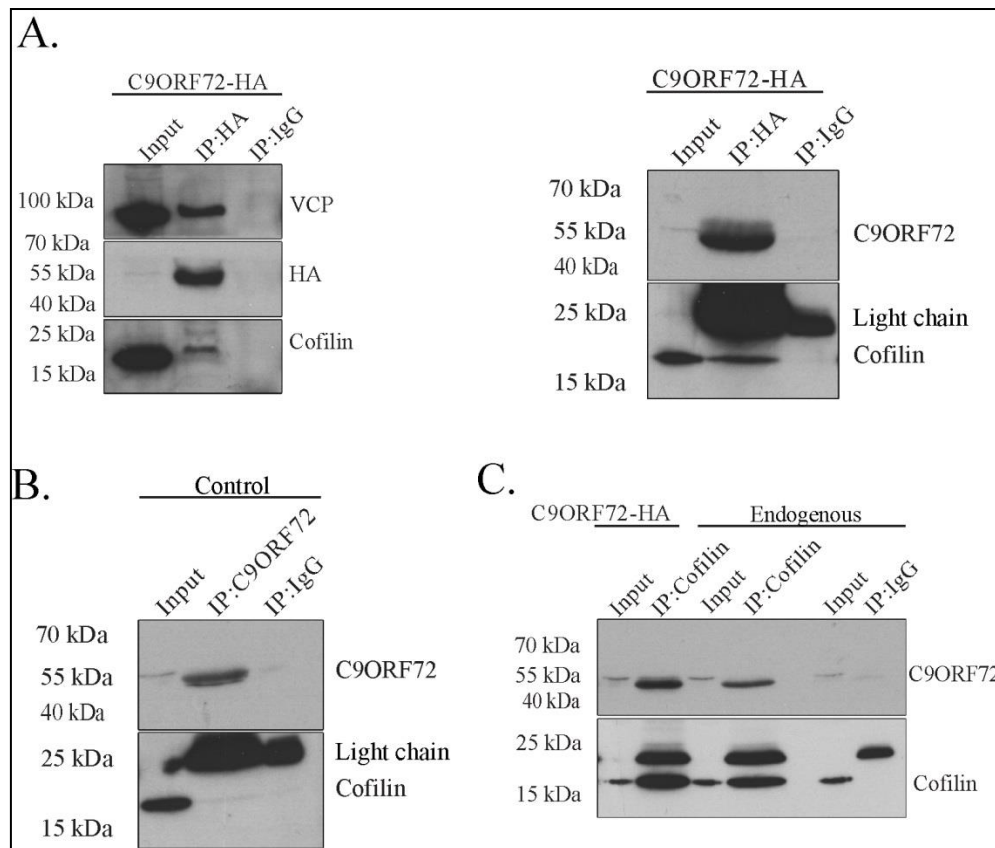


Figure 35: Immunoprecipitation confirming the interaction of C9ORF72 with cofilin from motoneurons.

(A) Confirmation of overexpressed huC9ORF72-HA interaction with cofilin. Left side blot shows that the HA-pulled down huC9ORF72-HA is positive for C9ORF72 and the right blot shows that it interacts with cofilin. (B) Pulldown of endogenous C9ORF72 showing interaction with cofilin. (C) Pulldown of endogenous cofilin confirming that cofilin interacts with overexpressed huC9orf72-HA and endogenous mouse C9ORF72. Control IgG mouse IgG was used.

6.15 C9ORF72 regulates cofilin phosphorylation.

Cofilin is an ubiquitous actin-binding factor required for the reorganization of actin filaments. It promotes actin assembly or disassembly depending on its concentration relative to actin and relative to the concentration of other actin binding proteins [221]. The activity of cofilin depends on phosphorylation at Ser3, which inactivates its function in F-actin assembly [223, 224]. To check if there is a mechanism by which cofilin phosphorylation is regulated with the expression of C9ORF72 protein, motoneuron cultures were infected with lentivirus for the overexpression and knockdown of C9ORF72 and after 7 DIV total protein was isolated. The protein concentration of each sample was quantified and subjected to Western blotting to test the level of cofilin phosphorylation. The results from N=3 experiments showed that overexpression of huC9ORF72-HA protein reduced cofilin phosphorylation while

knockdown increased it (Figure 36 A, B) without any change in total cofilin levels (Figure 36 C).

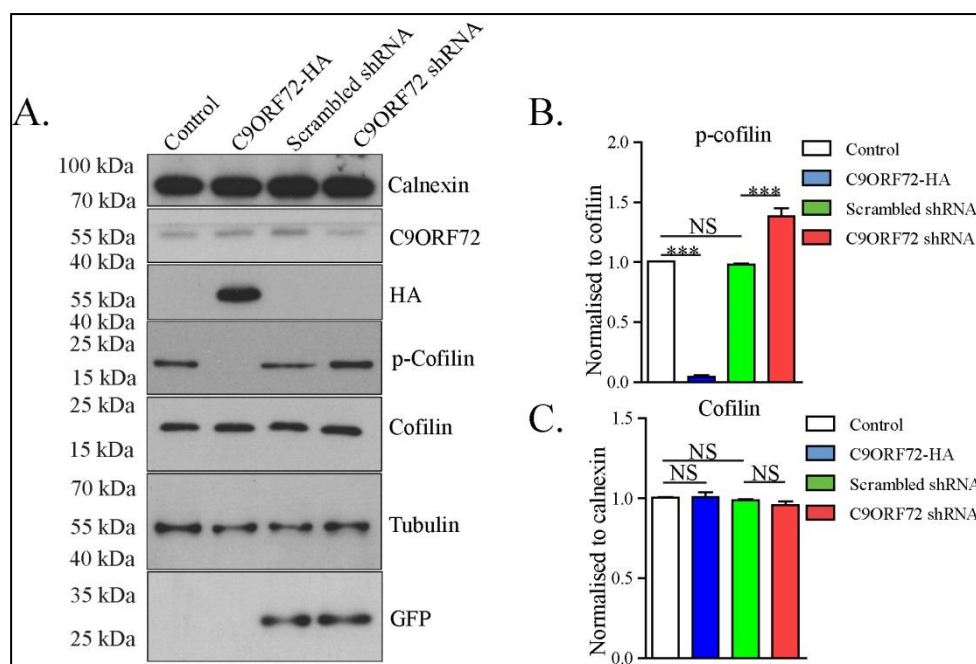


Figure 36: C9ORF72 modulates cofilin activity.

(A) Western blot analysis showing the upregulation or downregulation of p-cofilin with C9ORF72 overexpression or knockdown, respectively, (n=5) from primary cultured motoneurons. (B, C). Quantitative analysis of Western blots as shown in A for phospho-cofilin and total cofilin levels. Densitometric analysis of immunoblot scans was performed from five independent experiments. After normalization with loading controls, values of control samples were set to 1. Data represent mean \pm s.e.m.

As a recent publication has shown that patients with repeat expansion have reduced levels of C9ORF72 expression, it would be interesting to see if there is a difference in phosphorylation of cofilin [167]. To test whether actin dynamics is also altered in human cells with C9ORF72 expansion, we investigated immortalized lymphoblasts from 3 age matched controls and three corresponding samples of 3 C9ORF72 repeat expansion-carrier ALS patients. Immunoblots of lymphoblastoid cell extracts from these patient showed an upregulation of cofilin phosphorylation (Figure 37 A, B). From the above mentioned results we could confirm that C9ORF72 acts as an actin dynamics regulating protein by modulating the phosphorylation of cofilin.

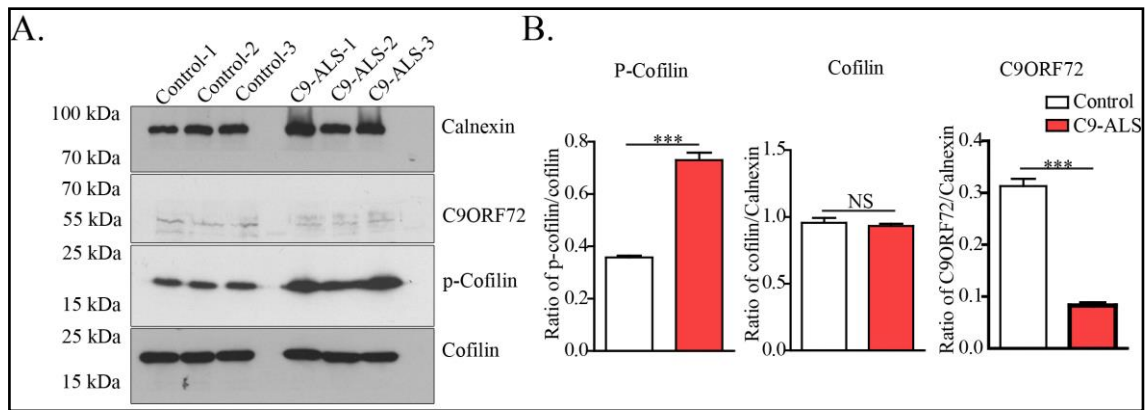


Figure 37: Upregulation of p-cofilin in lymphoblastoid cells from C9ORF72 repeat expansion patients.

(A.) Immunoblot showing the upregulation of p-cofilin in lymphoblastoid cell of 3 control individuals and 3 ALS patients with a more than 63 repeats expansion in the *C9ORF72* gene. (B) Quantitative analysis of Western blots as shown in A for phospho-cofilin and C9ORF72. Densitometric analysis of immunoblot scans was done from 4 independent experiments.

6.16 Cloning of a vector for combining actin visualisation with C9ORF72 knockdown.

To obtain deeper insights into the function of C9ORF72 we wanted to see how actin dynamics is altered by the phosphorylation of cofilin. To address this, live cell tools were developed to visualise actin dynamics. Cytoplasmic actin linked with GFP was cloned into an shRNA lentiviral vector for C9ORF72 repression or expression of scrambled shRNA (Figure 38A). For this experiment, a construct for actin linked with GFP was PCR out with restriction enzymes compatible to the eGFP in the pSIH-H1 shRNA vector (System Bioscience) containing scrambled or C9ORF72 shRNA and fused in frame to the actin coding cDNA to obtain a construct coding β -actin with a N-terminally fused GFP followed by a 11 amino acid linker sequence. This allowed us to study actin dynamics by live cell imaging in mouse motoneuron cultures lacking C9ORF72. A scrambled sequence was used for the control GFP-actin construct [201]. The expression of both constructs was confirmed by Western blotting and immunostaining (Figure 38 B, C), which showed clear of GFP-actin and phalloidin staining.

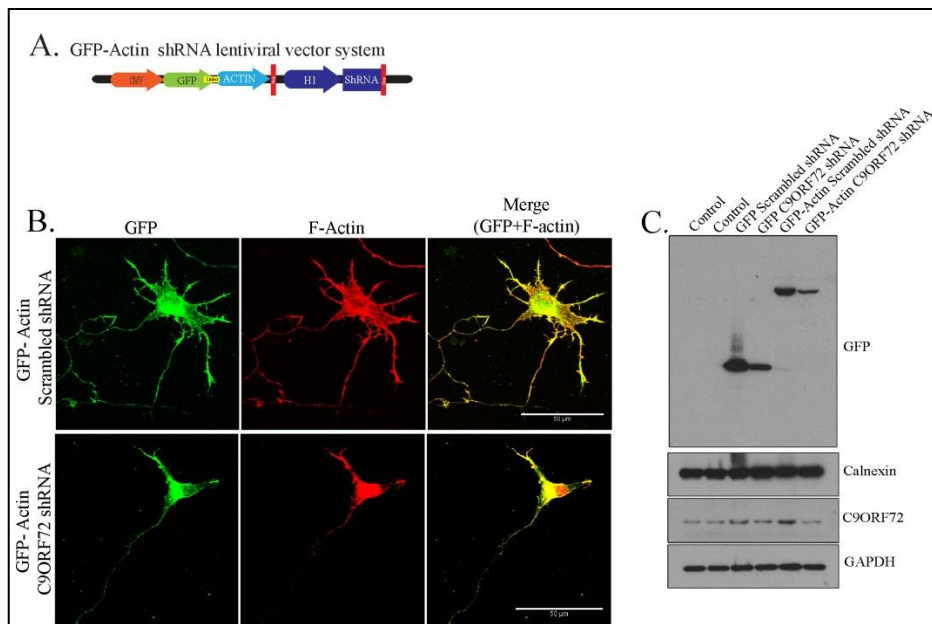


Figure 38: Construction and efficacy of viral constructs for C9ORF72 knockdown and coexpression of GFP-actin.

(A) Representative scheme of the C9ORF72 shRNA vector with coexpression of GFP-actin under the CMV promoter. (B) Motoneurons at 7 DIV transduced with C9ORF72 shRNA or scrambled shRNA lentiviruses were detected by coexpressed GFP-actin. GFP-actin colocalizes with actin and tubulin in axonal processes. Bars 100 μ m. (C) Western blot analysis of cultured motoneurons at 7 DIV transduced with shRNA for scrambled and C9ORF72 with coexpression of GFP and GFP-actin. The blot also shows the effect of knockdown on C9ORF72 protein levels when transduced with shRNA viruses in comparison to control scrambled constructs and untransfected controls.

6.17 Actin dynamics is disturbed after knockdown of mouse C9ORF72.

To study the actin dynamics in transduced cultured motoneurons at 5 DIV [74] with GFP-actin scrambled shRNA or GFP-actin C9ORF72 shRNA transduced motoneurons were seeded in μ -Dishes (35mm) at a density of 10,000 cell plated on laminin221. The motoneurons used for live cell imaging were washed three times with 37°C neurobasal medium and then incubated with fresh neurobasal medium with BDNF (5ng/ml) for 30 min at 37°C and 5% CO₂. Care was taken to make sure that temperature does not have an influence on actin dynamics. Imaging was performed using the Eclipse TE2000 microscope from Nikon equipped with a 60 \times Plan Apochromat NA 1.4 immersion objective combined with Perfect Focus System (Nikon) and a top stage incubation chamber and objective heater (Tokai Hit). Emission was filtered through a 493/574-nm dual-band beam splitter and recorded with an Orca Flash 4.0 (Hamamatsu) camera. Cells were imaged for 1350 sec at 15-sec intervals with an exposure time of 400msec with 2X2 binning. Kymographs were generated and analysed

using the ImageJ Kymograph plugin. Velocity of actin dynamics was calculated as the total track distance divided by the total time (1350sec) from each kymograph.

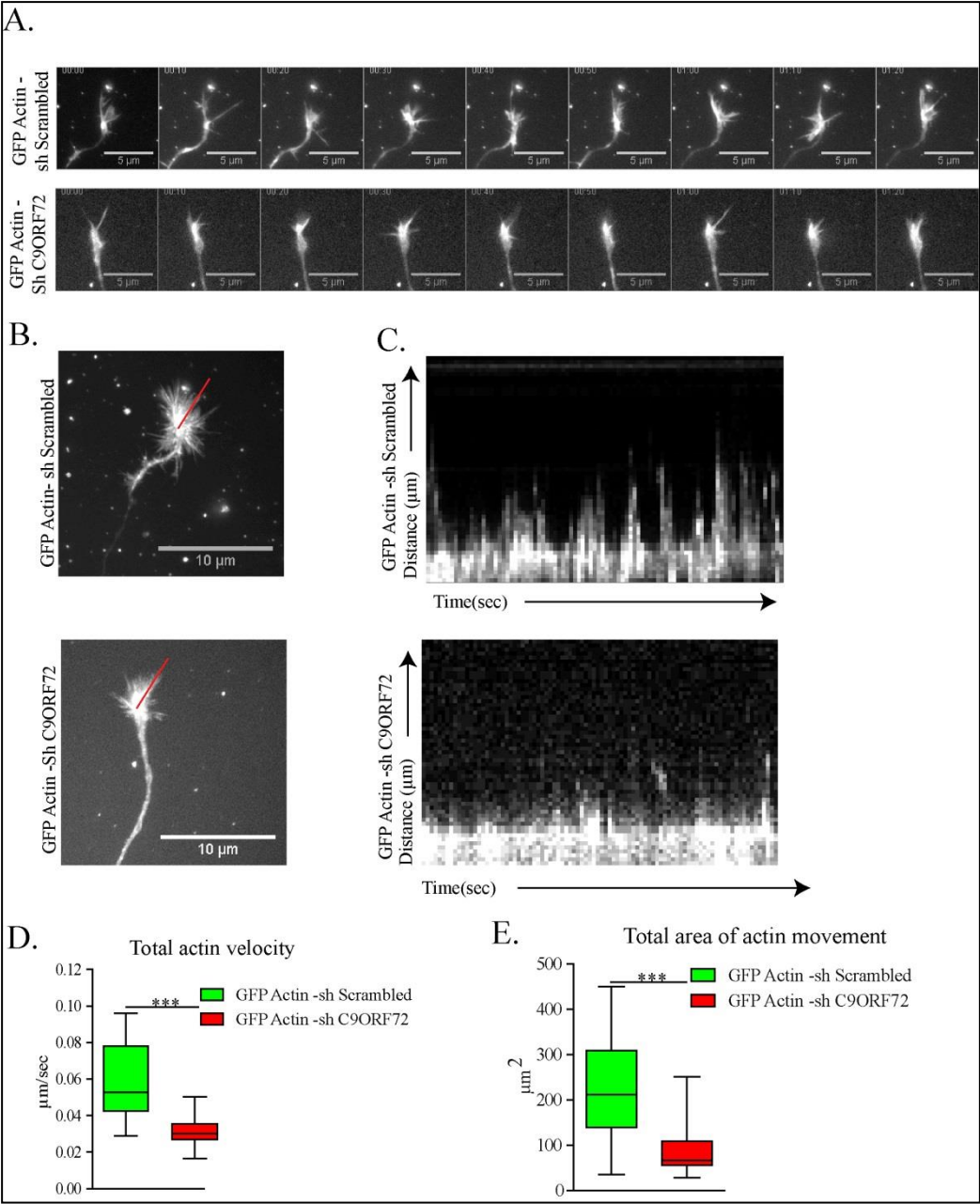


Figure 39: C9ORF72 regulates actin dynamics.

(A.) Live cell imaging of growth cones in motoneurons infected with GFP-actin and with C9ORF72 shRNA. Control cells were infected with scrambled shRNA. Time interval between each exposure 15 sec. (B) Z projection of 90 images with 15 sec intervals. (C) Kymogram of GFP-actin plus scrambled shRNA or C9ORF72 shRNA representing the same growth cone movements as shown in (B). X-axis represents time in sec and y-axis distance of movement in μm . (D) Quantification of total velocity of GFP-actin stained processes. Data from $n = 36$ independent experiments. $***, P < 0.001$; unpaired student t-test. Whiskers represent spread from Min to Max. (E.) Total area covered by movement of GFP-actin stained processes. Data in D and E from $n=36$ independent experiments. $***, P < 0.001$; unpaired sStudent's t-test. Whiskers represent spread from Min to Max.

From the live cell imaging analysis it can be concluded that the number of newly generated actin filaments was significantly reduced in C9ORF72 depleted motoneurons (Figure 39 A). C9ORF72 knockdown led to a significantly reduced velocity of actin movement in axonal growth cones compared to motoneurons transduced with scrambled control constructs (Figure 39 C, D). The dynamics of growth cone movement, as measured by the area into which the growth cone expanded over time was also significantly reduced (Figure 39 E). From the above-mentioned result it became clear that the actin dynamics is impaired when C9ORF72 levels are reduced in motoneurons.

6.18 Altered G/F actin ratio in motoneurons after overexpression and knockdown of C9ORF72.

In parallel to the live cell imaging, a biochemical method was also used to analyse if the G(globular)/F(filamentous) actin ratio was influenced by the expression of C9ORF72. For this analysis G/F actin ratios of 7 DIV cultured motoneurons transduced with lentivirus for overexpression of hu-C9ORF72HA and knockdown of C9ORF72. The culture samples were isolated and lysed in G actin stabilisation buffer to separate the G-actin from F-actin by centrifugal separation. The G/F actin ratio was quantified by western blotting. The results confirmed that the G/F actin ratios were altered. The overexpression of huC9ORF72-HA lead to significant increases in the G/Factin ratio whereas the knockdown of C9ORF72 lead to a reduced G/F actin ratio (Figure 40 A, B, C& D)

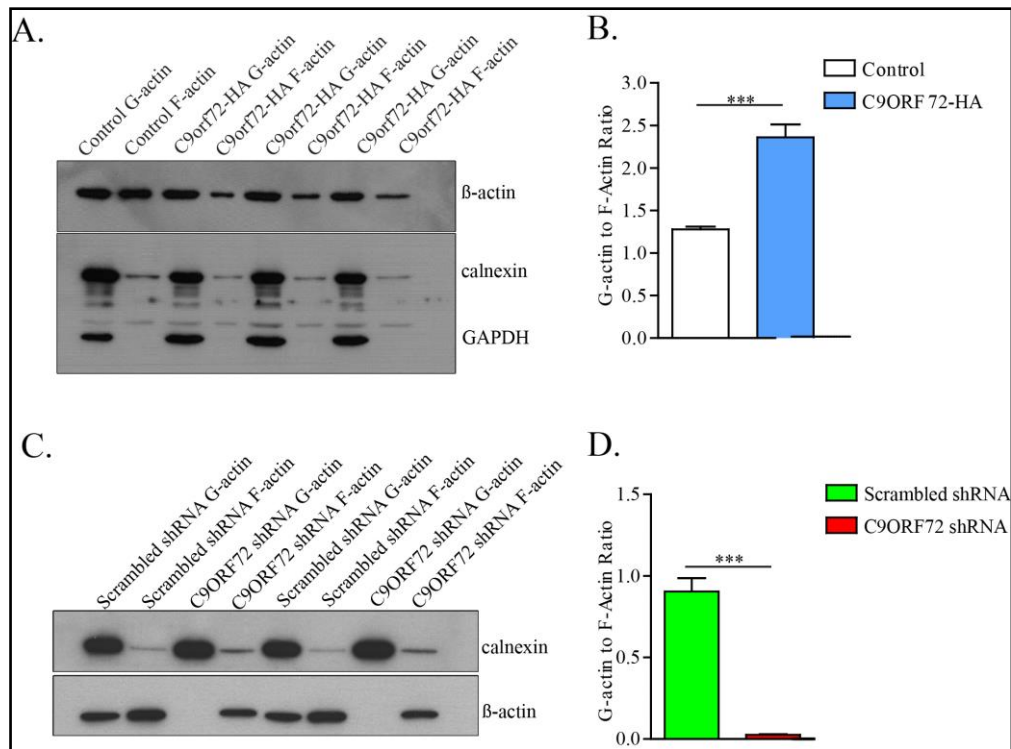


Figure 40: Altered G/F actin ratio in motoneurons after overexpression and knockdown of C9ORF72.

(A) Western blot analysis of G-actin and F-actin distribution in motoneurons cultured for 7DIV. Extracts were processed to separate F and G actin, and blots show the different fractions containing G-actin and F-actin in control motoneurons and motoneurons overexpressing C9ORF72. (B) Quantification of the G/F actin ratio determined by densitometric analysis of immunoblot scans after normalization with loading controls from 3 independent experiments. Data represent mean \pm s.e.m. (C). Western blot showing the G-actin and F-actin fractions from extracts of motoneurons transduced with lentiviruses for C9ORF72 knockdown. Two independent controls with scrambled shRNA constructs were used for comparison. (D) Western blot quantification of G/F actin ratio in control and C9ORF72 shRNA virus transduced motoneurons. Quantification of G/F ratios after normalization with loading controls from 3 independent experiments. Data represent mean \pm s.e.m. *** $P < 0.001$; unpaired student's t test.

7. DISCUSSION.

RNA binding proteins (RBPs) are proteins that play an important role in many cell regulatory processes [225]. hnRNP R and TDP-43 are two multifunctional RBPs involved in neurodegenerative diseases including ALS and FTLN [225]. Since the discovery of *SMN* mutations as cause of SMA multiple efforts have been made in elucidating the role of the corresponding protein in motoneuron function. Profoundly, *SMN* has a central cellular role in the assembly of spliceosomal snRNPs. It is now becoming increasingly clear that *SMN* also interacts with a number of RNA-binding proteins such as FMRP [226], KSRP [59], hnRNP R [227] and Q [61, 228], TDP-43 [229], FUS [230], IMP1 [231] and HuD [231]. The main goal of this study was to elucidate the role of hnRNP R and TDP-43 in relation to *SMN*. This study provides evidence about the following molecular mechanisms.

7.1 *SMN* interacts directly with hnRNP R and TDP-43 and regulates the binding to the 3'UTR of β -actin mRNA.

HnRNP R has been identified as an interaction partner for *SMN* [228]. Furthermore, hnRNP R binds to U-rich sequences within the 3'UTR of β -actin mRNA [61, 232] and participates in the translocation of this mRNA into axons and axon terminals [61]. Accordingly, loss of either *SMN* or hnRNP R reduces axon growth of isolated mouse motoneurons [61, 232]. Knockdown of *SMN* or hnRNP R in zebrafish results in similar phenotypes. Under both conditions, truncated axons and aberrant branching in peripheral regions are found and point to a common functional pathway *in vivo* [232, 233]

SMN, hnRNP R and TDP-43 are partially colocalizing in axons and axon terminals and also in the perinuclear region within the soma of motoneurons [227]. Since both hnRNP R, TDP-43 and *SMN* have numerous interaction partners with various functions, this spatial distribution and correlation is not surprising and indicates that dynamic interactions of *SMN*, hnRNP R and TDP-43 could take place in axons and axonal compartments, which need to be investigated in more detail. This hypothesis is supported by the observation of an axonal and presynaptic colocalization of hnRNP R and TDP-43 with *SMN* [227]. In order to corroborate this result, it was necessary first to see if hnRNP R and TDP-43 can directly bind to *SMN*. For this, recombinant protein was purified from *E. coli* and coimmunoprecipitation experiments were performed with *SMN*, hnRNP R and TDP-43. The results clearly show that they can interact directly. No previous studies had shown the direct interaction of *SMN* to hnRNP R and TDP-43 in mammalian cells or tissues before. Then present experiments revealed a direct interaction of hnRNP R and *SMN* predominantly in the cytosol of motoneurons and E18

spinal cord. In HEK293T cells, SMN and hnRNP R could not be coimmunoprecipiated, neither from nuclear nor from cytosolic extracts thus pointing to differences between neuronal and other cell populations.

What could be the function of the hnRNP R, TDP-43 and SMN interaction in motoneurons? HnRNP R and TDP-43 have multiple functions in transcription regulation and RNA processing [112, 234]. HnRNP R and TDP-43 contain consensus RNA-binding domains, and an RGG-rich domain, which is typical for many proteins involved in RNA-splicing and transport. As shown for the β -actin mRNA before, hnRNP R and TDP-43 bind to U-rich sequences in 3'UTRs [61, 118, 123, 228, 232]. The association with SMN could point towards the formation of an mRNA transporting granule, as demonstrated for SMN and HuD before [58, 60, 231]. We detected a modulation of binding activity of hnRNP R to its axonal target mRNA, the 3'UTR of β -actin. Adding of SMN in EMSAs to hnRNP R and TDP-43 leads to a higher affinity of hnRNP R to the β -actin 3'UTR indicating a potential regulation of RNA-binding protein activity in axons of spinal motoneurons. It is possible that SMN regulates the formation or stability of mRNA trafficking granules in spinal motoneurons. This hypothesis could explain the selective vulnerability of spinal motoneurons in SMA as the SMN level might be crucial for this function in axons.

7.2 Depletion of SMN alters the subcellular distribution of hnRNP R in motoneurons.

HnRNP R is located in the nucleus and in the cytosol of motoneurons. HnRNP R is also enriched together with SMN in axon terminals of motoneurons both in cell culture and *in vivo* [227]. The latter observation provides additional weight to the hypothesis that SMN, together with hnRNP R and possibly also other mRNA-binding proteins is involved in maturation and maintenance of neuromuscular synapses by a direct local action in the presynaptic compartment [235].

The SMN protein is found both in the nucleus and cytosol of motoneurons, and it is located in axons and axon terminals both *in vitro* and *in vivo* [227]. It has been reported also that SMN protein is present in the presynaptic compartment of neuromuscular junctions, particularly of postnatal mice [227]. Studies have shown by immunohistochemistry that SMN is localized at neuromuscular junctions in the diaphragm and that a specific signal is found in close vicinity to the presynaptic marker synaptophysin. SMN and hnRNP R show a partial colocalization in axons and axon terminals and a strong but not exclusive colocalization in the perinuclear region within the soma of motoneurons [227, 236]. Furthermore, colocalization

appears to change over time reaching the highest degree of overlap at periods when axon elongation is maximal [227].

In comparison to previous studies [232] a new shRNA construct targeting all known isoforms of hnRNP R was constructed. Interestingly, some hnRNP R isoforms that are described in databases only contain the N-terminus and therefore no nuclear localization sequence since the latter is located at the C-terminal end (Ensemble Database, 2014). Consequently, the application of N-terminal antibodies for visualization of hnRNP R covers all present isoforms. Upon hnRNP R depletion SMN levels and subcellular distribution appear to be unchanged. Furthermore, the number of gems is comparable [227]. Vice versa, knockdown of SMN does not interfere with total hnRNP R levels, which fits to previous data [61]. Although total hnRNP R levels are not affected, SMN depletion alters the translocation of hnRNP R from the nucleus to the cytoplasm, in particular to axons and axon terminals. Also *in vivo*, this alteration became apparent in spinal cord fractionations and sections from *Smn^{-/-}-SMN2tg* mouse embryos.

Thus, the availability of cytosolic hnRNP R strongly depends on SMN protein. This might explain why the knockdown of either SMN or hnRNP R, respectively, results in a similar phenotype in zebrafish and isolated mouse motoneurons [61, 232, 233, 237, 238]. Basically, in both cases cytosolic hnRNP R is reduced which could lead to impaired transport and translocation of specific mRNAs to axons and axon terminals, which in turn might be crucial for local translational events promoting maturation and differentiation processes.

Studies with cultured SMN deficient motoneurons revealed that the actin cytoskeleton is defective at specialized structures such as axonal growth cones, resulting in impaired differentiation of the developing growth cone to the presynaptic compartment of the neuromuscular junction [61, 238, 239]. The reduced availability of β -actin mRNA, possibly due to disturbed hnRNP R translocation, could account for decreased actin protein levels, particularly polymerized actin, which in turn could interfere with clustering of $Ca_v2.2$ calcium channels and eventually other transmembrane proteins on the surface, preventing calcium influx and the recognition of essential differentiation signals provided by direct interaction of $Ca_v2.2$ subunits and laminin $\beta 2$ chains [238, 240]. Microarray analyses have also shown that β -actin mRNA was also found as one downregulated target after SMN knockdown [241]. It still remains an open question to relate the data from the microarray analysis to presynaptic structural and functional abnormalities [235, 242] and furthermore to determine, if other RNA-binding proteins like TDP-43, FUS/TLS or HuD, respectively, might also be translocated to axons and axon terminals by SMN protein, which could significantly

contribute to the observed diversity of misregulated axonal mRNA upon SMN knockdown. It has recently been reported that SMN impacts the axonal localization of IMP1 which is also involved in axonal transport and recruitment of β -actin mRNA [231]. Notably, mutant FUS/TLS appears to sequester SMN thus reducing its axonal levels [243], which in turn might alter as a secondary consequence the translocation of several SMN interaction partners affecting ultimately synaptic integrity by misplacing essential mRNAs. Thus, SMA and ALS apparently share common mechanisms of pathogenesis [244, 245].

7.3 Mutations in the C-terminal region of TDP-43 regulate the binding of protein and RNA.

RNA binding proteins play a critical role in providing the connection between the gene expression steps that lead to the production of a mature RNA [246]. Important RBPs play a distinct role in the assembly of multimeric complexes for the control of specific RNA life cycles [247, 248]. In terms of numbers and quantity, the RBPs responsible for creating the “backbone” of these multimeric complexes belong for the most part to the heterogeneous ribonucleoprotein (hnRNP) family [249]. From a structural point of view, almost all hnRNPs contain one or more RNA binding domains that allow them to specifically bind to RNA sequences. They also contain specific sequences of variable composition, such as arginine-glycine-glycine (RGG) boxes that mediate their biological functions [250, 251]. This fundamental role played by hnRNPs is especially highlighted in neurons, where there is an extremely high level of differential RNA expression that is mainly generated through the cooperation of these ubiquitous hnRNP proteins with other tissue-specific RNA binding factors [236].

The most studied hnRNP proteins that have been shown to play a major and direct role in neurodegenerative processes are represented by TDP-43 [103, 252], FUS/TLS [104, 105] and very recently two hnRNP A/B family members [253]. It is important to note that mutations of these proteins by themselves do not mediate neurodegeneration. It has been demonstrated that mutant FUS sequesters axonal SMN [243], disturbs snRNP localization [243], reduces the number of gems [230] and leads to synaptic defects at neuromuscular junctions [254, 255], thus establishing a potential correlation between ALS and SMA [244]. Similar results were reported for TDP-43 [256]. Mutant TDP-43 reveals impaired transport of cytoplasmic mRNP granules [257].

The results from this study clearly show that TDP-43 can bind to the 3'UTR of β -actin at the N-terminal region containing the RRM and that the C-terminal glycine rich domain

region alone cannot bind to the RNA. However, the mutation in the C-terminal region influences the binding of protein and RNA, as we see a change in the binding affinities to the interacting RNA (3'UTR of β -actin and TDP-43) and to proteins like hnRNP R, FUS/TLS and SMN. One hypothesis is that point mutations at the C-terminal region lead to structural changes in the protein conformation. Although the crystal structures of the TDP-43 RRM1 and RRM2 bound to a single-stranded DNA [121, 258] as well as the NMR solution structure of RRM1-RRM2 bound to a single-stranded RNA [122] have revealed how the two RNA recognition motifs interact with nucleic acids, they do not provide a clear link between missense mutations in TDP-43 relevant to ALS.

ALS-linked mutants of TDP-43 have been suggested to be more prone to aggregation and more potent in inducing cell death than wild-type TDP-43. Compared to the mutation in the RRM region of TDP-43, the mutation in the C-terminal region like Q331K and M337V accelerate spontaneous TDP-43 aggregation [259], A315T, G348C and A382T induce neuron cell death [114, 260], and Q331K and M337V more strongly induce oxidative injury of motoneuron like cells [261]. Moreover, the ALS-linked mutants, G298S, Q331K, M337V, exhibit longer protein half-lives and enhance interactions with FUS/TLS43, whereas the D169G mutation in the RRM1-RRM2 domain increases protein thermal stability [258] or half-life [210, 262]. TDP-43 protein has an auto-regulatory function of regulating its own transcript expression [263]. This supports the finding that lethal mutations in TDP-43 like those at positions 337 and 379 show increased binding of TDP-43 transcript compared to TDP-43 with mutation at 348. This could be one of the reasons why these mutations in TDP-43 lead to retention or enhancement of TDP-43 function in splicing of most pre-mRNAs and selective loss-of-function for splicing of specific pre-mRNAs [263].

In summary these data strongly suggest that SMN does not only impact the subcellular location of hnRNP R and possibly also other RNA-binding proteins like TDP-43, but additionally has profound effects on the subcellular transport and distribution of mRNAs with specific functions for synaptic vesicle release, maintenance of axonal and presynaptic cytoskeleton and other biological parameters which are important for axonal and presynaptic maturation and function.

7.4 C9ORF72 interaction with cofilin modulates actin dynamics in motoneurons.

The discovery of the hexanucleotide repeat expansion of non-coding GGGGCC repeats in a gene named Chromosome 9 open reading frame 72 (*C9orf72*) has been identified as a cause of ~40% of hereditary ALS and 25% of familial frontotemporal dementia (FTLD)

cases. The conditions are generally termed C9FTLD/ALS [110, 111]. Pathological findings in cells and tissues of *C9ORF72*-linked ALS/FTLD patients suggest three possible pathogenic mechanisms of disease. The evidence that cells derived from *C9ORF72* patients have decreased levels of *C9ORF72* transcripts suggests a loss-of-function mechanism. In addition, increasing lines of evidence point at RNA gain of function as the most likely mechanisms [147, 173, 264].

One of the possible mechanisms discussed in the field is the RNA-mediated gain-of-function toxicity in C9FTLD/ALS. The GGGGCC-repeat (G4C2) region lies between two alternatively spliced non-coding exons of the *C9ORF72* gene [110, 166]. The findings of various independent studies indicate that the expression level of *C9ORF72* transcripts is reduced [110, 137, 166, 172] and that the amount of the corresponding protein is altered in C9FTLD/ALS patients with the GGGGCC repeat expansion [162]. These finding supports the hypothesis that G4C2 repeat transcript as well as the antisense repeat transcript may accumulate in RNA foci which can bind to RNA binding proteins, whereby the RNA metabolism could be disrupted [147, 173]. *C9ORF72* RNA containing G4C2 repeats has been reported to form RNA foci [110, 173, 265]. It also has been identified that there is an inverse correlation between RNA foci and age-at-onset of C9FTLD/ALS. It has been shown by biochemical and microscopic investigations that *C9ORF72* RNA is capable of recruiting cellular proteins to RNA foci [266]. Among these proteins are RNA-binding proteins such as hnRNPs [174, 218, 267] and RNA export factors [148, 174]. Recent publications have shown that extensive alternative splicing and alternative polyadenylation defects are observed in the cerebellum of C9ALS subjects, including changes in ALS-associated genes like *ATXN2* and *FUS* in subjects with sporadic ALS [175]. Furthermore, heterogeneous nuclear ribonucleoprotein H (hnRNP-H) and other RNA-binding proteins like hnRNP R and TDP-43 are predicted to be potential regulators of cassette exon alternative splicing events in both *C9ORF72* ALS and sporadic ALS [175].

The recruitment of these proteins to *C9ORF72* RNA foci compromises their cellular functions, leading to C9FTLD/ALS pathologies. Resent advance in trimethylation of H3 and H4 core histones at particular lysine residues associated with gene silencing [268] have showed that the gene expression level of *C9ORF72* was reduced in patients presented with H3K9, H3K27, H3K79 and H4K20 trimethylation [166]. Also the appearance of four consecutive guanine nucleotides in DNA leads to the formation of a meta-stable DNA secondary structure termed a G-quadruplex [147]. It has been shown that the formation of G-

quadruplex DNA plays a regulatory role in various cellular processes, such as gene transcription control [269] and that the formation of GGGGCC DNA G-quadruplex structure halts the transcription of *C9ORF72*, which provides an alternative explanation for the down-regulation of *C9ORF72* gene expression observed in C9FTLD/ALS [147]. However, it is not yet clear, whether one mechanism predominates over the other or whether they both contribute to neurodegeneration.

Although the focus of most recent research has been directed at the repeat expansion of *C9ORF72* and studied related toxic effects of the repeat expansion, few studies have worked on the endogenous function of *C9ORF72*. Clearly, understanding this function is necessary for elucidating its role in neurodegeneration disease. Recent publications show that reduction of *C9ORF72* levels in both cortical and motoneurons does not affect survival *in vitro* [167] and *in vivo* [168]. However, reduced axon length of motoneurons and locomotion defects are induced in zebrafish by antisense oligonucleotide-mediated reduction of *C9ORF72* protein [139]. With these observations one could conclude that basic information on the actual function of the protein is very vital. To address the loss-of-function hypothesis, lentiviral based knockdown and overexpression was used to try to understand the cellular function of *C9ORF72*. The overexpression or the knockdown of the protein did not affect the survival of the cultured motoneurons but interestingly, axon length in 7 day cultures and growth cone area in 5 day cultures were significantly increased in *C9ORF72* overexpressing motoneurons compared to controls, while knockdown of *C9orf72* led to significantly shorter axons and reduced growth cone area. These results indicate that *C9orf72* modulates axonal growth and growth cone size in mouse spinal motoneurons. However, this could be a contradiction to recent publications that conditional knockdown of *C9orf72* in mouse does not cause motoneuron degeneration or motor deficits [170]. But it must be noted that the paper suggests that *C9ORF72* plays a role during embryonic and postnatal development, because of the presence of neuronal *C9orf72* expression at several sites in the embryonic nervous system, as well as in non-neuronal tissues [170]. This observation is in line with zebrafish embryo data which also show both inside and outside the nervous system expression of *C9ORF72* [139].

One of the possible functions of *C9ORF72* has been implicated in intra-cellular membrane trafficking [186, 187]. Our mass spectrometry (LC-MS), immunoprecipitation and immunocytochemistry identified *C9ORF72* to interact with key regulators of actin dynamics such as cofilin, arp2/3 and coronin. Cofilin plays a central role in the regulation of actin dynamics which could be responsible for reduced axon growth and reduced size of axonal

growth cones [222]. Endogenous cofilin pulldown also revealed strong binding both of overexpressed C9ORF72-HA and endogenous C9orf72. This interaction was also confirmed by immunostaining in cultured mouse motoneurons, showing that C9ORF72-HA co-localizes with cofilin in the cell body, axonal shaft and growth cone.

Cofilin is an ubiquitous actin-binding factor required for the reorganization of actin filaments [221]. The activity of cofilin depends on phosphorylation at Ser3 which inactivates its function in F-actin assembly [223, 224]. Further investigation in the dynamics of cofilin activity clearly proved that overexpression of C9ORF72-HA protein reduced phosphorylation, while knockdown increased cofilin phosphorylation without any change in total cofilin levels. This observation was further supported with the studies on human immortalized lymphoblastoid cells from ALS patients with reduced C9ORF72 expression, which showed an upregulation of cofilin phosphorylation compared to control patients.

Lastly the live cell actin dynamics study clearly showed that the numbers of newly generated actin filaments were reduced in C9orf72 depleted motoneurons and the depletion of C9orf72 lead to significantly reduced velocity of actin movement and growth cone movement area. This approach demonstrated that actin dynamics is impaired when C9orf72 levels are reduced in motoneurons. In parallel to the live cell imaging, protein fractionation of F-actin and G-actin also confirmed that G/F actin ratios are altered when C9orf72 is knocked down or overexpressed. These data provide evidence that C9orf72 plays a cellular role in regulating actin dynamics, via interaction with cofilin and possibly other proteins active in shaping the actin cytoskeleton. Our data also explain the axonal phenotype observed in zebrafish after C9orf72 suppression [139]. Thus, loss of function of C9ORF72 could contribute to the clinical phenotype in ALS and FTL, based on observations that reduced actin dynamics influences synaptic strength [270], maintenance [271] and axon stability [61].

8. REFERENCES FOR THIS THESIS

1. Werdnig, G., *Two early infantile hereditary cases of progressive muscular atrophy simulating dystrophy, but on a neural basis.* 1891. Arch Neurol, 1971. **25**(3): p. 276-8.
2. Sugarman, E.A., et al., *Pan-ethnic carrier screening and prenatal diagnosis for spinal muscular atrophy: clinical laboratory analysis of >72,400 specimens.* Eur J Hum Genet, 2012. **20**(1): p. 27-32.
3. Prior, T.W., *Spinal muscular atrophy: newborn and carrier screening.* Obstet Gynecol Clin North Am, 2010. **37**(1): p. 23-36, Table of Contents.
4. Prior, T.W., et al., *Newborn and carrier screening for spinal muscular atrophy.* Am J Med Genet A, 2010. **152A**(7): p. 1608-16.
5. Feldkotter, M., et al., *Quantitative analyses of SMN1 and SMN2 based on real-time lightCycler PCR: fast and highly reliable carrier testing and prediction of severity of spinal muscular atrophy.* Am J Hum Genet, 2002. **70**(2): p. 358-68.
6. Crawford, T.O. and C.A. Pardo, *The neurobiology of childhood spinal muscular atrophy.* Neurobiol Dis, 1996. **3**(2): p. 97-110.
7. Mercuri, E., E. Bertini, and S.T. Iannaccone, *Childhood spinal muscular atrophy: controversies and challenges.* Lancet Neurol, 2012. **11**(5): p. 443-52.
8. Roper, H., R. Quinlivan, and P. Workshop, *Implementation of "the consensus statement for the standard of care in spinal muscular atrophy" when applied to infants with severe type 1 SMA in the UK.* Arch Dis Child, 2010. **95**(10): p. 845-9.
9. Wang, C.H., et al., *Consensus statement for standard of care in spinal muscular atrophy.* J Child Neurol, 2007. **22**(8): p. 1027-49.
10. Palladino, A., et al., *Cardiac involvement in patients with spinal muscular atrophies.* Acta Myol, 2011. **30**(3): p. 175-8.
11. Rudnik-Schoneborn, S., et al., *Congenital heart disease is a feature of severe infantile spinal muscular atrophy.* J Med Genet, 2008. **45**(10): p. 635-8.
12. Shababi, M., et al., *Cardiac defects contribute to the pathology of spinal muscular atrophy models.* Hum Mol Genet, 2010. **19**(20): p. 4059-71.
13. Kaufmann, P., et al., *Observational study of spinal muscular atrophy type 2 and 3: functional outcomes over 1 year.* Arch Neurol, 2011. **68**(6): p. 779-86.
14. Yuan, P. and L. Jiang, *Clinical characteristics of three subtypes of spinal muscular atrophy in children.* Brain Dev, 2015. **37**(5): p. 537-41.
15. Piepers, S., et al., *A natural history study of late onset spinal muscular atrophy types 3b and 4.* J Neurol, 2008. **255**(9): p. 1400-4.
16. Burghes, A.H. and C.E. Beattie, *Spinal muscular atrophy: why do low levels of survival motor neuron protein make motor neurons sick?* Nat Rev Neurosci, 2009. **10**(8): p. 597-609.
17. Liu, Q. and G. Dreyfuss, *A novel nuclear structure containing the survival of motor neurons protein.* EMBO J, 1996. **15**(14): p. 3555-65.
18. Matera, A.G. and M.R. Frey, *Coiled bodies and gems: Janus or gemini?* Am J Hum Genet, 1998. **63**(2): p. 317-21.
19. Young, P.J., et al., *Nuclear gems and Cajal (coiled) bodies in fetal tissues: nucleolar distribution of the spinal muscular atrophy protein, SMN.* Exp Cell Res, 2001. **265**(2): p. 252-61.
20. Setola, V., et al., *Axonal-SMN (α -SMN), a protein isoform of the survival motor neuron gene, is specifically involved in axonogenesis.* Proc Natl Acad Sci U S A, 2007. **104**(6): p. 1959-64.
21. Burghes, H.M., *Other forms of survival motor neuron protein and spinal muscular atrophy: an opinion.* Neuromuscul Disord, 2008. **18**(1): p. 82-3.
22. Battaglia, G., et al., *Expression of the SMN gene, the spinal muscular atrophy determining gene, in the mammalian central nervous system.* Hum Mol Genet, 1997. **6**(11): p. 1961-71.

23. Cartegni, L. and A.R. Krainer, *Disruption of an SF2/ASF-dependent exonic splicing enhancer in SMN2 causes spinal muscular atrophy in the absence of SMN1*. Nat Genet, 2002. **30**(4): p. 377-84.
24. Coovert, D.D., et al., *The survival motor neuron protein in spinal muscular atrophy*. Hum Mol Genet, 1997. **6**(8): p. 1205-14.
25. Jones, K.W., et al., *Direct interaction of the spinal muscular atrophy disease protein SMN with the small nucleolar RNA-associated protein fibrillarin*. J Biol Chem, 2001. **276**(42): p. 38645-51.
26. Kashima, T. and J.L. Manley, *A negative element in SMN2 exon 7 inhibits splicing in spinal muscular atrophy*. Nat Genet, 2003. **34**(4): p. 460-3.
27. Monani, U.R., et al., *A single nucleotide difference that alters splicing patterns distinguishes the SMA gene SMN1 from the copy gene SMN2*. Hum Mol Genet, 1999. **8**(7): p. 1177-83.
28. DiDonato, C.J., et al., *Regulation of murine survival motor neuron (Smn) protein levels by modifying Smn exon 7 splicing*. Hum Mol Genet, 2001. **10**(23): p. 2727-36.
29. Burnett, B.G., et al., *Regulation of SMN protein stability*. Mol Cell Biol, 2009. **29**(5): p. 1107-15.
30. Lorson, C.L. and E.J. Androphy, *An exonic enhancer is required for inclusion of an essential exon in the SMA-determining gene SMN*. Hum Mol Genet, 2000. **9**(2): p. 259-65.
31. Gupta, K., et al., *Oligomeric Properties of Survival Motor Neuron.Gemin2 Complexes*. J Biol Chem, 2015. **290**(33): p. 20185-99.
32. Young, P.J., et al., *The exon 2b region of the spinal muscular atrophy protein, SMN, is involved in self-association and SIP1 binding*. Hum Mol Genet, 2000. **9**(19): p. 2869-77.
33. Giesemann, T., et al., *A role for polyproline motifs in the spinal muscular atrophy protein SMN. Profilins bind to and colocalize with smn in nuclear gems*. J Biol Chem, 1999. **274**(53): p. 37908-14.
34. Talbot, K., et al., *Missense mutation clustering in the survival motor neuron gene: a role for a conserved tyrosine and glycine rich region of the protein in RNA metabolism?* Hum Mol Genet, 1997. **6**(3): p. 497-500.
35. Fischer, U., Q. Liu, and G. Dreyfuss, *The SMN-SIP1 complex has an essential role in spliceosomal snRNP biogenesis*. Cell, 1997. **90**(6): p. 1023-9.
36. Gubitz, A.K., W. Feng, and G. Dreyfuss, *The SMN complex*. Exp Cell Res, 2004. **296**(1): p. 51-6.
37. Liu, Q., et al., *The spinal muscular atrophy disease gene product, SMN, and its associated protein SIP1 are in a complex with spliceosomal snRNP proteins*. Cell, 1997. **90**(6): p. 1013-21.
38. Pellizzoni, L., J. Yong, and G. Dreyfuss, *Essential role for the SMN complex in the specificity of snRNP assembly*. Science, 2002. **298**(5599): p. 1775-9.
39. Raker, V.A., et al., *Spliceosomal U snRNP core assembly: Sm proteins assemble onto an Sm site RNA nonanucleotide in a specific and thermodynamically stable manner*. Mol Cell Biol, 1999. **19**(10): p. 6554-65.
40. Meister, G., et al., *A multiprotein complex mediates the ATP-dependent assembly of spliceosomal U snRNPs*. Nat Cell Biol, 2001. **3**(11): p. 945-9.
41. Carissimi, C., et al., *Gemin8 is a novel component of the survival motor neuron complex and functions in small nuclear ribonucleoprotein assembly*. J Biol Chem, 2006. **281**(12): p. 8126-34.
42. Carissimi, C., et al., *Gemin8 is required for the architecture and function of the survival motor neuron complex*. J Biol Chem, 2006. **281**(48): p. 37009-16.
43. Meister, G., et al., *Characterization of a nuclear 20S complex containing the survival of motor neurons (SMN) protein and a specific subset of spliceosomal Sm proteins*. Hum Mol Genet, 2000. **9**(13): p. 1977-86.
44. Otter, S., et al., *A comprehensive interaction map of the human survival of motor neuron (SMN) complex*. J Biol Chem, 2007. **282**(8): p. 5825-33.
45. Glinka, M., et al., *The heterogeneous nuclear ribonucleoprotein-R is necessary for axonal beta-actin mRNA translocation in spinal motor neurons*. Human molecular genetics, 2010. **19**(10): p. 1951-66.

46. Rossoll, W., et al., *Smn, the spinal muscular atrophy-determining gene product, modulates axon growth and localization of beta-actin mRNA in growth cones of motoneurons*. The Journal of cell biology, 2003. **163**(4): p. 801-12.
47. Rossoll, W., et al., *Specific interaction of Smn, the spinal muscular atrophy determining gene product, with hnRNP R and gry-rbp/hnRNP-Q: a role for Smn in RNA processing in motor axons?* Human molecular genetics, 2002. **11**(1): p. 93-105.
48. Fallini, C., G.J. Bassell, and W. Rossoll, *The ALS disease protein TDP-43 is actively transported in motor neuron axons and regulates axon outgrowth*. Hum Mol Genet, 2012. **21**(16): p. 3703-18.
49. Lee, S., et al., *Identification of a subnuclear body involved in sequence-specific cytokine RNA processing*. Nat Commun, 2015. **6**: p. 5791.
50. Turner, B.J., et al., *TDP-43 expression in mouse models of amyotrophic lateral sclerosis and spinal muscular atrophy*. BMC Neurosci, 2008. **9**: p. 104.
51. Yamazaki, T., et al., *FUS-SMN protein interactions link the motor neuron diseases ALS and SMA*. Cell reports, 2012. **2**(4): p. 799-806.
52. Akten, B., et al., *Interaction of survival of motor neuron (SMN) and HuD proteins with mRNA cpG15 rescues motor neuron axonal deficits*. Proc Natl Acad Sci U S A, 2011. **108**(25): p. 10337-42.
53. Fallini, C., et al., *Dynamics of survival of motor neuron (SMN) protein interaction with the mRNA-binding protein IMP1 facilitates its trafficking into motor neuron axons*. Dev Neurobiol, 2014. **74**(3): p. 319-32.
54. Fallini, C., et al., *The survival of motor neuron (SMN) protein interacts with the mRNA-binding protein HuD and regulates localization of poly(A) mRNA in primary motor neuron axons*. J Neurosci, 2011. **31**(10): p. 3914-25.
55. Hubers, L., et al., *HuD interacts with survival motor neuron protein and can rescue spinal muscular atrophy-like neuronal defects*. Hum Mol Genet, 2011. **20**(3): p. 553-79.
56. Tadesse, H., et al., *KH-type splicing regulatory protein interacts with survival motor neuron protein and is misregulated in spinal muscular atrophy*. Hum Mol Genet, 2008. **17**(4): p. 506-24.
57. Zhang, H., et al., *Multiprotein complexes of the survival of motor neuron protein SMN with Gemins traffic to neuronal processes and growth cones of motor neurons*. J.Neurosci., 2006. **26**(33): p. 8622-8632.
58. Hubers, L., et al., *HuD interacts with survival motor neuron protein and can rescue spinal muscular atrophy-like neuronal defects*. Hum.Mol.Genet., 2011. **20**(3): p. 553-579.
59. Tadesse, H., et al., *KH-type splicing regulatory protein interacts with survival motor neuron protein and is misregulated in spinal muscular atrophy*. Hum.Mol.Genet., 2008. **17**(4): p. 506-524.
60. Fallini, C., et al., *The Survival of Motor Neuron (SMN) Protein Interacts with the mRNA-Binding Protein HuD and Regulates Localization of Poly(A) mRNA in Primary Motor Neuron Axons*. J.Neurosci., 2011. **31**(10): p. 3914-3925.
61. Rossoll, W., et al., *Smn, the spinal muscular atrophy-determining gene product, modulates axon growth and localization of beta-actin mRNA in growth cones of motoneurons*. J.Cell Biol., 2003. **163**(4): p. 801-812.
62. Ruggiu, M., et al., *A role for SMN exon 7 splicing in the selective vulnerability of motor neurons in spinal muscular atrophy*. Mol Cell Biol, 2012. **32**(1): p. 126-38.
63. Pellizzoni, L., et al., *A functional interaction between the survival motor neuron complex and RNA polymerase II*. J Cell Biol, 2001. **152**(1): p. 75-85.
64. Watkins, N.J., et al., *Assembly and maturation of the U3 snoRNP in the nucleoplasm in a large dynamic multiprotein complex*. Mol Cell, 2004. **16**(5): p. 789-98.
65. Matera, A.G., R.M. Terns, and M.P. Terns, *Non-coding RNAs: lessons from the small nuclear and small nucleolar RNAs*. Nat Rev Mol Cell Biol, 2007. **8**(3): p. 209-20.
66. Park, H.B., et al., *Survival analysis of spinal muscular atrophy type I*. Korean J Pediatr, 2010. **53**(11): p. 965-70.

67. Schrank, B., et al., *Inactivation of the survival motor neuron gene, a candidate gene for human spinal muscular atrophy, leads to massive cell death in early mouse embryos*. Proc Natl Acad Sci U S A, 1997. **94**(18): p. 9920-5.
68. Monani, U.R., et al., *The human centromeric survival motor neuron gene (SMN2) rescues embryonic lethality in Smn(-/-) mice and results in a mouse with spinal muscular atrophy*. Hum Mol Genet, 2000. **9**(3): p. 333-9.
69. Jablonka, S., et al., *Reduced survival motor neuron (Smn) gene dose in mice leads to motor neuron degeneration: an animal model for spinal muscular atrophy type III*. Hum Mol Genet, 2000. **9**(3): p. 341-6.
70. Le, T.T., et al., *SMNDelta7, the major product of the centromeric survival motor neuron (SMN2) gene, extends survival in mice with spinal muscular atrophy and associates with full-length SMN*. Hum Mol Genet, 2005. **14**(6): p. 845-57.
71. Jablonka, S., et al., *The role of SMN in spinal muscular atrophy*. Journal of neurology, 2000. **247 Suppl 1**: p. 137-42.
72. Pellizzoni, L., *Chaperoning ribonucleoprotein biogenesis in health and disease*. EMBO Rep, 2007. **8**(4): p. 340-5.
73. Li, D.K., et al., *SMN control of RNP assembly: from post-transcriptional gene regulation to motor neuron disease*. Semin Cell Dev Biol, 2014. **32**: p. 22-9.
74. Jablonka, S., et al., *Defective Ca²⁺ channel clustering in axon terminals disturbs excitability in motoneurons in spinal muscular atrophy*. The Journal of cell biology, 2007. **179**(1): p. 139-49.
75. Rowland, L.P., *Diagnosis of amyotrophic lateral sclerosis*. J Neurol Sci, 1998. **160 Suppl 1**: p. S6-24.
76. Przedborski, S., H. Mitsumoto, and L.P. Rowland, *Recent advances in amyotrophic lateral sclerosis research*. Curr Neurol Neurosci Rep, 2003. **3**(1): p. 70-7.
77. Rowland, L.P., *Ameliorating amyotrophic lateral sclerosis*. N Engl J Med, 2010. **362**(10): p. 953-4.
78. Mizutani, T., et al., *Amyotrophic-Lateral-Sclerosis with Ophthalmoplegia and Multisystem Degeneration in Patients on Long-Term Use of Respirators*. Acta Neuropathologica, 1992. **84**(4): p. 372-377.
79. Giordana, M.T., et al., *Neuropathology of olfactory ensheathing cell transplantation into the brain of two amyotrophic lateral sclerosis (ALS) patients*. Brain Pathol, 2010. **20**(4): p. 730-7.
80. Hirano, A., *Neuropathology of ALS: an overview*. Neurology, 1996. **47**(4 Suppl 2): p. S63-6.
81. Ikemoto, A., A. Hirano, and I. Akiguchi, *Neuropathology of amyotrophic lateral sclerosis with extra-motor system degeneration: characteristics and differences in the molecular pathology between ALS with dementia and Guamanian ALS*. Amyotroph Lateral Scler Other Motor Neuron Disord, 2000. **1**(2): p. 97-104.
82. Mackenzie, I.R., *The neuropathology of FTD associated With ALS*. Alzheimer Dis Assoc Disord, 2007. **21**(4): p. S44-9.
83. Yates, D., *Motor neuron disease: Misfolded wild-type SOD1 may link sporadic and familial ALS*. Nat Rev Neurol, 2010. **6**(12): p. 645.
84. Armon, C., *The underestimation of familial ALS and counseling patients with sporadic ALS*. Neurology, 2014. **82**(1): p. 13-4.
85. Gibson, S.B., et al., *Familial clustering of ALS in a population-based resource*. Neurology, 2014. **82**(1): p. 17-22.
86. Benkler, C., et al., *Recent advances in amyotrophic lateral sclerosis research: perspectives for personalized clinical application*. EPMA J, 2010. **1**(2): p. 343-61.
87. Mitchell, J.D., *Guidelines in motor neurone disease (MND)/amyotrophic lateral sclerosis (ALS) - from diagnosis to patient care*. J Neurol, 2000. **247 Suppl 6**: p. VI/7-12.
88. Zoccollella, S., et al., *Signs and symptoms at diagnosis of amyotrophic lateral sclerosis: a population-based study in southern Italy*. Eur J Neurol, 2006. **13**(7): p. 789-92.
89. Barbeito, L.H., et al., *A role for astrocytes in motor neuron loss in amyotrophic lateral sclerosis*. Brain Res Brain Res Rev, 2004. **47**(1-3): p. 263-74.

90. Al-Chalabi, A., et al., *The genetics and neuropathology of amyotrophic lateral sclerosis*. Acta Neuropathol, 2012. **124**(3): p. 339-52.
91. Ravits, J., et al., *Deciphering amyotrophic lateral sclerosis: what phenotype, neuropathology and genetics are telling us about pathogenesis*. Amyotroph Lateral Scler Frontotemporal Degener, 2013. **14 Suppl 1**: p. 5-18.
92. Teyssou, E., et al., *Mutations in SQSTM1 encoding p62 in amyotrophic lateral sclerosis: genetics and neuropathology*. Acta Neuropathol, 2013. **125**(4): p. 511-22.
93. Hasegawa, M., et al., *Phosphorylated TDP-43 in frontotemporal lobar degeneration and amyotrophic lateral sclerosis*. Ann Neurol, 2008. **64**(1): p. 60-70.
94. Lin, W.L. and D.W. Dickson, *Ultrastructural localization of TDP-43 in filamentous neuronal inclusions in various neurodegenerative diseases*. Acta Neuropathol, 2008. **116**(2): p. 205-13.
95. Mizuno, Y., et al., *Peripherin partially localizes in Bunina bodies in amyotrophic lateral sclerosis*. J Neurol Sci, 2011. **302**(1-2): p. 14-8.
96. Mori, F., et al., *Co-localization of Bunina bodies and TDP-43 inclusions in lower motor neurons in amyotrophic lateral sclerosis*. Neuropathology, 2014. **34**(1): p. 71-6.
97. Vinsant, S., et al., *Characterization of early pathogenesis in the SOD1(G93A) mouse model of ALS: part II, results and discussion*. Brain Behav, 2013. **3**(4): p. 431-57.
98. Fujita, Y. and K. Okamoto, *Golgi apparatus of the motor neurons in patients with amyotrophic lateral sclerosis and in mice models of amyotrophic lateral sclerosis*. Neuropathology, 2005. **25**(4): p. 388-94.
99. Ramamohan, P.Y., et al., *Cerebrospinal fluid from amyotrophic lateral sclerosis patients causes fragmentation of the Golgi apparatus in the neonatal rat spinal cord*. Amyotroph Lateral Scler, 2007. **8**(2): p. 79-82.
100. Dupuis, L. and J.P. Loeffler, *Neuromuscular junction destruction during amyotrophic lateral sclerosis: insights from transgenic models*. Curr Opin Pharmacol, 2009. **9**(3): p. 341-6.
101. Rosen, D.R., et al., *Mutations in Cu/Zn superoxide dismutase gene are associated with familial amyotrophic lateral sclerosis*. Nature, 1993. **362**(6415): p. 59-62.
102. Nishimura, A.L., et al., *A mutation in the vesicle-trafficking protein VAPB causes late-onset spinal muscular atrophy and amyotrophic lateral sclerosis*. Am J Hum Genet, 2004. **75**(5): p. 822-31.
103. Neumann, M., et al., *Ubiquitinated TDP-43 in frontotemporal lobar degeneration and amyotrophic lateral sclerosis*. Science, 2006. **314**(5796): p. 130-3.
104. Kwiatkowski, T.J., Jr., et al., *Mutations in the FUS/TLS gene on chromosome 16 cause familial amyotrophic lateral sclerosis*. Science, 2009. **323**(5918): p. 1205-8.
105. Vance, C., et al., *Mutations in FUS, an RNA processing protein, cause familial amyotrophic lateral sclerosis type 6*. Science, 2009. **323**(5918): p. 1208-11.
106. McCann, C., et al., *The Ataxin-2 protein is required for microRNA function and synapse-specific long-term olfactory habituation*. Proc Natl Acad Sci U S A, 2011. **108**(36): p. E655-62.
107. Deng, H.X., et al., *Mutations in UBQLN2 cause dominant X-linked juvenile and adult-onset ALS and ALS/dementia*. Nature, 2011. **477**(7363): p. 211-5.
108. Chen, Y.Z., et al., *Senataxin, the yeast Sen1p orthologue: characterization of a unique protein in which recessive mutations cause ataxia and dominant mutations cause motor neuron disease*. Neurobiol Dis, 2006. **23**(1): p. 97-108.
109. Hadano, S., et al., *Loss of ALS2/Alsln exacerbates motor dysfunction in a SOD1-expressing mouse ALS model by disturbing endolysosomal trafficking*. PLoS One, 2010. **5**(3): p. e9805.
110. DeJesus-Hernandez, M., et al., *Expanded GGGGCC hexanucleotide repeat in noncoding region of C9ORF72 causes chromosome 9p-linked FTD and ALS*. Neuron, 2011. **72**(2): p. 245-56.
111. Renton, A.E., et al., *A hexanucleotide repeat expansion in C9ORF72 is the cause of chromosome 9p21-linked ALS-FTD*. Neuron, 2011. **72**(2): p. 257-68.
112. Lagier-Tourenne, C., M. Polymenidou, and D.W. Cleveland, *TDP-43 and FUS/TLS: emerging roles in RNA processing and neurodegeneration*. Hum Mol Genet, 2010. **19**(R1): p. R46-64.
113. Pesiridis, G.S., V.M. Lee, and J.Q. Trojanowski, *Mutations in TDP-43 link glycine-rich domain functions to amyotrophic lateral sclerosis*. Hum Mol Genet, 2009. **18**(R2): p. R156-62.

114. Barmada, S.J. and S. Finkbeiner, *Pathogenic TARDBP mutations in amyotrophic lateral sclerosis and frontotemporal dementia: disease-associated pathways*. Rev Neurosci, 2010. **21**(4): p. 251-72.
115. Buratti, E., et al., *Nuclear factor TDP-43 and SR proteins promote in vitro and in vivo CFTR exon 9 skipping*. EMBO J, 2001. **20**(7): p. 1774-84.
116. Ayala, Y.M., et al., *TDP-43 regulates its mRNA levels through a negative feedback loop*. EMBO J, 2011. **30**(2): p. 277-88.
117. Buratti, E., et al., *Nuclear factor TDP-43 can affect selected microRNA levels*. FEBS J, 2010. **277**(10): p. 2268-81.
118. Wang, I.F., et al., *TDP-43, the signature protein of FTLD-U, is a neuronal activity-responsive factor*. J Neurochem, 2008. **105**(3): p. 797-806.
119. Mackenzie, I.R., R. Rademakers, and M. Neumann, *TDP-43 and FUS in amyotrophic lateral sclerosis and frontotemporal dementia*. Lancet Neurol, 2010. **9**(10): p. 995-1007.
120. Buratti, E. and F.E. Baralle, *Characterization and functional implications of the RNA binding properties of nuclear factor TDP-43, a novel splicing regulator of CFTR exon 9*. J Biol Chem, 2001. **276**(39): p. 36337-43.
121. Kuo, P.H., et al., *Structural insights into TDP-43 in nucleic-acid binding and domain interactions*. Nucleic Acids Res, 2009. **37**(6): p. 1799-808.
122. Lukavsky, P.J., et al., *Molecular basis of UG-rich RNA recognition by the human splicing factor TDP-43*. Nat Struct Mol Biol, 2013. **20**(12): p. 1443-9.
123. Tollervey, J.R., et al., *Characterizing the RNA targets and position-dependent splicing regulation by TDP-43*. Nature neuroscience, 2011. **14**(4): p. 452-8.
124. Fuentealba, R.A., et al., *Interaction with polyglutamine aggregates reveals a Q/N-rich domain in TDP-43*. J Biol Chem, 2010. **285**(34): p. 26304-14.
125. Cushman, M., et al., *Prion-like disorders: blurring the divide between transmissibility and infectivity*. J Cell Sci, 2010. **123**(Pt 8): p. 1191-201.
126. Kim, S.H., et al., *Amyotrophic lateral sclerosis-associated proteins TDP-43 and FUS/TLS function in a common biochemical complex to co-regulate HDAC6 mRNA*. J Biol Chem, 2010. **285**(44): p. 34097-105.
127. Lagier-Tourenne, C. and D.W. Cleveland, *Rethinking ALS: the FUS about TDP-43*. Cell, 2009. **136**(6): p. 1001-4.
128. Lerga, A., et al., *Identification of an RNA binding specificity for the potential splicing factor TLS*. J Biol Chem, 2001. **276**(9): p. 6807-16.
129. Iko, Y., et al., *Domain architectures and characterization of an RNA-binding protein, TLS*. J Biol Chem, 2004. **279**(43): p. 44834-40.
130. Polymenidou, M., et al., *Long pre-mRNA depletion and RNA missplicing contribute to neuronal vulnerability from loss of TDP-43*. Nat Neurosci, 2011. **14**(4): p. 459-68.
131. Freibaum, B.D., et al., *Global analysis of TDP-43 interacting proteins reveals strong association with RNA splicing and translation machinery*. J Proteome Res, 2010. **9**(2): p. 1104-20.
132. Buratti, E. and F.E. Baralle, *TDP-43: gumming up neurons through protein-protein and protein-RNA interactions*. Trends Biochem Sci, 2012. **37**(6): p. 237-47.
133. Baker, M., et al., *Mutations in progranulin cause tau-negative frontotemporal dementia linked to chromosome 17*. Nature, 2006. **442**(7105): p. 916-9.
134. Cruts, M., et al., *Null mutations in progranulin cause ubiquitin-positive frontotemporal dementia linked to chromosome 17q21*. Nature, 2006. **442**(7105): p. 920-4.
135. Ayala, V., et al., *Cell stress induces TDP-43 pathological changes associated with ERK1/2 dysfunction: implications in ALS*. Acta Neuropathol, 2011. **122**(3): p. 259-70.
136. Igaz, L.M., et al., *Dysregulation of the ALS-associated gene TDP-43 leads to neuronal death and degeneration in mice*. J Clin Invest, 2011. **121**(2): p. 726-38.
137. Gijssels, I., et al., *A C9orf72 promoter repeat expansion in a Flanders-Belgian cohort with disorders of the frontotemporal lobar degeneration-amyotrophic lateral sclerosis spectrum: a gene identification study*. Lancet Neurol, 2012. **11**(1): p. 54-65.

138. Majounie, E., et al., *Frequency of the C9orf72 hexanucleotide repeat expansion in patients with amyotrophic lateral sclerosis and frontotemporal dementia: a cross-sectional study*. *Lancet Neurol*, 2012. **11**(4): p. 323-30.
139. Ciura, S., et al., *Loss of function of C9orf72 causes motor deficits in a zebrafish model of amyotrophic lateral sclerosis*. *Ann Neurol*, 2013. **74**(2): p. 180-7.
140. Cooper-Knock, J., et al., *Clinico-pathological features in amyotrophic lateral sclerosis with expansions in C9ORF72*. *Brain*, 2012. **135**(Pt 3): p. 751-64.
141. Tomiyama, H., [*C9orf72 in Japanese amyotrophic lateral sclerosis (ALS)*]. *Rinsho Shinkeigaku*, 2013. **53**(11): p. 1074-6.
142. Konno, T., et al., *Japanese amyotrophic lateral sclerosis patients with GGGGCC hexanucleotide repeat expansion in C9ORF72*. *J Neurol Neurosurg Psychiatry*, 2013. **84**(4): p. 398-401.
143. La Spada, A.R. and J.P. Taylor, *Repeat expansion disease: progress and puzzles in disease pathogenesis*. *Nat Rev Genet*, 2010. **11**(4): p. 247-58.
144. Ling, S.C., M. Polymenidou, and D.W. Cleveland, *Converging mechanisms in ALS and FTD: disrupted RNA and protein homeostasis*. *Neuron*, 2013. **79**(3): p. 416-38.
145. Lagier-Tourenne, C., et al., *Targeted degradation of sense and antisense C9orf72 RNA foci as therapy for ALS and frontotemporal degeneration*. *Proc Natl Acad Sci U S A*, 2013. **110**(47): p. E4530-9.
146. Mizielińska, S., et al., *C9orf72 frontotemporal lobar degeneration is characterised by frequent neuronal sense and antisense RNA foci*. *Acta Neuropathol*, 2013. **126**(6): p. 845-57.
147. Haeusler, A.R., et al., *C9orf72 nucleotide repeat structures initiate molecular cascades of disease*. *Nature*, 2014. **507**(7491): p. 195-200.
148. Cooper-Knock, J., et al., *Sequestration of multiple RNA recognition motif-containing proteins by C9orf72 repeat expansions*. *Brain*, 2014. **137**(Pt 7): p. 2040-51.
149. Gascon, E. and F.B. Gao, *Cause or Effect: Misregulation of microRNA Pathways in Neurodegeneration*. *Front Neurosci*, 2012. **6**: p. 48.
150. Reddy, K., et al., *The disease-associated r(GGGGCC)_n repeat from the C9orf72 gene forms tract length-dependent uni- and multimolecular RNA G-quadruplex structures*. *J Biol Chem*, 2013. **288**(14): p. 9860-6.
151. Su, Z., et al., *Discovery of a biomarker and lead small molecules to target r(GGGGCC)-associated defects in c9FTD/ALS*. *Neuron*, 2014. **83**(5): p. 1043-50.
152. Moseley, M.L., et al., *Bidirectional expression of CUG and CAG expansion transcripts and intranuclear polyglutamine inclusions in spinocerebellar ataxia type 8*. *Nat Genet*, 2006. **38**(7): p. 758-69.
153. Zu, T., et al., *Non-ATG-initiated translation directed by microsatellite expansions*. *Proc Natl Acad Sci U S A*, 2011. **108**(1): p. 260-5.
154. Mori, K., et al., *The C9orf72 GGGGCC repeat is translated into aggregating dipeptide-repeat proteins in FTL/ALS*. *Science*, 2013. **339**(6125): p. 1335-8.
155. Mori, K., et al., *Bidirectional transcripts of the expanded C9orf72 hexanucleotide repeat are translated into aggregating dipeptide repeat proteins*. *Acta Neuropathol*, 2013. **126**(6): p. 881-93.
156. Kwon, I., et al., *Poly-dipeptides encoded by the C9orf72 repeats bind nucleoli, impede RNA biogenesis, and kill cells*. *Science*, 2014. **345**(6201): p. 1139-45.
157. Mizielińska, S., et al., *C9orf72 repeat expansions cause neurodegeneration in Drosophila through arginine-rich proteins*. *Science*, 2014. **345**(6201): p. 1192-4.
158. Zu, T., et al., *RAN proteins and RNA foci from antisense transcripts in C9ORF72 ALS and frontotemporal dementia*. *Proc Natl Acad Sci U S A*, 2013. **110**(51): p. E4968-77.
159. Mackenzie, I.R., et al., *Pathological TDP-43 distinguishes sporadic amyotrophic lateral sclerosis from amyotrophic lateral sclerosis with SOD1 mutations*. *Ann Neurol*, 2007. **61**(5): p. 427-34.

160. Walsh, M.J., et al., *Invited review: decoding the pathophysiological mechanisms that underlie RNA dysregulation in neurodegenerative disorders: a review of the current state of the art.* *Neuropathol Appl Neurobiol*, 2015. **41**(2): p. 109-34.
161. Al-Sarraj, S., et al., *p62 positive, TDP-43 negative, neuronal cytoplasmic and intranuclear inclusions in the cerebellum and hippocampus define the pathology of C9orf72-linked FTL and MND/ALS.* *Acta Neuropathol*, 2011. **122**(6): p. 691-702.
162. Waite, A.J., et al., *Reduced C9orf72 protein levels in frontal cortex of amyotrophic lateral sclerosis and frontotemporal degeneration brain with the C9ORF72 hexanucleotide repeat expansion.* *Neurobiol Aging*, 2014. **35**(7): p. 1779 e5-1779 e13.
163. Cooper-Knock, J., et al., *C9ORF72 transcription in a frontotemporal dementia case with two expanded alleles.* *Neurology*, 2013. **81**(19): p. 1719-21.
164. Xi, Z., et al., *Hypermethylation of the CpG-island near the C9orf72 G(4)C(2)-repeat expansion in FTL patients.* *Hum Mol Genet*, 2014. **23**(21): p. 5630-7.
165. Xi, Z., et al., *Hypermethylation of the CpG island near the G4C2 repeat in ALS with a C9orf72 expansion.* *Am J Hum Genet*, 2013. **92**(6): p. 981-9.
166. Belzil, V.V., et al., *Reduced C9orf72 gene expression in c9FTD/ALS is caused by histone trimethylation, an epigenetic event detectable in blood.* *Acta Neuropathol*, 2013. **126**(6): p. 895-905.
167. Wen, X., et al., *Antisense Proline-Arginine RAN Dipeptides Linked to C9ORF72-ALS/FTD Form Toxic Nuclear Aggregates that Initiate In Vitro and In Vivo Neuronal Death.* *Neuron*, 2014. **84**(6): p. 1213-25.
168. Therrien, M., et al., *Deletion of C9ORF72 results in motor neuron degeneration and stress sensitivity in C. elegans.* *PLoS One*, 2013. **8**(12): p. e83450.
169. Tronche, F., et al., *Disruption of the glucocorticoid receptor gene in the nervous system results in reduced anxiety.* *Nat Genet*, 1999. **23**(1): p. 99-103.
170. Koppers, M., et al., *C9orf72 ablation in mice does not cause motor neuron degeneration or motor deficits.* *Ann Neurol*, 2015.
171. Harms, M.B., et al., *Lack of C9ORF72 coding mutations supports a gain of function for repeat expansions in amyotrophic lateral sclerosis.* *Neurobiol Aging*, 2013. **34**(9): p. 2234 e13-9.
172. Fratta, P., et al., *Homozygosity for the C9orf72 GGGGCC repeat expansion in frontotemporal dementia.* *Acta Neuropathol*, 2013. **126**(3): p. 401-9.
173. Donnelly, C.J., et al., *RNA toxicity from the ALS/FTD C9ORF72 expansion is mitigated by antisense intervention.* *Neuron*, 2013. **80**(2): p. 415-28.
174. Sareen, D., et al., *Targeting RNA foci in iPSC-derived motor neurons from ALS patients with a C9ORF72 repeat expansion.* *Sci Transl Med*, 2013. **5**(208): p. 208ra149.
175. Prudencio, M., et al., *Distinct brain transcriptome profiles in C9orf72-associated and sporadic ALS.* *Nat Neurosci*, 2015.
176. Zhang, Y., et al., *An RNA-sequencing transcriptome and splicing database of glia, neurons, and vascular cells of the cerebral cortex.* *J Neurosci*, 2014. **34**(36): p. 11929-47.
177. Zhang, Y., et al., *Purification and Characterization of Progenitor and Mature Human Astrocytes Reveals Transcriptional and Functional Differences with Mouse.* *Neuron*, 2016. **89**(1): p. 37-53.
178. Suzuki, N., et al., *The mouse C9ORF72 ortholog is enriched in neurons known to degenerate in ALS and FTD.* *Nat Neurosci*, 2013. **16**(12): p. 1725-7.
179. Atanasio, A., et al., *C9orf72 ablation causes immune dysregulation characterized by leukocyte expansion, autoantibody production, and glomerulonephropathy in mice.* *Sci Rep*, 2016. **6**: p. 23204.
180. O'Rourke, J.G., et al., *C9orf72 is required for proper macrophage and microglial function in mice.* *Science*, 2016. **351**(6279): p. 1324-9.
181. Boillee, S., et al., *Onset and progression in inherited ALS determined by motor neurons and microglia.* *Science*, 2006. **312**(5778): p. 1389-92.
182. Ilieva, H., M. Polymenidou, and D.W. Cleveland, *Non-cell autonomous toxicity in neurodegenerative disorders: ALS and beyond.* *J Cell Biol*, 2009. **187**(6): p. 761-72.

183. Chew, J., et al., *Neurodegeneration. C9ORF72 repeat expansions in mice cause TDP-43 pathology, neuronal loss, and behavioral deficits*. Science, 2015. **348**(6239): p. 1151-4.
184. Peters, O.M., et al., *Human C9ORF72 Hexanucleotide Expansion Reproduces RNA Foci and Dipeptide Repeat Proteins but Not Neurodegeneration in BAC Transgenic Mice*. Neuron, 2015. **88**(5): p. 902-9.
185. Bruijn, L.I., et al., *Aggregation and motor neuron toxicity of an ALS-linked SOD1 mutant independent from wild-type SOD1*. Science, 1998. **281**(5384): p. 1851-4.
186. Levine, T.P., et al., *The product of C9orf72, a gene strongly implicated in neurodegeneration, is structurally related to DENN Rab-GEFs*. Bioinformatics, 2013. **29**(4): p. 499-503.
187. Zhang, D., et al., *Discovery of Novel DENN Proteins: Implications for the Evolution of Eukaryotic Intracellular Membrane Structures and Human Disease*. Front Genet, 2012. **3**: p. 283.
188. Yoshimura, S., et al., *Family-wide characterization of the DENN domain Rab GDP-GTP exchange factors*. J Cell Biol, 2010. **191**(2): p. 367-81.
189. Bhui, T. and J.K. Roy, *Rab proteins: the key regulators of intracellular vesicle transport*. Exp Cell Res, 2014. **328**(1): p. 1-19.
190. Farg, M.A., et al., *C9ORF72, implicated in amyotrophic lateral sclerosis and frontotemporal dementia, regulates endosomal trafficking*. Hum Mol Genet, 2014. **23**(13): p. 3579-95.
191. Verhoeven, K., et al., *Mutations in the small GTP-ase late endosomal protein RAB7 cause Charcot-Marie-Tooth type 2B neuropathy*. Am J Hum Genet, 2003. **72**(3): p. 722-7.
192. Topp, J.D., et al., *Alsin is a Rab5 and Rac1 guanine nucleotide exchange factor*. J Biol Chem, 2004. **279**(23): p. 24612-23.
193. Freibaum, B.D., et al., *GGGGCC repeat expansion in C9orf72 compromises nucleocytoplasmic transport*. Nature, 2015. **525**(7567): p. 129-33.
194. Jovicic, A., et al., *Modifiers of C9orf72 dipeptide repeat toxicity connect nucleocytoplasmic transport defects to FTD/ALS*. Nat Neurosci, 2015. **18**(9): p. 1226-9.
195. Zhang, K., et al., *The C9orf72 repeat expansion disrupts nucleocytoplasmic transport*. Nature, 2015. **525**(7567): p. 56-61.
196. Zhang, Y.J., et al., *C9ORF72 poly(GA) aggregates sequester and impair HR23 and nucleocytoplasmic transport proteins*. Nat Neurosci, 2016. **19**(5): p. 668-77.
197. Haeusler, A.R., C.J. Donnelly, and J.D. Rothstein, *The expanding biology of the C9orf72 nucleotide repeat expansion in neurodegenerative disease*. Nat Rev Neurosci, 2016. **17**(6): p. 383-95.
198. Wiese, S., et al., *Isolation and enrichment of embryonic mouse motoneurons from the lumbar spinal cord of individual mouse embryos*. Nature protocols, 2010. **5**(1): p. 31-8.
199. Bender, F.L., et al., *High-efficiency gene transfer into cultured embryonic motoneurons using recombinant lentiviruses*. Histochemistry and cell biology, 2007. **127**(4): p. 439-48.
200. Chong, S. and M.Q. Xu, *Protein splicing of the Saccharomyces cerevisiae VMA intein without the endonuclease motifs*. J Biol Chem, 1997. **272**(25): p. 15587-90.
201. Fischer, M., et al., *Rapid actin-based plasticity in dendritic spines*. Neuron, 1998. **20**(5): p. 847-54.
202. Sanger, F., S. Nicklen, and A.R. Coulson, *DNA sequencing with chain-terminating inhibitors*. Proc Natl Acad Sci U S A, 1977. **74**(12): p. 5463-7.
203. van Dijk, T.B., et al., *Friend of Prmt1, a novel chromatin target of protein arginine methyltransferases*. Mol Cell Biol, 2010. **30**(1): p. 260-72.
204. Yamazaki, T., et al., *FUS-SMN protein interactions link the motor neuron diseases ALS and SMA*. Cell Rep, 2012. **2**(4): p. 799-806.
205. Kim, J.H., et al., *Protein-protein interaction among hnRNPs shuttling between nucleus and cytoplasm*. J Mol Biol, 2000. **298**(3): p. 395-405.
206. Huang, J., et al., *Cloning and expression of a novel isoform of heterogeneous nuclear ribonucleoprotein-R*. Neuroreport, 2005. **16**(7): p. 727-30.
207. Gitcho, M.A., et al., *TDP-43 A315T mutation in familial motor neuron disease*. Annals of neurology, 2008. **63**(4): p. 535-8.

208. Maekawa, S., et al., *TDP-43 is consistently co-localized with ubiquitinated inclusions in sporadic and Guam amyotrophic lateral sclerosis but not in familial amyotrophic lateral sclerosis with and without SOD1 mutations*. *Neuropathology : official journal of the Japanese Society of Neuropathology*, 2009. **29**(6): p. 672-83.
209. Sreedharan, J., et al., *TDP-43 mutations in familial and sporadic amyotrophic lateral sclerosis*. *Science*, 2008. **319**(5870): p. 1668-72.
210. Ling, S.C., et al., *ALS-associated mutations in TDP-43 increase its stability and promote TDP-43 complexes with FUS/TLS*. *Proceedings of the National Academy of Sciences of the United States of America*, 2010. **107**(30): p. 13318-23.
211. Tollervey, J.R., et al., *Characterizing the RNA targets and position-dependent splicing regulation by TDP-43*. *Nat Neurosci*, 2011. **14**(4): p. 452-8.
212. Kabashi, E., et al., *TARDBP mutations in individuals with sporadic and familial amyotrophic lateral sclerosis*. *Nat Genet*, 2008. **40**(5): p. 572-4.
213. Peritz, T., et al., *Immunoprecipitation of mRNA-protein complexes*. *Nat Protoc*, 2006. **1**(2): p. 577-80.
214. Avendano-Vazquez, S.E., et al., *Autoregulation of TDP-43 mRNA levels involves interplay between transcription, splicing, and alternative polyA site selection*. *Genes Dev*, 2012. **26**(15): p. 1679-84.
215. Vance, C., et al., *Familial amyotrophic lateral sclerosis with frontotemporal dementia is linked to a locus on chromosome 9p13.2-21.3*. *Brain*, 2006. **129**(Pt 4): p. 868-76.
216. Shatunov, A., et al., *Chromosome 9p21 in sporadic amyotrophic lateral sclerosis in the UK and seven other countries: a genome-wide association study*. *Lancet Neurol*, 2010. **9**(10): p. 986-94.
217. Smith, B.N., et al., *The C9ORF72 expansion mutation is a common cause of ALS+/-FTD in Europe and has a single founder*. *Eur J Hum Genet*, 2013. **21**(1): p. 102-8.
218. Lee, Y.B., et al., *Hexanucleotide repeats in ALS/FTD form length-dependent RNA foci, sequester RNA binding proteins, and are neurotoxic*. *Cell Rep*, 2013. **5**(5): p. 1178-86.
219. Keilhauer, E.C., M.Y. Hein, and M. Mann, *Accurate protein complex retrieval by affinity enrichment mass spectrometry (AE-MS) rather than affinity purification mass spectrometry (AP-MS)*. *Mol Cell Proteomics*, 2015. **14**(1): p. 120-35.
220. May, S., et al., *C9orf72 FTL/ALS-associated Gly-Ala dipeptide repeat proteins cause neuronal toxicity and Unc119 sequestration*. *Acta Neuropathol*, 2014. **128**(4): p. 485-503.
221. Bravo-Cordero, J.J., et al., *Functions of cofilin in cell locomotion and invasion*. *Nat Rev Mol Cell Biol*, 2013. **14**(7): p. 405-15.
222. Stern, S., et al., *The transcription factor serum response factor stimulates axon regeneration through cytoplasmic localization and cofilin interaction*. *J Neurosci*, 2013. **33**(48): p. 18836-48.
223. Agnew, B.J., L.S. Minamide, and J.R. Bamburg, *Reactivation of phosphorylated actin depolymerizing factor and identification of the regulatory site*. *J Biol Chem*, 1995. **270**(29): p. 17582-7.
224. Moriyama, K., K. Iida, and I. Yahara, *Phosphorylation of Ser-3 of cofilin regulates its essential function on actin*. *Genes Cells*, 1996. **1**(1): p. 73-86.
225. Romano, M. and E. Buratti, *Targeting RNA binding proteins involved in neurodegeneration*. *J Biomol Screen*, 2013. **18**(9): p. 967-83.
226. Piazzon, N., et al., *In vitro and in cellulo evidences for association of the survival of motor neuron complex with the fragile X mental retardation protein*. *J.Biol.Chem.*, 2008. **283**(9): p. 5598-5610.
227. Dombert, B., et al., *Presynaptic localization of Smn and hnRNP R in axon terminals of embryonic and postnatal mouse motoneurons*. *PLoS One*, 2014. **9**(10): p. e110846.
228. Rossoll, W., et al., *Specific interaction of Smn, the spinal muscular atrophy determining gene product, with hnRNP R and gry-rbp/hnRNP-Q: a role for Smn in RNA processing in motor axons?* *Hum.Mol.Genet.*, 2002. **11**(1): p. 93-105.

229. Tsuiji, H., et al., *Spliceosome integrity is defective in the motor neuron diseases ALS and SMA*. EMBO Mol.Med., 2013. **5**(2): p. 221-234.
230. Yamazaki, T., et al., *FUS-SMN protein interactions link the motor neuron diseases ALS and SMA*. Cell Rep., 2012. **2**(4): p. 799-806.
231. Fallini, C., et al., *Dynamics of survival of motor neuron (SMN) protein interaction with the mRNA-binding protein IMP1 facilitates its trafficking into motor neuron axons*. Dev.Neurobiol., 2013.
232. Glinka, M., et al., *The heterogeneous nuclear ribonucleoprotein-R is necessary for axonal beta-actin mRNA translocation in spinal motor neurons*. Hum.Mol.Genet., 2010. **19**(10): p. 1951-1966.
233. McWhorter, M.L., et al., *Knockdown of the survival motor neuron (Smn) protein in zebrafish causes defects in motor axon outgrowth and pathfinding*. J.Cell Biol., 2003. **162**(5): p. 919-931.
234. Chaudhury, A., P. Chander, and P.H. Howe, *Heterogeneous nuclear ribonucleoproteins (hnRNPs) in cellular processes: Focus on hnRNP E1's multifunctional regulatory roles*. RNA., 2010. **16**(8): p. 1449-1462.
235. Kong, L., et al., *Impaired synaptic vesicle release and immaturity of neuromuscular junctions in spinal muscular atrophy mice*. J.Neurosci., 2009. **29**(3): p. 842-851.
236. Zubovic, L., M. Baralle, and F.E. Baralle, *Mutually exclusive splicing regulates the Nav 1.6 sodium channel function through a combinatorial mechanism that involves three distinct splicing regulatory elements and their ligands*. Nucleic Acids Res, 2012. **40**(13): p. 6255-69.
237. Boon, K.L., et al., *Zebrafish survival motor neuron mutants exhibit presynaptic neuromuscular junction defects*. Hum.Mol.Genet., 2009. **18**(19): p. 3615-3625.
238. Jablonka, S., et al., *Defective Ca²⁺ channel clustering in axon terminals disturbs excitability in motoneurons in spinal muscular atrophy*. J.Cell Biol., 2007. **179**(1): p. 139-149.
239. Jablonka, S., et al., *Mechanisms for axon maintenance and plasticity in motoneurons: alterations in motoneuron disease*. J.Anat., 2014. **224**(1): p. 3-14.
240. Nishimune, H., J.R. Sanes, and S.S. Carlson, *A synaptic laminin-calcium channel interaction organizes active zones in motor nerve terminals*. Nature, 2004. **432**(7017): p. 580-587.
241. Saal, L., et al., *Subcellular transcriptome alterations in a cell culture model of spinal muscular atrophy point to widespread defects in axonal growth and presynaptic differentiation*. RNA, 2014. **20**(11): p. 1789-802.
242. Ruiz, R., et al., *Altered intracellular Ca²⁺ homeostasis in nerve terminals of severe spinal muscular atrophy mice*. J.Neurosci., 2010. **30**(3): p. 849-857.
243. Groen, E.J., et al., *ALS-associated mutations in FUS disrupt the axonal distribution and function of SMN*. Hum.Mol.Genet., 2013. **22**(18): p. 3690-3704.
244. Achsel, T., et al., *The intriguing case of motor neuron disease: ALS and SMA come closer*. Biochem.Soc.Trans., 2013. **41**(6): p. 1593-1597.
245. Gerbino, V., et al., *Mislocalised FUS mutants stall spliceosomal snRNPs in the cytoplasm*. Neurobiol.Dis., 2013. **55**: p. 120-128.
246. Dreyfuss, G., V.N. Kim, and N. Kataoka, *Messenger-RNA-binding proteins and the messages they carry*. Nat Rev Mol Cell Biol, 2002. **3**(3): p. 195-205.
247. Swanson, M.S. and G. Dreyfuss, *RNA binding specificity of hnRNP proteins: a subset bind to the 3' end of introns*. EMBO J, 1988. **7**(11): p. 3519-29.
248. Pinol-Roma, S., et al., *Immunopurification of heterogeneous nuclear ribonucleoprotein particles reveals an assortment of RNA-binding proteins*. Genes Dev, 1988. **2**(2): p. 215-27.
249. Glisovic, T., et al., *RNA-binding proteins and post-transcriptional gene regulation*. FEBS Lett, 2008. **582**(14): p. 1977-86.
250. Cartegni, L., et al., *hnRNP A1 selectively interacts through its Gly-rich domain with different RNA-binding proteins*. J Mol Biol, 1996. **259**(3): p. 337-48.
251. Buratti, E., et al., *TDP-43 binds heterogeneous nuclear ribonucleoprotein A/B through its C-terminal tail: an important region for the inhibition of cystic fibrosis transmembrane conductance regulator exon 9 splicing*. J Biol Chem, 2005. **280**(45): p. 37572-84.

252. Arai, T., et al., *TDP-43 is a component of ubiquitin-positive tau-negative inclusions in frontotemporal lobar degeneration and amyotrophic lateral sclerosis*. *Biochem Biophys Res Commun*, 2006. **351**(3): p. 602-11.
253. Kim, H.J., et al., *Mutations in prion-like domains in hnRNPA2B1 and hnRNPA1 cause multisystem proteinopathy and ALS*. *Nature*, 2013. **495**(7442): p. 467-473.
254. Armstrong, G.A. and P. Drapeau, *Loss and gain of FUS function impair neuromuscular synaptic transmission in a genetic model of ALS*. *Hum.Mol.Genet.*, 2013. **22**(21): p. 4282-4292.
255. Shahidullah, M., et al., *Defects in synapse structure and function precede motor neuron degeneration in Drosophila models of FUS-related ALS*. *J.Neurosci.*, 2013. **33**(50): p. 19590-19598.
256. Shan, X., et al., *Altered distributions of Gemini of coiled bodies and mitochondria in motor neurons of TDP-43 transgenic mice*. *Proc.Natl.Acad.Sci.U.S.A*, 2010. **107**(37): p. 16325-16330.
257. Alami, N.H., et al., *Axonal transport of TDP-43 mRNA granules is impaired by ALS-causing mutations*. *Neuron*, 2014. **81**(3): p. 536-543.
258. Kuo, P.H., et al., *The crystal structure of TDP-43 RRM1-DNA complex reveals the specific recognition for UG- and TG-rich nucleic acids*. *Nucleic Acids Res*, 2014. **42**(7): p. 4712-22.
259. Johnson, B.S., et al., *TDP-43 is intrinsically aggregation-prone, and amyotrophic lateral sclerosis-linked mutations accelerate aggregation and increase toxicity*. *J Biol Chem*, 2009. **284**(30): p. 20329-39.
260. Kabashi, E., et al., *Gain and loss of function of ALS-related mutations of TARDBP (TDP-43) cause motor deficits in vivo*. *Hum Mol Genet*, 2010. **19**(4): p. 671-83.
261. Duan, W., et al., *Mutant TAR DNA-binding protein-43 induces oxidative injury in motor neuron-like cell*. *Neuroscience*, 2010. **169**(4): p. 1621-9.
262. Austin, J.A., et al., *Disease causing mutants of TDP-43 nucleic acid binding domains are resistant to aggregation and have increased stability and half-life*. *Proc Natl Acad Sci U S A*, 2014. **111**(11): p. 4309-14.
263. Ling, S.C., et al., *ALS-associated mutations in TDP-43 increase its stability and promote TDP-43 complexes with FUS/TLS*. *Proc Natl Acad Sci U S A*, 2010. **107**(30): p. 13318-23.
264. Gendron, T.F., D.M. Cosio, and L. Petrucelli, *c9RAN translation: a potential therapeutic target for the treatment of amyotrophic lateral sclerosis and frontotemporal dementia*. *Expert Opin Ther Targets*, 2013. **17**(9): p. 991-5.
265. Almeida, S., et al., *Modeling key pathological features of frontotemporal dementia with C9ORF72 repeat expansion in iPSC-derived human neurons*. *Acta Neuropathol*, 2013. **126**(3): p. 385-99.
266. Vatovec, S., A. Kovanda, and B. Rogelj, *Unconventional features of C9ORF72 expanded repeat in amyotrophic lateral sclerosis and frontotemporal lobar degeneration*. *Neurobiol Aging*, 2014. **35**(10): p. 2421 e1-2421 e12.
267. Mori, K., et al., *hnRNP A3 binds to GGGGCC repeats and is a constituent of p62-positive/TDP43-negative inclusions in the hippocampus of patients with C9orf72 mutations*. *Acta Neuropathol*, 2013. **125**(3): p. 413-23.
268. Barski, A., et al., *High-resolution profiling of histone methylations in the human genome*. *Cell*, 2007. **129**(4): p. 823-37.
269. Lam, E.Y., et al., *G-quadruplex structures are stable and detectable in human genomic DNA*. *Nat Commun*, 2013. **4**: p. 1796.
270. Cingolani, L.A., et al., *Activity-dependent regulation of synaptic AMPA receptor composition and abundance by beta3 integrins*. *Neuron*, 2008. **58**(5): p. 749-62.
271. Huang, W., et al., *mTORC2 controls actin polymerization required for consolidation of long-term memory*. *Nat Neurosci*, 2013. **16**(4): p. 441-8.

9. APPENDIX

9.1 List of Figures:

Figure 1: Genetics of SMA in humans.....	7
Figure 2: SMN-dependent RNP assembly pathways and their link to SMA.....	11
Figure 3: TDP-43 and FUS/TLS mutations in ALS.....	17
Figure 4: Pathogenic mechanisms for G4C2 repeat expansion.....	20
Figure 5: Cellular processes impaired by the C9ORF72 nucleotide repeat expansion.....	27
Figure 6: Crosslinking of beads with antibody.	64
Figure 7: Purification scheme of recombinant hnRNP R expressed as His-tagged protein in <i>E. coli</i> strain BL21.....	69
Figure 8: Affinity purification profile on a fast protein liquid chromatography (FPLC) of hnRNP R and SDS-PAGE of recombinant hnRNP R purification steps visualized by silver staining.	69
Figure 9: Purification scheme of recombinant SMN expressed as His-tagged protein in <i>E. coli</i> strain BL21.	70
Figure 10: Affinity purification profile on a FPLC of SMN and SDS-PAGE of recombinant SMN purification steps visualized by colloidal staining.....	70
Figure 11: TDP-43 Full length, fragments and mutants.....	71
Figure 12: Cloning of TDP-43 mutants.....	72
Figure 13: Western blot for TDP43, mutants and fragments.	72
Figure 14: Coimmunoprecipitation of SMN and hnRNP R in primary motoneurons, native spinal cord and HEK293T cells.	74
Figure 15: SMN immunoprecipitations from recombinant proteins and co-immunoprecipitations of hnRNP R.....	76
Figure 16: Recombinant hnRNP R immunoprecipitations and co-immunoprecipitations of SMN.....	76

Figure 17: Lentiviral knockdown of hnRNP R and SMN in motoneurons.....	77
Figure 18: Subcellular distribution of SMN and hnRNP R protein in primary mouse motoneurons.....	78
Figure 19: Subcellular distribution of hnRNP R is altered in SMA type I primary motoneurons.....	79
Figure 20: Cytoplasmic hnRNP R is reduced in SMA type I E18 spinal cord.....	81
Figure 21: TDP-43 wildtype and mutant protein pull down from NSC-34 cells.....	82
Figure 22: Quantification of pull-down of hnRNP R, FUS/TLS, and SMN by wildtype and mutant TDP-43 from NSC-34 cells.....	83
Figure 23: Recombinant TDP-43 immunoprecipitations.....	84
Figure 24: Co-immunoprecipitations of recombinant SMN by TDP-43 antibodies.....	84
Figure 25: Electrophoretic mobility shift assay of radioactively labeled β -actin 3'UTR with recombinant hnRNP R and SMN.....	86
Figure 26: 3'UTR of β -actin interaction with TDP-43.....	87
Figure 27: EMSA for TDP-43 interaction with the 3'UTR of β -actin and the influence of SMN enhancing the binding of the 3'UTR of β -actin to TDP-43.....	89
Figure 28: Quantification of RNA pull down of overexpressed HA-tagged TDP-43 and mutants in NSC-34.....	90
Figure 29: Localisation of shRNA site in the mouse <i>C9orf72</i> gene with its splice isoforms..	92
Figure 30: Confirmation of C9ORF72 overexpression and knockdown in cultured mouse motoneurons.....	93
Figure 31: Altered C9ORF72 expression does not affect motoneuron survival but axonal length.....	94
Figure 32: Interactome of C9ORF72 in NSC34 cells.....	96
Figure 33: Interactome analysis of huC9ORF72 protein.....	97

Figure 34: C9ORF72 colocalization with overexpressed huC9ORF72-HA at 5DIV cultured motoneurons.	98
Figure 35: Immunoprecipitation confirming the interaction of C9ORF72 with cofilin from motoneurons.	99
Figure 36: C9ORF72 modulates cofilin activity.	100
Figure 37: Upregulation of p-cofilin in lymphoblastoid cells from C9ORF72 repeat expansion patients.	101
Figure 38: Construction and efficacy of viral constructs for C9ORF72 knockdown and coexpression of GFP-actin.	102
Figure 39: C9ORF72 regulates actin dynamics.	103
Figure 40: Altered G/F actin ratio in motoneurons after overexpression and knockdown of C9ORF72.	105

9.2 List of Tables:

Table 1: Genes associated with familial ALS.	13
Table 2: cell lines and primary culture used in the study.	28
Table 3: Bacterial strains used.	28
Table 4: Antibiotics used for bacterial culture.	29
Table 5: Requirements for mouse motoneuronal culture.	29
Table 6: Buffer for Immunofluorescence.	31
Table 7: Buffer for Western blotting.	32
Table 8: Commercial kits and molecular ladders.	33
Table 9: Stock buffer for protein purification.	33
Table 10: Columns used for protein purification.	36
Table 11: Primary antibodies used for Western blotting (WB), immunofluorescence (IF).....	36
Table 12: Secondary antibodies used for immunofluorescence.	37
Table 13: Buffer used for EMSA.	39
Table 14: Plasmid concentration required for lentivirus production.	47
Table 15: Recombinant protein binding buffer	50
Table 16: EMSA reaction setup.	51
Table 17: Linearisation of beta-actin plasmid.	52
Table 18: Radiolabeling beta-actin 3'UTR mRNA.	52
Table 19: Cytosolic fractionation buffer:	53
Table 20: Nuclear fractionation buffer.	53
Table 21: G-actin stabilization buffer.	55
Table 22: F-actin depolymerization buffer.	56
Table 23: Resolving Gel.	56

Table 24: Stacking Gel.....	57
Table 25: Blot size for protein blotting.	57
Table 26: Gel fixing solution:	58
Table 27: Coomassie stain.....	58
Table 28: Destain solution.....	59
Table 29: PCR cycling conditions.....	59
Table 30: Ligation reaction setup.....	60
Table 31: Lysis buffer for plasmid purification.	62
Table 32: Table of affinity of protein A and protein G coupled beads to mouse and rabbit antibody.....	64

9.3 Abbreviations.

ALS	Amyotrophic lateral sclerosis
ANOVA	Analysis of variance
ARE	Adenylate-Uridylate Rich Element
AD	Autosomal dominant
ALS	Amyotrophic lateral sclerosis
ALYREF	Aly/REF export factor
AR	Autosomal recessive
BDNF	Brain derived neurotrophic factor
Bcl-2	B-cell lymphoma 2
BIM	Bcl-2 interacting mediator of cell death
bp	Base pair
CMV	Cyto megalovirus
CNS	Central nervous system
DIV	Days in-vitro
DNA	Deoxyribonucleic acid
DPRs	Dipeptide repeat proteins
FALS	Familial ALS
FTLD	Frontotemporal lobar degeneration
FUS/TLS	Fused in Sarcoma/Translocated in Sarcoma
GAPDH	Glyceraldehyde 3-phosphate dehydrogenase
Gem	Gemini of coiled body
GDNF	Glial derived neurotrophic factor
GFP	Green fluorescent protein

HBSS	Hank's balanced salt solution
HEK293	Human embryonic kidney cell line 293
HDAC6	Histone deacetylase 6
hnRNPR	Heterogeneous ribonuclear protein R
HuD	ELAV-like protein 4
IgG	Immunoglobulin G
IMP	Insulin-like growth factor-II mRNA-binding proteins
kDa	kilo Dalton
KHSRP	KH-type splicing regulatory protein
KO	Knock-out
LC-MS	Liquid chromatography–mass spectrometry
NMJ	Neuro muscular junction
NSC-34	Mouse Motor Neuron-Like Hybrid Cell Line
MIAT	Myocardial infarction associated transcript
NLS	Nuclear localization signal
NES	Nuclear export signal
PCR	Polymerase chain reaction
PD	Parkinson disease.
RNA	Ribonucleic acid
RRM	RNA-recognition motif
RBPs	RNA-binding proteins
SALS	sporadic ALS
SDS-PAGE	Sodium-dodecyl sulfate polyacrylamide gel electrophoresis

SEM	Standard error of mean
siRNA	Small interference RNA
STRAP	Serine/Threonine Kinase Receptor Associated Protein
SMA	Spinal muscular atrophy
SMN	Survival motor neuron
snoRNPs	Small nucleolar ribonucleoproteins
SOD1	Superoxide dismutase 1
snRNP's	Small nuclear ribonuclear proteins
shRNA	Short hairpin RNA
TDP43	TAR DNA binding protein 43
UNRIP	UNR-interacting protein
UTR	Untranslated region
VCP	Valosin-containing protein
WT	Wildtype

10. AFFIDAVIT

Affidavit

I hereby confirm that my thesis entitled “**The role of RNA binding proteins in motoneuron diseases**” is the result of my own work. I did not receive any help or support from commercial consultants. All sources and / or materials applied are listed and specified in the thesis.

Furthermore, I confirm that this thesis has not yet been submitted as part of another examination process neither in identical nor in similar form.

Place, Date

Signature

Eidesstattliche Erklärung

Hiermit erkläre ich an Eides statt, die Dissertation “**Die Rolle von RNA-bindenden Proteinen in Motoneuronenerkrankungen.**” eigenständig, d.h. insbesondere selbständig und ohne Hilfe eines kommerziellen Promotionsberaters, angefertigt und keine anderen als die von mir angegebenen Quellen und Hilfsmittel verwendet zu haben.

Ich erkläre außerdem, dass die Dissertation weder in gleicher noch in ähnlicher Form bereits in einem anderen Prüfungsverfahren vorgelegen hat.

Ort, Datum

Unterschrift

11. ACKNOWLEDGMENTS

“Progress through Education & Strength through Organization”

Sree Narayana Guru....

I would like to express the deepest appreciation and deep sense of gratitude to Professor. Dr. Michael Sendtner, my principle supervisor, for giving me an opportunity to work under his guidance. I extend my deep indebtedness for the freedom of experimentation, wholehearted interest, constant motivation, ever willing help and insightful ideas throughout the research. His line of advice will always remain with me “Never give up by saying No for an answer”. I would also thank him for the critical scrutiny of the thesis.

I express my sincere gratitude to Prof. Dr. Hermann Schindelin, my second supervisor for his open handed help in introducing me to the world of crystallography and protein purification. His timely advice and suggestion were pivotal role with my protein purification experiments. Thank you very much.

I have been extremely privileged to know and interact with Prof. Dr. Erich Buchner and extend my deep-hearted gratitude for been my supervisor as well. You have been indispensable part of my achievement during my Ph.D. I would also like to appreciate the time and effort you had put in times of difficulties and helping me with the correction of my thesis. Thank you very much.

I owe my sincere gratitude to Dr. Carsten Drepper and Dr. Thomas Herrmann for teaching me the basic techniques and helping me to get acquainted to the lab atmosphere. I would like to thank specially Dr. Michael Glinka for getting me acquainted with basic radioactive technique and working safely in radioactive labs.

It gives me great pleasure in acknowledging Prof. Dr. Anna Maria Musti, Dr. Robert Blum & Prof. Dr. Villmann Carmen for their invaluable scientific inputs and advice both scientifically and personally. I would like to make a special appreciation for Hildegard Troll for the virus production. Regine Sendtner, Buterus Viktor and Buterus Viktor from the animal house facility without which most of my experiment was not possible.

I am indebted to all my colleagues who have supported me. Special thanks to Dr. Lidia Albanito, Dr. Benjamin Dombert, Dr. Christian Simon. Dr. Preeti Yadav, Dr. Reena Rathod, Dr. Chandrakanth Reddy, Lena Saal, Dominique Schmitt, Steven Havlicek, Dr. Andrea Wetzel, Dr. Rudolf Götz, Dr. Sibylle Jablonka, Dr. Frank Kreiger, Dr. Dirk Püringher, Dr. Patrick Lüningschr, Dr. Stefanie Rauskolb, Dr. Michael Briese, Mehri Moradi, Dr. Samera Samtleben, Dr. Beatriz Blanco, Thomas Andreska, Ghanawi Hanaa, Sasi Manju, Martin Corinna, Skoruppa Michael and Surrey Verena. I will cherish all the fun and joy we had with you guys till my end.

I would like to thank all the technical and administrative assistance I received from Michaela Keßler, Judita Grimm, Zuzana Fouskova, Manuela Kohles, Nicole Elflein, Christian Mehling, Urveen Oberoi-Lehrieder. Thank you very much will keep it close to me forever.

Words were hard to find to appreciate these people in my life. First of all my Papa and Mamma who always believed in me and gave me the best in life. I have to thank my wife from the bottom of my heart for all the sacrificed in her life to make time and space for me to work during the late night is one of them. Karthika thank you. I can never thank her more for the two handsome boys she gave me

Adithya and Aarav. Their love and affection during hard time was the lantern that showed light through the dark times of my life. I will always regret the time when I notice that the best of my kid's childhood was lost with my work. Adithya and Aarav thank you for this affection and love. I dedicate not just my Ph.D but also all my achievement to these special people in my life.

I also like specially thanking my grandfather, grandmother, uncles (Raju Sadashivan, Jayan Sadashivan and Biju Sadashivan) and Aunties (Reena Raju, Deepa Jayan and Deepa Biju) for their prayers and love. My prayer goes with my belated father-in-law who I miss a lot. A mere thank you would not be enough to thank my dearest mother-in-law who came down to stay with me to take care of my wife and kids when we need her the most. I also humbled by the love and affection from Kiran, Dhanya, Arjun and Aryan. I would like to express my sincere gratitude to Dr. Lysamma Vettom, Dr. Wegener and Dr. Elsamma Wegener for care and constant support.

This thesis would be a dream without the excellent funding that supported me. I would like to sincerely thank them all for giving me this opportunity.

Last but not the least I would like to thank everyone I have meet in Wurzburg and thank them all for the great time I had with them. Thank you all for your wishes and prayers.

Rajeeve Sivadasan

12. CURRICULUM VITAE

Rajeeve Sivadasan.

DATE OF BIRTH: 18-02-1980

EDUCATION:

Institute of Clinical Neurobiology, University of Würzburg

Ph.D., Molecular neurobiology, expected by December 2016

Dr. N.G.P. Arts & Science College, Coimbatore, INDIA

Master of Science (Biotechnology), April 2002-2004, Aggregate-63.24%

NSS College (University of Kerala), Kollam, Kerala, INDIA.

Bachelor of Science (Biochemistry), April 1999-2002, Aggregate-79.80 %

RESEARCH EXPERIENCE

Ph.D (2009-2016) at Institut für Klinische Neurobiologie, Versbacherstr. 5, 97078 Würzburg under the guidance of Prof. Michael Sendtner. The projects involved in include the characterization of the cellular function of C9ORF72 protein in mouse motoneuron. This study proved for the first time that C9ORF72 regulate actin dynamics with the phosphorylation of cofilin. The other project involved in was the *In vitro* study into the function of RNA binding protein like hnRNP R, TDP-43 and FUS/TLS in motoneuron disease.

Senior Research Fellow (2005-2008) at the Rajiv Gandhi Institute for Biotechnology, Trivandrum, Kerala, India under the guidance of Dr. T. R. Santhosh Kumar. The project involved in was finding and characterization of natural plant products for anti-cancer effect. This project led to establishment of high throughput screening techniques of mass screening of products for anticancer properties. The second project was the establishment of immortalized HUVEC cells to clot artificial blood vessels to prevent post operational rejection in patients.

Junior Research Fellow (2004-2005) at the College of Agriculture, Vellayani, Kerala, India under the guidance of Prof. K. Rajmohan. The project involved includes Research in DNA

methylation in relation to maturation of *Eucalyptus camaldulensis*. The other project includes the establishment of gene bank for *Anacardium occidentale* by RAPD (Random Amplification of Polymorphic DNA) and RFPL (Restriction Fragment Length Polymorphism) methods.

PUBLICATION

Sivadasan R, Hornburg D, Drepper C, Frank N, Jablonka S, Hansel A, Lojewski X, Sterneckert J, Hermann A, Shaw PJ, Ince PG, Mann M, Meissner F, Sendtner M. C9ORF72 interaction with cofilin modulates actin dynamics in motor neurons. *Nature Neuroscience*. 2016 (In Press).

Yadav P, Selvaraj BT, Bender FL, Behringer M, Moradi M, **Sivadasan R**, Dombert B, Blum R, Asan E, Sauer M, Julien JP, Sendtner M. Neurofilament depletion improves microtubule dynamics via modulation of Stat3/stathmin signaling. *Acta Neuropathol*. 2016 Jul;132(1):93-110. doi: 10.1007/s00401-016-1564-y. Epub 2016 Mar 28. PMID: 27021905

Dombert B*, **Sivadasan R***, Simon CM, Jablonka S, Sendtner M. Presynaptic localization of Smn and hnRNP R in axon terminals of embryonic and postnatal mouse motoneurons. *PLoS One*. 2014 Oct 22;9(10):e110846. (* equal contribution)

Joy B*, **Sivadasan R***, Abraham T E, John M, Sobhan PK, Seervi M, T R S. Lysosomal destabilization and cathepsin B contributes for cytochrome c release and caspase activation in embelin-induced apoptosis, *Mol Carcinog*. 2010 Apr;49(4):324-36. (* equal contribution)

Rajmohan, K., Gomathi, S. and **Sivadasan, R.** (2006) DNA methylation in relation to maturation of *Eucalyptus camaldulensis*. *Biochemi. Cell. Arch.* 6(2): 229-32. (ISSN 09725075).

POSTER PRESENTATION

SFB 487. Molecular Pharmacology of Receptors, Channels and Transporters. Poster title: "TDP-43 Recombinant Protein Production for Functional Studies and Structural Analysis. July 28-30, 2011

NGF 2012. Neurotrophic Factors and Plasticity of the Nervous System. Poster title: “TDP-43 Recombinant Protein Production for Functional Studies and Structural Analysis. June 21-24, 2012

SfN 2012. Society for Neuroscience. Poster title: “Overexpression of hnRNP R rescues axon pathology in Smn-deficient motoneurons”. October 13-17, 2012

For IPS. BAVARIAN RESEARCH COOPERATION induced pluripotent stem cells. Poster title: “Deep Proteomic Evaluation of Primary and Cell Line Motoneuron Disease Models Delineates Major Differences in Neuronal Characteristics“. October 2-3, 2015.